Università degli Studi di Pisa

Facoltà di Scienze Matematiche, Fisiche e Naturali

Corso di Laurea in Fisica

Simulation of opto-mechanical systems in the presence of ponderomotive squeezing effects

Tesi di Laurea Magistrale

Candidato
Eleonora Capocasa

Relatore
Dott. Giancarlo Cella

Anno Accademico 2013/2014

Contents

1 Introduction

An interferometric gravitational wave detector aims to reveal the relative displacement of the mirrors which constitute the optical cavities caused by the transit of a gravitational wave. Such displacement generates a revealable optical signal whose detection is made harder by many sources of noises able to produce spurious optical signals. The sensitivity of first generation detectors was basically limited by seismic and thermal noise while new generation detectors will eventually have to face the sensitivity limits imposed by the quantum nature of the light used for the detection (see Figure 1.1).

It is possible to separate such "quantum noise" into two contributions[1]:

- shot noise caused by the fluctuations of the number of photons in laser beams which is higher when the laser power is low.
- radiation pressure noise caused by quantum fluctuations of the laser amplitude. Its effect increases for high values of the power and at low frequencies where the mechanical response of the mirror is larger.

As we will see, it is possible to write the expression for the quantum noise strain equivalent spectral power for a resonant detector in a form where these two contributions can be easily identified, namely

$$S_h(f) = \frac{h^2_{SQL}(f)}{2}\left[K(f) + \frac{1}{K(f)}\right] \tag{1.1}$$

Here I_0 is the laser power, $K \propto I_0 f^{-2}$ and $h_{SQL} \propto f^{-1}$. Radiation pressure noise is represented by $Kh^2_{SQL} \propto I_0 f^{-4}$ while shot noise by $K^{-1}h^2_{SQL} \propto I_0^{-1}$. They both show the correct dependence from I_0.

Given a frequency $\overline{f}$ it is possible to vary the laser power and strike the best balance between shot noise and radiation pressure noise. This is achieved for the value of I_0 that gives $K(\overline{f}) = 1$. In this case the spectral power becomes

$$S_h^{MIN}(\overline{f}) = h^2_{SQL}(\overline{f}) = \frac{\hbar}{\pi^2 L^2 M \overline{f}^2} \tag{1.2}$$

[1]There exist also classical fluctuations of light, which will not concern us in this thesis.

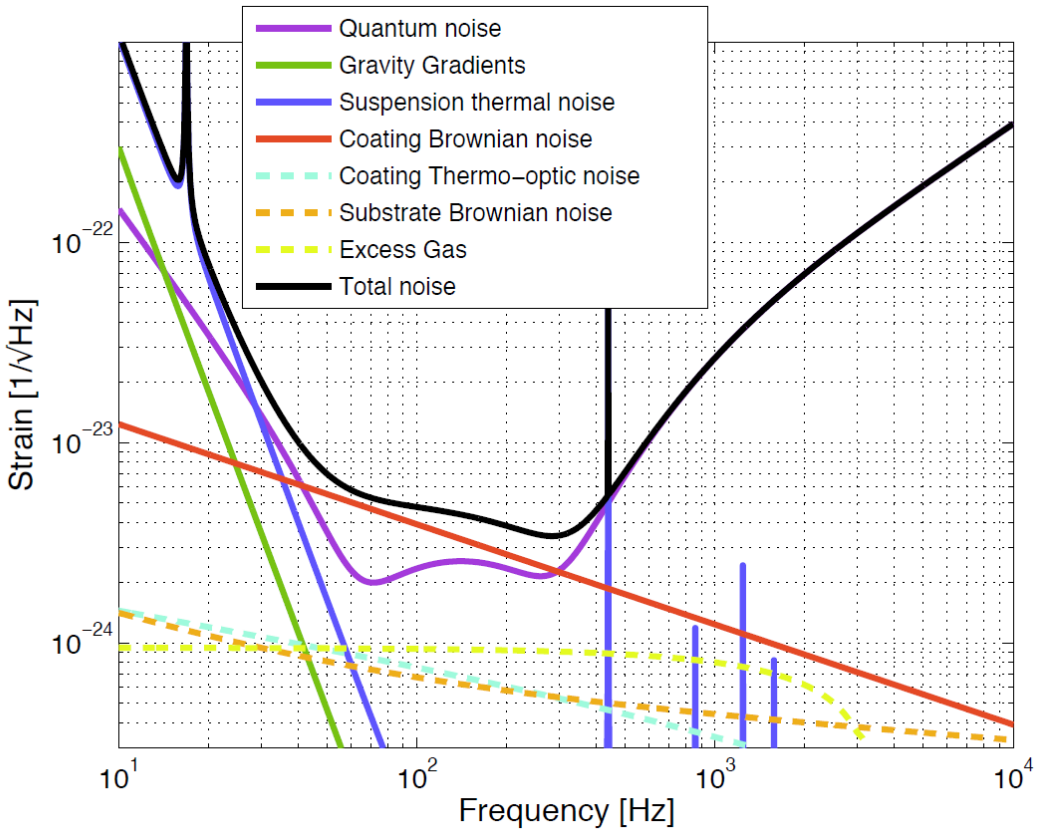

Figure 1.1: Sensitivity curve of advanced gravitational wave detectors, which will be operative in 2015 and 2016. Note that sensitivity details are subject to change. See [1] for up to date estimates of second generation detector sensitivities. The curve shows a relevant contribution of quantum noise to total noise in many regions therefore its reduction would improve significantly the sensitivity of the detector.

where L is the cavity length and M the mass of the mirrors. This quantity, referred to as Standard Quantum Limit (SQL) , is a lower bound for the noise which seems to be connected to the impossibility of measuring repeatedly the position of the mirrors with arbitrary precision [2] and could be interpreted as a consequence of Heisenberg's uncertainty principle where radiation pressure and shot noise are non commuting, conjugate observables. Since the Hamiltonian which describes time evolution for a mode of the electromagnetic radiation is formally identical to the one of an harmonic oscillator we can write the relation

$$\Delta E \Delta \left(\overline{E}\phi\right) \geq k \tag{1.3}$$

where E is the amplitude of the field, $\overline{E}$ its mean value, ϕ is the phase and k is a suitable constant.

Although connected to the fundamental uncertainty principle of quantum mechanics, SQL is not a fundamental limit itself: in fact we are not interested in determining the position of the mirrors but in measuring the classical force which acts on them by means of laser light. The Hamiltonian of this process is the same as the one of a classical force coupled to a quantum-mechanical oscillator for which strategies to evade SQL have been successfully studied [3]. Moreover the SQL is derived assuming the standard properties of the electromagnetic field: for an ordinary laser, which can be described conveniently by a coherent state, the amplitude uncertainty equals the phase uncertainty multiplied by the mean amplitude value

$$\Delta E = \Delta \left(\overline{E}\phi\right) \tag{1.4}$$

However, quantum physics does not prevent us from modifying quantum fluctuation and new quantum states can be obtained, so that (1.4) is no longer true. For this states, referred to as squeezed states, the phase uncertainty can be reduced at the expense of amplitude uncertainty which is bound to increase in order to make (1.3) hold true. If the information we need is kept in the phase of the field (as it happen for the mirror displacement in gravitational wave detectors) we can have an intuitive idea of how, for these states, noise can go below SQL [4][5].

Squeezed light can be generated by introducing correlations between amplitude and phase fluctuations of a coherent state. So far the most effective techniques to do that make use of non-linear means to create such correlation. For example, in a non linear crystal where the polarization P and the electric field E are related by an equation of the kind

$$P = \epsilon_o \left(\chi_1 E + \chi_2 E^2 + \chi_3 E^2 + ...\right)$$

the term proportional to χ_2 induces a cubic interaction which is describable by

means of an Hamiltonian like

$$\hat{H}_I = i\hbar g \left[\hat{b}^\dagger \hat{a}_1 \hat{a}_2 - \hat{b}\hat{a}_1^\dagger \hat{a}_2^\dagger\right]$$

Here a single photon in the mode $\hat{b}$ of angular frequency ω_b can be converted into a pair of photons in the modes $\hat{a}_1$ e $\hat{a}_2$ with angular frequencies ω_{a_1} and ω_{a_2} such that $\omega_{a_1} + \omega_{a_2} = \omega_b$ in order to conserve energy. Analogously a pair of photons can merge in a single one. These mechanisms are respectively known as "down conversion" and "up conversion".

However, in theory, the mere interaction of the laser light with a movable mirror is capable of creating noise correlations: in effect an amplitude fluctuation of the input field generates a displacement of the suspended mirror which in turn will affect the phase fluctuations [6, 7]. This effect is referred to as ponderomotive squeezing and it is particularly interesting as it naturally arises in interferometric detectors, but due to the intrinsic weakness of radiation pressure fluctuation with respect to other noise sources, it is extremely difficult to observe.

This thesis focuses on the generation of ponderomotive squeezing and arises within the collaboration "*Progetto PRIN di Ponderomotive Squeezing*" (see `http://www.ppps.it/`) which aims to build a dedicated interferometer to observe directly this squeezing effect. The main goal of this work is the development of a code able to simulate opto-mechanical effects in optical systems providing a useful tool to predict the system behavior and also to investigate interesting theoretical aspects of the coupling between mechanical and optical modes. Indeed, there are many other effects due to radiation pressure that are worth to be considered. In particular, the interplay between radiation pressure and change in cavity length and circulating power results in an effective stiffness of the cavity called optical spring effect which can be exploited in many ways [8], for example to cool a mechanical system to its quantum ground state [9] or to shift the frequency at which the squeezing occurs from the free pendulum one.

In order to improve the accuracy of the simulation, optical fields are not regarded as plane waves but are decomposed in Hermite Gauss (HG) modes. This allows to take into account accurately tilting effects on the mirrors due to a non-zero momentum of the radiation pressure force.

For each HG mode the field is split in a classical part and in a fluctuating part. The first is evaluated using a classical model and it defines the equilibrium point for the mirrors, around which we will linearize the dynamics. In order to describe the quantum fluctuations around a classical carrier we used the two photon formalism [10][11], where such fluctuations are treated as amplitude and phase fluctuations for sidebands of the laser carrier. It provides an effective way to describe the correlations introduced by the interaction of the field with optical elements like movable mirrors. We use a simple generalization of this

formalism, which was developed for plane waves, to the case of HG modes.

In the first part of the work we describe classical opto-mecanical effects in a Fabry-Pérot cavity with movable mirrors where the circulating light is decomposed in HG modes. Afterwards the light fields are quantized and also the opto-mechanical effects are presented from a quantum point of view.

In the second part we illustrate the operating principles of the simulation and present some results for the squeezing which can be obtained, both in the case of a large interferometric gravitational wave detector and in a smaller dedicated cavity such as the one proposed in the PRIN project or in [12]. We also included the possibility of simulating thermal noise in the system in order to compare its modulation effect on the mirrors with those generated by quantum fluctuations and investigate which system configurations allow to reduce its spoiling effects on ponderomotive squeezing.

Lastly we briefly discuss the possibility of a further development of the simulation in order to take into account effects which go beyond the linear approximation used.

2 Ponderomotive effects in a resonant cavity

2.1 Classical description of a resonant cavity

Optical cavities are among the simplest devices used to study the coupling of light and mechanical modes. This interaction takes place between the light modes excited in the cavity and the mechanical modes of the mirrors which form it. The simplest optical cavity is composed of two mirrors with curvature radii R_1, R_2 separated by some distance L and from these three parameters it is possible to classify a cavity as stable or unstable and work out the features of electromagnetic fields which resonate inside it.

2.1.1 Electromagnetic fields in a cavity: Hermite Gauss modes

We will describe the electromagnetic field propagating inside a cavity as a classical one, and we will use the paraxial approximation because we are interested in the description of a narrow beam propagating along a well defined optical axis. We will ignore also polarization degrees of freedom, so our field will represent the relevant transverse component of the electric field, which in the monochromatic case is a solution of the Helmholtz equation

$$\left(\nabla^2 + k^2\right) E = 0 \tag{2.1}$$

where $k = \omega/c$. The paraxial approximation is obtained by searching solutions like

$$E = e^{ikz - i\omega t}\phi\left(x, y, z\right) + c.c$$

where ϕ , which represents the difference between our field and a plane wave, changes slowly on the length scale defined by the wavelength, namely

$$\frac{\partial \phi}{\partial z} \ll k\phi \tag{2.2}$$

This solution will represent a beam propagating in the positive z direction if $k > 0$, in the negative one otherwise. With the assumption (2.2) we can rewrite

Eq.(2.1) as

$$\left(\nabla_T^2 + \frac{\partial^2}{\partial z^2} + 2ik\frac{\partial}{\partial z}\right)\phi = 0$$

which can be approximated using Eq. (2.2) as

$$\left(\nabla_T^2 + 2ik\frac{\partial}{\partial z}\right)\phi = 0 \tag{2.3}$$

Here ∇_T^2 is the Laplacian operator restricted to the transverse coordinates,

$$\nabla_T^2 = \frac{\partial^2}{\partial x^2} + \frac{\partial^2}{\partial y^2}$$

The paraxial equation is a first order equation in the z derivative: this means that the knowledge of the field on a given plane $z = z_1$ is enough to evaluate the field in the direction of the propagation (or backward if needed).

If we Fourier transform in the transverse coordinates we get

$$\left(2ik\frac{\partial}{\partial z} - p^2 - q^2\right)\tilde{\phi}\,(p, q, z) = 0$$

which can be solved as

$$\tilde{\phi}\,(p, q, z_2) = \exp\left[-i\frac{p^2 + q^2}{2k}\,(z_2 - z_2)\right]\tilde{\phi}\,(p, q, z_1)$$

This defines the propagator of the field in the Fourier domain.

A useful set of solutions of the paraxial equation (2.3) is given by the Hermite Gauss modes [13]

$$\begin{aligned}\mathrm{HG}_{(m,n,\omega)}\,(x, y; z) &= c_{mn}e^{ikz}e^{-i\eta_{mn}(z)}e^{\frac{ikr^2}{2q(z)}}H_m\left(\frac{\sqrt{2}x}{w(z)}\right)H_n\left(\frac{\sqrt{2}y}{w(z)}\right) \\ &\equiv c_{mn}e^{ikz}e^{-i\eta_{mn}(z)}\varphi_{mnk}\,(x, y; z)\end{aligned} \tag{2.4}$$

where m, n are nonnegative integers and

- $H_m\,(X)$ is the m-th Hermite polynomial which accounts for the field intensity in the transverse plane;
- q is a complex parameter which can be written as

$$q = -\frac{1}{w^2(z)} + \frac{ik}{2R(z)}$$

and gives information about the curvature of the phase front and the variation of the beam intensity in the transverse plane. In particular $R(z)$ is the curvature radius of the wavefront which intersects the axis in z and $w(z)$, usually referred to as beam radius or spot size, measures the decrease of the field intensity as we go away from the optical axis. Its minimum value w_0 known as beam waist is usually taken as the zero for the optical axis z.

- $\eta_{mn}$is an extra-phase

$$\eta_{mn}(z) = (m+n+1)\arctan\frac{z}{b}$$

called Gouy phase, appearing during propagation with respect to a plane wave. Physically it represent the diffraction effects which arise near the beam waist;

- c_{mn} is a normalization factor

$$c_{mn} = \sqrt{\frac{2}{\pi w^2}\frac{1}{2^{m+n}m!n!}}$$

which assures that the integral of the square modulus of (2.4) in the transverse plane equals one for every mode.

The following relations, holding for these parameters, will be useful in future:

$$q(z) = -ib + z \tag{2.5a}$$

$$b = \frac{kw_0^2}{2} \tag{2.5b}$$

$$\frac{ik}{2q(z)} = \frac{1}{z+\frac{b^2}{z}} + \frac{i}{b+\frac{z^2}{b}} = -\frac{1}{w^2(z)} + \frac{ik}{2R(z)} \tag{2.5c}$$

$$w(z) = w_0\sqrt{1+\frac{z^2}{b^2}} \tag{2.5d}$$

$$R(z) = z\left(1+\frac{b^2}{z^2}\right) \tag{2.5e}$$

Since a set of HG functions $HG^q_{z,mn}(x,y)$ with $m,n = 0,1,...,\infty$ is a basis for the transverse field at each z, any optical amplitude $E(x,y)$ can be written as

$$E(x,y) = \sum_{m,n} E_{mn} HG^q_{z,mn}(x,y)$$

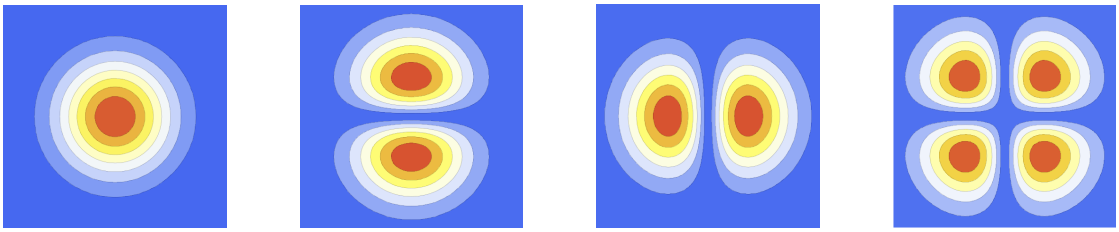

Figure 2.1: Intensity pattern of the lowest-order HG modes: from left to right, HG_{00}, HG_{01}, HG_{10} and HG_{11}. The intensity profile of a HG_{mn} mode has m nodes in the vertical direction and n nodes in the horizontal direction.

An $HG^q_{z,mn}(x,y)$ basis (for every z) is completely determined by the value w_0 and the expression (2.4) provides a natural connection between bases with the same w_0 at different z. The element of a HG basis with $m = n = 0$ is referred to as fundamental Transverse Electric and Magnetic (TEM) mode and has a Gaussian intensity profile whose full width at half maximum is $2w(z)$. From (2.5d) we see that $w(z)$ is a hyperbola with a minimum in $z = 0$ corresponding to the beam waist and asymptotes that form an angle $\theta_g = \frac{2}{kw_0}$ with the z axis, known as aperture angle. Therefore the intensity distribution for the fundamental mode TEM_{00} is Gaussian at each z and its width increases during propagation.

2.1.2 Propagation through optical devices and matched modes

The free propagation of a HG mode can be read from Eq. (2.4) and Eq. (2.5a). Things become more complicated when the propagating field interacts with optical devices such as lenses or mirrors. It is possible to associate a 2×2 matrix, called ray transfer matrix, with any optical system and use it to work out the relation between q parameters of the input and output beam. If $M = \begin{bmatrix} A & B \\ C & D \end{bmatrix}$ is the ray transferred matrix of an optical system (usually also referred to as $ABCD$ matrix) we have

$$q_{out} = \frac{A\, q_{in} + B}{C\, q_{in} + D} \tag{2.6}$$

The most used $ABCD$ matrices, when studying simple optical cavities, are the one which describes a free propagation over a distance L

$$M_L = \begin{bmatrix} 1 & L \\ 0 & 1 \end{bmatrix}$$

and the one which describes the reflection from a mirror with curvature radius R

$$M_R = \begin{bmatrix} 1 & 0 \\ -2R^{-1} & 1 \end{bmatrix}$$

This description for the free propagation of $q(z)$ allows us to recover Eq. (2.5a) and can be used to find the eigenmodes of a cavity. These are defined as self-consistent configurations which reproduce themselves after one round trip. The $ABCD$ matrix M^{rt} associated with a round trip in a Fabry-Pérot cavity is

$$M^{rt} = M_{R_1} M_L M_{R_2} M_L$$

which is obtained by multiplying in the right order the matrices relative to the free propagation M_L, to the reflection from the end mirror M_{R_2} and to the front mirror M_{R_1}. By using Eq. (2.6)

$$q_{out} = \frac{M_{11}^{rt} q_{in} + M_{12}^{rt}}{M_{21}^{rt} q_{in} + M_{22}^{rt}} \tag{2.7}$$

Self-consistency requires $q_{in} = q_{out} = q$. Solving Eq. (2.7) we find q_{in} and, from it, we derive q at every z. Then we can deduce $w(z)$ and $R(z)$. We will find out that the curvature radius of a mode $R(\bar{z})$, where $\bar{z}$ is the mirror position, must be equal to the curvature radius of the mirror, which means that the mirror surface coincides with the phase front of the resonant mode. We can also find the value of the waist w_0 and its distances d_1, d_2 from the mirrors. As we said, the value w_0 of the waist and its position determine univocally (except for the wave vector $k = 2\pi\nu/c$) a $HG_{z,mn}^{q}(x, y)$ basis, and so for a stable cavity it is always possible to find a matched $HG_{z,mn}^{q}(x, y)$ basis whose parameters depend only on the geometry of the cavity (curvature radius of the mirrors $R_1 R_2$ and their distance L). The value w_0 of the waist is given by

$$w_0^2 = \left(\frac{\lambda}{\pi}\right)^2 \frac{L(R_1 - L)(R_2 - L)(R_1 + R_2 - L)}{(R_1 + R_2 - 2L)^2}$$

while the distances from the mirrors, as shown in Figure 2.2 are

$$d_1 = \frac{L(R_2 - L)}{R_1 + R_2 - 2L}$$

$$d_2 = \frac{L(R_1 - L)}{R_1 + R_2 - 2L}$$

Now we want find the resonant condition for the wave vector k. We know that

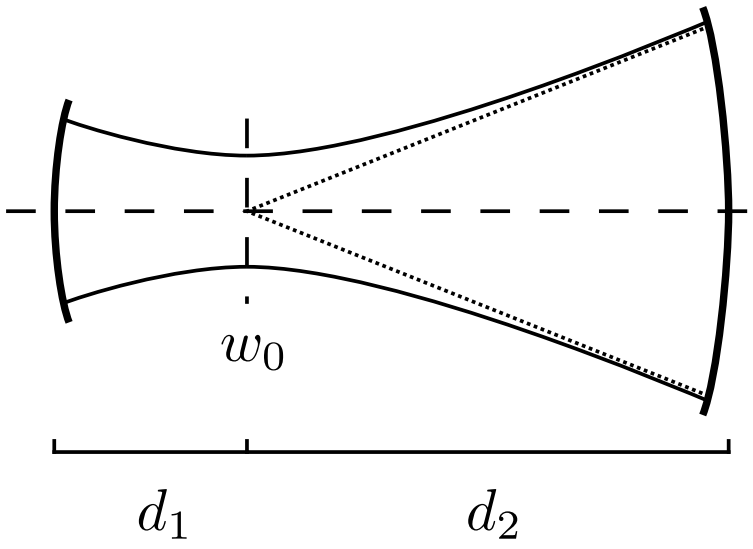

Figure 2.2: Matched Gaussian beam profile.

modes of different order belonging to the same basis have different phase velocity because of the Gouy phase. Thus imposing the resonant condition (phase shift equals to $2n\pi$ after a round trip) we find a condition, depending on the mode number, that reads

$$\frac{\nu_{mn,p}}{\nu^{(FSR)}} = p + (m+n+1)\,\frac{1}{\pi}\arccos\sqrt{\left(1-\frac{L}{R_1}\right)\left(1-\frac{L}{R_2}\right)} \tag{2.8}$$

where $\nu^{(FSR)} = \frac{c}{2L}$, is the Free Spectral Range (FSR), the frequency gap between two successive resonances of a given mode, labeled by the integer p.

For our purposes it will be useful to study the distance of the resonant frequency ν_{00,p_0} for a fundamental mode from higher modes (especially the ones at first order TEM_{01}, TEM_{10}). From (2.8) we have

$$\delta\nu_{mn,p} = \nu_{mn,p} - \nu_{00,p_0} = \nu_0\left(p - p_0 + (m+n)\,\alpha\right)$$

where

$$\alpha = \frac{1}{\pi}\arccos\sqrt{\left(1-\frac{L}{R_1}\right)\left(1-\frac{L}{R_2}\right)}$$

The distribution being periodic, it suffices to study it over a FSR. In our case we have

$$\delta\nu_{01} = \delta\nu_{10} = \nu_0\alpha = \frac{c}{2\pi L}\arccos\sqrt{\left(1-\frac{L}{R_1}\right)\left(1-\frac{L}{R_2}\right)}$$

2.1.3 Coupling of different modes

In a cavity with perfectly matched mirrors each mode propagates independently but a linear coupling between them is likely to occur in the presence of perturbed mirrors. Let us consider the case of a mirror rotated from the "matched position" by a small amount. The effect of such a rotation on an incoming mode HG_{kl}^{in} can be represented by a matrix

$$HG_{mn}^{out} = \sum_{kl} R_{kl,mn} HG_{kl}^{in}$$

This means that part of the incoming mode amplitude will be redistributed between higher order modes, according to the $R_{kl,mn}$ coefficients. We will now look for an explicit expression for this matrix whose coefficients should depend on the mirror displacement. We describe small displacements of the mirror with parameters $\delta\theta_x$ and $\delta\theta_y$ that represent a rotation of the x and y axes. For symmetry reasons a rotation $\delta\theta_z$ of the z axes won't have any effect on the coupling at the first order, unless an astigmatic mirror is used. This can be the case in a real optical device, but we will not deal with this possibility here. The operator associated with a reflection by a mirror is

$$R = \exp 2ikf\,(x,y) \tag{2.9}$$

where $f\,(x,y)$ represents the displaced surface of the mirror with respect to its matched position. The coefficients of $R_{kl,mn}$ can be found by applying the reflection operator to the incoming mode and then projecting it on a HG basis:

$$R_{kl,mn} = \langle HG_{mn}|\, e^{2ikf(x,y)}\, |HG_{kl}\rangle$$

After substituting the expression for the HG modes we gave in (2.4), this becomes

$$\begin{aligned} R_{kl,mn} = c_{mn}c_{kl}\int H_m\left(\sqrt{2}\frac{x}{w}\right) H_n\left(\sqrt{2}\frac{y}{w}\right) H_k\left(\sqrt{2}\frac{x}{w}\right) H_l\left(\sqrt{2}\frac{y}{w}\right)\cdot \\ \times \exp\left[-2\frac{x^2+y^2}{w^2}\right] e^{2ikf(x,y)}dxdy \end{aligned} \tag{2.10}$$

By defining the new variables $X = \sqrt{2}\frac{x}{w}$ and $Y = \sqrt{2}\frac{y}{w}$ we obtain

$$R_{kl,mn} = \frac{w^2}{2} c_{mn} c_{kl} \int H_m(X) H_n(Y) H_k(X) H_l(Y) \cdot \\ \times \exp\left[-X^2\right] \exp\left[-Y^2\right] \exp\left[2ikf\left(\frac{wX}{\sqrt{2}}, \frac{wY}{\sqrt{2}}\right)\right] dX dY$$

If X, Y and Z are the coordinates of the rotated frame, where the parabolic mirror equation is

$$Z = \frac{X^2 + Y^2}{2R}$$

we know they are linked to the former frame x, y, z by a rotation, and we have

$$\delta\vec{R} = \delta\vec{\theta} \wedge \vec{r} = \begin{vmatrix} \hat{x} & \hat{y} & \hat{z} \\ \delta\theta_x & \delta\theta_y & \delta\theta_z \\ x & y & z \end{vmatrix}$$

from which

$$X = x + \delta\theta_y z - \delta\theta_z y \\ Y = y - \delta\theta_x z + \delta\theta_z x \\ Z = z + \delta\theta_x y - \delta\theta_y x$$

and

$$Z = \frac{X^2 + Y^2}{2R} \Rightarrow \\ z + \delta\theta_x y - \delta\theta_y x = \frac{(x + \delta\theta_y z - \delta\theta_z y)^2 + (y - \delta\theta_x z + \delta\theta_z x)^2}{2R} \Rightarrow \\ z = \frac{x^2 + y^2}{2R} - \delta\theta_x y + \delta\theta_y x + \frac{1}{R}\left[\delta\theta_y z x + \delta\theta_x z y\right] \tag{2.11}$$

We can neglect the last term as both $\delta\theta_y$ and z are small compared with x and y which are at most of order w and so $\frac{x}{R} \simeq \frac{w}{R} \simeq \sin\theta_g$ which is small to be consistent with the paraxial approximation and we obtain the rotated mirror equation from which we can deduce the function

$$f(x, y) = \delta\theta_x y - \delta\theta_y x$$

The integral (2.10) becomes

$$\begin{aligned} R_{mn,kl} &= c_{mn}c_{kl}\int H_m\left(\sqrt{2}\frac{x}{w}\right)H_k\left(\sqrt{2}\frac{x}{w}\right)\exp\left[-\frac{2x^2}{w^2}\right]\exp\left(2ik\delta\theta_y x\right)dx \\ &\cdot H_n\left(\sqrt{2}\frac{y}{w}\right)H_l\left(\sqrt{2}\frac{y}{w}\right)\exp\left[-\frac{2x^2}{w^2}\right]\exp\left(-2ik\delta\theta_x y\right)dy \end{aligned}$$

We have to calculate integrals of the form

$$I_{mk}\left(p\right)=\int_{-\infty}^{+\infty}H_m\left(X\right)H_n\left(X\right)e^{-X^2}e^{ipX}dX$$

It is possible to prove that

$$I_{mk}\left(p\right)=\sqrt{\pi}i^{m+k}e^{-p^2/4}Q_{mk}\left(p\right)$$

where we introduced the displacement polynomials

$$Q_{mk}\left(p\right)=\sum_{s=0}^{min(m,k)}\left(-2\right)^s\frac{m!k!}{s!\left(m-s\right)!\left(k-s\right)!}p^{m+k-2s}$$

Our rotation matrix becomes

$$R_{mn,kl}\left(p,q\right)=\frac{i^{m+n+k+l}}{\sqrt{2^{m+n+k+l}m!n!k!l!}}Q_{mk}\left(p\right)Q_{nl}\left(q\right)e^{-\frac{1}{4}\left(p^2+q^2\right)} \tag{2.12}$$

with

$$\begin{aligned} p &= \sqrt{2}kw\delta\theta_y \\ q &= -\sqrt{2}kw\delta\theta_x \end{aligned}$$

In Figure 2.3 it is shown the power coupled from the fundamental mode TEM_{00} into higher order modes as a function of the rotation parameter p. It is evident that for small rotations, when p is close to zero, the stronger coupling takes place with the closer mode TEM_{00}. From the Table 2.1, which shows the coupling between TEM_{00}, TEM_{10}, TEM_{01} modes, we see that at first order in the rotation parameters p and q only the modes which differ by one index are coupled. Since we will deal with small displacements of the mirror, we will restrict our interest to first order coupled modes.

Note that the elements in Table 2.1 $\mathcal{R}_{mn,kl}$ are not exactly the ones of Eq. 2.12

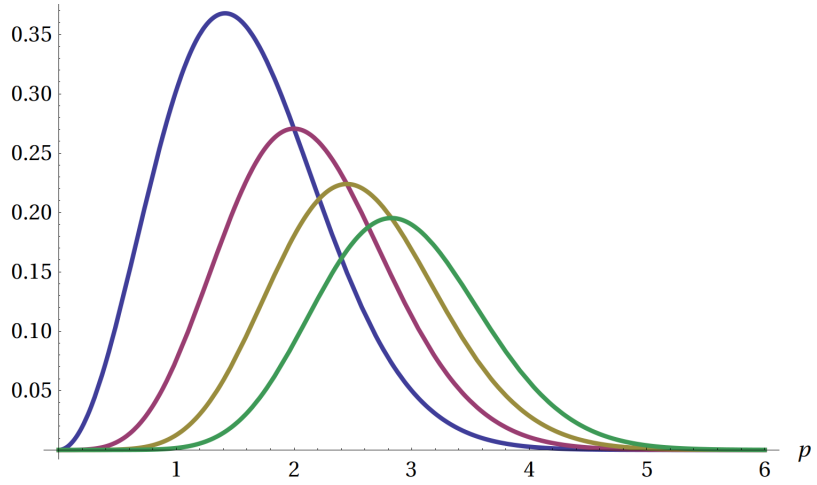

Figure 2.3: Coupling of TEM_{00}.

	TEM_{00}	TEM_{10}	TEM_{01}
TEM_{00}	1	$i\frac{p}{\sqrt{2}}$	$i\frac{q}{\sqrt{2}}$
TEM_{10}	$i\frac{p}{\sqrt{2}}$	$1-\frac{p^2}{2}$	$-\frac{pq}{2}$
TEM_{01}	$i\frac{q}{\sqrt{2}}$	$-\frac{pq}{2}$	$1-\frac{p^2}{2}$

Table 2.1: The couplings $\mathcal{R}_{mn,kl}$ between TEM_{00}, TEM_{10}, TEM_{01} modes induced by a mirror rotation.

but they are proportional by an exponential factor:

$$R_{mn,kl}\left(p,q\right)=\mathcal{R}_{mn,kl}\left(p,q\right)e^{-\frac{1}{4}\left(p^2+q^2\right)}$$

such term has been left not expanded in order to obtain a better accuracy in numerical simulation, even when the expansion parameters are not infinitesimal.

It is possible to show that a translation of the mirror by a small amount $\delta\epsilon_x$ or $\delta\epsilon_y$ along the x or y axes can be regarded as a rotation and expressed in terms of $\delta\theta_y$ and $\delta\theta_x$. For the translated frame we have

$$\begin{aligned}X&=x-\delta\epsilon_x\\Y&=y-\delta\epsilon_y\\Z&=z\end{aligned}$$

The equation for the mirror surface becomes

$$\begin{aligned} Z &= \frac{X^2+Y^2}{2R} \Rightarrow \\ z &= \frac{(x-\delta\epsilon_x)^2+(y-\delta\epsilon_y)^2}{2R} \Rightarrow \\ z &= \frac{x^2+y^2}{2R} - \frac{1}{R}\left[\delta\epsilon_x x + \delta\epsilon_y y\right] \end{aligned} \tag{2.13}$$

Comparing Eq. (2.11) with Eq. (2.13) we deduce

$$\begin{aligned} \delta\theta_y &= -\frac{\delta\epsilon_x}{R} \\ \delta\theta_x &= \frac{\delta\epsilon_y}{R} \end{aligned}$$

2.1.4 Classical ponderomotive effects

We have seen that a displacement of the mirror from its matched position can generate a coupling between different modes. Now we want to investigate how such a displacement can be caused by light interacting with the mirror by means of its radiation pressure.

A general expression for radiation pressure and momentum transferred by light can be calculated classically using the momentum conservation theorem

$$\frac{d}{dt}\left(P_m + P_{em}\right)_i = \oint_S T_{ij}\hat{n}_j dS \tag{2.14}$$

were P_m, P_{em} are the mechanical and the electromagnetic momentum and

$$T_{ij} = \varepsilon_o\left[E_iE_j + c^2B_iB_j - \frac{1}{2}\left(E^2+c^2B^2\right)\delta_{ij}\right]$$

is the Maxwell electromagnetic stress tensor. Eq. (2.14) can be used to calculate the force exerted by light on the mirror. We can imagine to enclose our mirror (here supposed plane for the sake of simplicity) inside a closed surface S and find $\frac{d}{dt}\left(P_m\right)_i$ as the i-th component of the flux of T_{ij} through the surface S.

Assuming that the field propagates along the z axis, the electric field $\vec{E}$ oscillates along the x axis and $\vec{B}$ along y axis, the Maxwell stress tensor will be a

diagonal tensor of the form

$$T_{ij} = \frac{1}{2}\varepsilon_0 \begin{pmatrix} E^2 & 0 & 0 \\ 0 & c^2B^2 & 0 \\ 0 & 0 & -E^2 - c^2B^2 \end{pmatrix} \tag{2.15}$$

Choosing $\hat{n} = (0, 0, -1)$, the only non-zero component of the product with T_{ij} is T_{33} and Eq. (2.14) becomes

$$\left\langle \frac{dP_m}{dt} \right\rangle = -\oint_S \langle T_{33} \rangle \, dS \tag{2.16}$$

where we considered an average on the oscillation period.

The radiation pressure just evaluated is responsible for a modulation effect. We can give a classical intuitive picture of this effect by considering a perfectly reflective mirror whose oscillation around its zero position is described by $\delta z_M(t) = \epsilon \cos \Omega t$. Supposing we are in a non-relativistic regime (i.e $\epsilon\Omega \ll c$) let's consider an incoming monochromatic wave in the region $x < 0$ of the form

$$E_{IN} = E_0 \cos \omega_0 \left(t - \frac{z}{c} \right)$$

For the reflected field we can write

$$E_R = E_0 \cos \omega_0 \left(t - \frac{2\delta z_M(t)}{c} + \frac{z}{c} \right)$$

and expanding we have

$$\begin{aligned} E_R &\simeq E_0 \left[1 + O\left(\frac{\omega_0 \delta z_M}{c} \right)^2 \right] \cos \omega_0 \left(t + \frac{z}{c} \right) + \\ &+ E_0 \left[\frac{2\omega_0 \delta z_M(t)}{c} + O\left(\frac{\omega_0 \delta z_M}{c} \right)^3 \right] \sin \omega_0 \left(t + \frac{z}{c} \right) \end{aligned} \tag{2.17}$$

If we write the field in terms of sine and cosine quadrature

$$E(t) = E_1(t) \cos \omega_0 t + E_2(t) \sin \omega_0 t \tag{2.18}$$

we see that the mirror motion introduces a temporal dependency in the amplitudes of $\cos \omega_0 t$ and $\sin \omega_0 t$ quadratures. If the oscillation amplitude of the mirror is small compared with the wavelength of the carrier (i.e $\omega_0 \delta z_M / c \ll 1$) , as we assume in order to neglect the higher order terms in Eq. (2.17), the quadrature amplitudes become

$$E_1(t) = E_0 \tag{2.19}$$

$$E_2(t) = \frac{2E_0\omega_0\epsilon}{c}\cos\Omega t \tag{2.20}$$

This modulation in time for amplitude results in the appearance of two components in addition to the carrier: two sidebands, whose frequencies are symmetrically displaced above and below the carrier by an amount Ω which is usually small compared with the carrier angular frequency ω_0.

$$E(t) = E_1(t)\cos\omega_0 t + E_2\cos(\Omega t)\sin(\omega_0 t)$$

Using prosthaphaeresis identities we obtain explicitly a decomposition of the modulated field in carrier and sideband components[1]

$$E(t) = E_0\cos\omega_0 t + \frac{E_2}{2}\left[\sin(\omega_0+\Omega)\,t + \sin(\omega_0-\Omega)\,t\right]$$

We consider now an impinging field of the form

$$E(t) = (E_0 + \delta E_1(t))\cos\omega_0 t + \delta E_2(t)\sin\omega_0 t$$

where E_0 is a carrier so that $\delta E_1(t)$ and $\delta E_2(t)$ can be regarded as phase and amplitude fluctuations. The reflected field will be

$$\begin{aligned} E^r(t) &= E\left(t - 2\frac{\delta z_M(t)}{c}\right) \\ &= \left[E_0 + \delta E_1\left(t - 2\frac{\delta z_M(t)}{c}\right)\right]\cos\omega_0\left(t - 2\frac{\delta z_M(t)}{c}\right) \\ &+ \delta E_2\left(t - 2\frac{\delta z_M(t)}{c}\right)\sin\omega_0\left(t - 2\frac{\delta z_M(t)}{c}\right) \end{aligned} \tag{2.21}$$

which after neglecting second order fluctuation becomes

$$E^r(t) \simeq \left[E_0 + \delta E_1(t)\right]\left[\cos\omega_0 t + \frac{2\omega_0}{c}\delta z_M(t)\sin\omega_0 t\right] + \delta E_2(t)\sin\omega_0 t$$

[1] In Section 2.5 we will give a quantum description of this effect introducing, after quantization, a specific formalism to describe the modulation in terms of coherent conversion of a photon of the carrier into a pair of correlated photons of frequencies $\omega_0 \pm \Omega$.

$$\simeq \quad [E_0 + \delta E_1(t)] \cos\omega_0 t + \left[\delta E_2(t) + \frac{2\omega_0}{c}\delta z_M(t)\right] \sin\omega_0 t$$

from which

$$\delta E_1^r(t) = \delta E_1(t) \tag{2.22a}$$

$$\delta E_2^r(t) = \delta E_2(t) + \frac{2\omega_0}{c}\delta z_M(t) \tag{2.22b}$$

Considering that the mirror oscillations are caused by the fluctuating part of the radiation pressure of the incident wave which is proportional to its the amplitude fluctuations, we find that

$$\delta z_M(t) \propto \delta P \propto \overline{\delta E^2} \propto E_0 \delta E_1(t)$$

from which we see that a correlation as been induced between phase and amplitude fluctuations of the reflected field. Such correlation will be described in terms of squeezing after switching to a quantum description of our fields.

Radiation pressure can apply to the mirror not only a force (2.16), but also a torque. In order to evaluate it we calculate the torque transferred to the mirror per unity of surface, using the center of the mirror as a pole

$$\vec{m}(x,y) = \begin{pmatrix} m_x \\ m_y \\ m_z \end{pmatrix}$$

$$\vec{m}(x,y) = \vec{r} \times \langle T_{ij}\hat{n}_j \rangle = -\begin{vmatrix} \hat{x} & \hat{y} & \hat{z} \\ x & y & z \\ 0 & 0 & \langle T_{33}\rangle \end{vmatrix} = \begin{pmatrix} -y\langle T_{33}\rangle \\ x\langle T_{33}\rangle \\ 0 \end{pmatrix}$$

Then, integrating $\vec{m}$ over the surface, we find $\vec{M}^{tot}$ acting on the mirror

$$\begin{pmatrix} M_x^{tot} \\ M_y^{tot} \\ M_z^{tot} \end{pmatrix} = \begin{pmatrix} \int y\langle T_{33}\rangle\, dxdy \\ \int -x\langle T_{33}\rangle\, dxdy \\ 0 \end{pmatrix}$$

In order to calculate T_{33}, all we need to know is the value of the electric and the magnetic field at the surface S. Considering a plane wave, where the electric and the magnetic fields don't depend on x, y, everything becomes trivial, especially for the total torque which is always zero for symmetry considerations.

More interesting effects arise when we consider HG modes: when calculating E^2, terms from different modes combine with one another and produce a non-

symmetric force distribution over the x, y surface. In Figure 2.4 the intensity profile for the superposition of different HG modes are shown. It can be seen that the combination of two modes which differs by one index gives a non symmetric force in the x, y plane and so a non-zero torque on the mirror. Assuming the mirror rotation caused by this non-zero torque to be small we model it as harmonic oscillations:

$$\delta\ddot{\theta}_x + \omega_x^2 \delta\theta_x = \frac{M_x^{tot}}{I} \tag{2.23}$$

$$\delta\ddot{\theta}_y + \omega_y^2 \delta\theta_y = \frac{M_y^{tot}}{I} \tag{2.24}$$

In the previous section we have discussed the mechanism through which a tilted mirror can transfer power for example from the fundamental mode and excite higher order modes. Here we have seen that, in turn, the presence of more than one mode can produce a torque (if the coupled modes differ by one index) which makes the mirror tilt.

Now we see that putting together these two effects we obtain a modulation effect that can be seen as a direct generalization of Eq. (2.22a) and (2.22b). Explicitly, an amplitude fluctuation in a given HG mode can be converted to a phase fluctuation in another one if $\Delta m = \pm 1$, $\Delta n = 0$ or $\Delta m = 0$ and $\Delta n = \pm 1$.

2.1.5 Circulating power in a cavity

An expression for the circulating power in a Fabry-Pérot cavity can be deduced from a simple classical model by considering plane waves. With reference to the Figure 2.1.5, where the incoming field is A, B is the intracavity field (taken at the first mirror) and where C is the outgoing field. We assume the mirrors to be characterized from a reflectivity r and a transmitivity t such that

$$r^2 + t^2 = 1$$

so we neglect losses[2] . With the convention[3]

$$A_{ref} = irA_{in} \qquad A_{tran} = tA_{in}$$

We have the following equations for A, B and C

[2] They will be described later from a quantum point of view.

[3] Other convention can be found in literature. The essential point is that the relation between input and output fields must be unitary. Phase factors can be reabsorbed by redefining the fields and play not a relevant role.

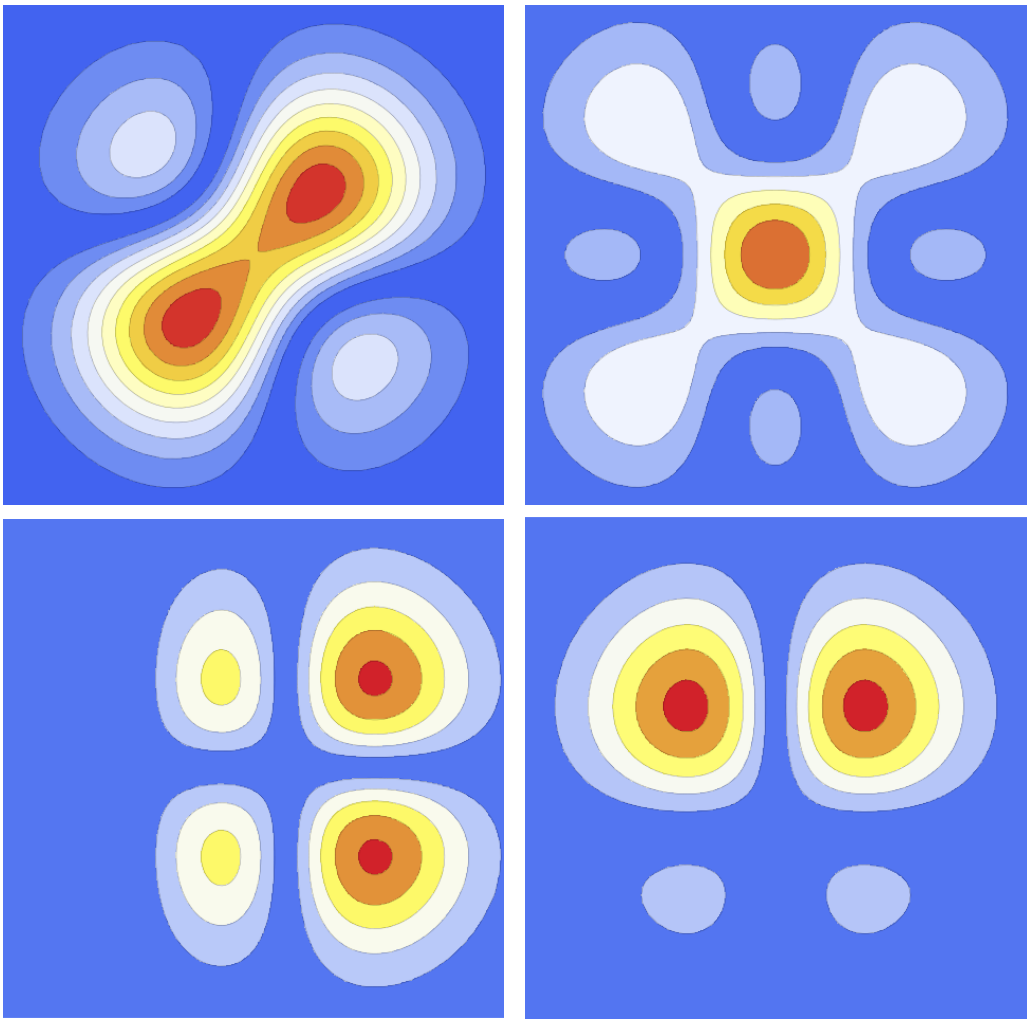

Figure 2.4: The intensity profiles of a superposition of modes are plotted in the first row for two modes which differ by more then one index (a linear combination of HG_{00}, HG_{11} on the left side, a linear combination of HG_{00} and HG_{22} on the right side). In the second row the same is done for modes which differ by exactly one index (a linear combination of HG_{11} and HG_{21} on the left side, a linear combination of HG_{11} and HG_{10} on the right side). In the first row the force is symmetric while in the second row it is not and it produce a torque which rotates the mirror.

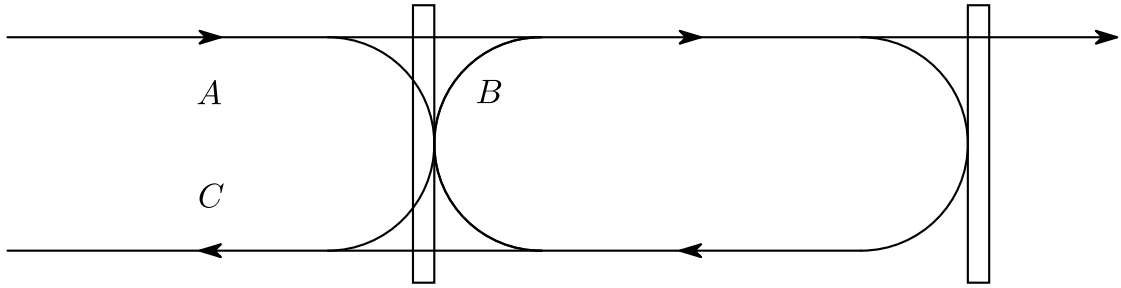

Scheme for the classical fields in a Fabry-Pérot cavity with just an incoming field.

$$B = t_1 A - r_1 r_2 e^{2ikL} B$$
$$C = i r_1 A + i r_2 t_1 e^{2ikL} B$$

From the first we find

$$B = \frac{t_1}{1 + r_1 r_2 e^{2ikL}} A \tag{2.25}$$

Noting that resonance occurs when $e^{2ikL} = -1$ we can re-express (2.25) as a function of the displacement x of the end mirror from the resonance position:

$$B = \frac{t_1}{1 - r_1 r_2 e^{2ikx}} A$$

The intracavity power is proportional to the square modulus of the field B, so we can write

$$P = \frac{t_1^2}{\left|1 - r_1 r_2 e^{2ikx}\right|^2} P_{in} = \frac{t_1^2}{\left(1 - r_1 r_2\right)^2 + 4 r_1 r_2 \sin^2(kx)} P_{in} \tag{2.26}$$

where $P_{in} = |A|^2$ is the input power. As we said maximum power is achieved at the resonance, when $x = 0$, and it is

$$P_{max} = \frac{t_1^2}{\left(1 - r_1 r_2\right)^2} P_{in}$$

The reflectivity and transmissivity coefficients of the mirror determine the field behavior in the cavity when the source is switched off. A parameter, called Finesse, is associated with each cavity and it is defined as

$$F = \frac{\pi\sqrt{r_1 r_2}}{1 - r_1 r_2}$$

From it we define the storage time of an optical cavity

$$\tau = \frac{2LF}{\pi c}$$

which is the time taken by a field initially present inside the cavity field to decay by a factor of $1/e$. It gives clearly the typical time scale needed by the cavity to adapt to an external fluctuation of the field.

2.1.6 Optical spring effect

The circulating power in the cavity is connected to the force exerted by radiation pressure on a mirror by

$$F_{rp} = \frac{\left(1 + r^2 - t^2\right) P}{c} = \frac{\left(2r^2 + a\right) P}{c}$$

with $r^2 + t^2 + a = 1$, where A is an absorption coefficient which we consider zero for our mirrors. Using Eq. (2.26) we find an expression for the radiation force as a function of the end mirror position (supposing that the first is fixed)

$$F_{rp}\left(x\right) = \frac{\left(2r_2^2\right)}{c} \frac{t^2 P_{in}}{\left(1 - r_1 r_2\right)^2 + 4 r_1 r_2 \sin^2\left(kx\right)}$$

As we saw, x is a displacement from the resonance condition. When $x \ll \lambda/(2\pi)$ we can approximate this expression as

$$F_{rp}\left(x\right) = \frac{\left(2r_2^2\right)}{c} \frac{t^2 P_{in}}{\left(1 - r_1 r_2\right)^2 + 4 r_1 r_2 \left(kx\right)^2}$$

We can see from Figure (2.5) that if the equilibrium position of a mirror is displaced from the resonance then the radiation force depends (for small displacements) linearly on its position. The force gradient creates a so-called "optical spring" effect on the mirror: if the cavity is longer than the resonant length the optical spring constant will be positive ad it will increase the total spring constant. Conversely if it is shorter the optical spring constant will be negative, reducing the total spring constant. The spring constant is given by

$$k_{opt} = -\frac{dF_{rp}\left(x\right)}{dx} = -\frac{d}{dx}\left[\frac{\left(2r_2^2\right)}{c} \frac{t^2 P_{in}}{\left(1 - r_1 r_2\right)^2 + 4 r_1 r_2 \left(kx\right)^2}\right] \tag{2.27}$$

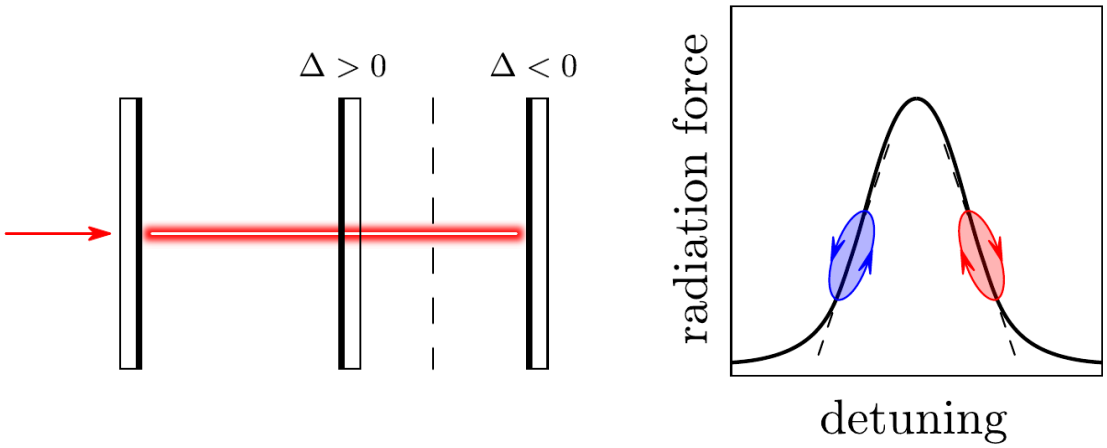

Figure 2.5: Optical spring effect induced in a detuned cavity.

and it is shown in Figure 2.6 together with the radiation pressure force as a function of the detuning.

As the optical restoring force and the mechanical one act in parallel on the mirror the total spring constant will be

$$k_{tot} = k_{mech} + k_{opt}$$

If k_{opt} is negative but its absolute value is larger than k_{mech}, the total spring constant k_{tot} will be negative and the system will become unstable.

This modification of the spring constant of the mirror is not the only effect of the radiation pressure on a detained mirror: in a high finesse cavity, the storage time of the cavity τ_{cav} causes the force to lag the displacement.

For example an oscillating mirror placed on the slope of the resonance, moving back and forth along the slope because of thermal fluctuations will undergo a force smaller than expected, when it moves toward the resonance, due to the time lag, while the force will remain larger when the mirror comes back. The radiation force extracts work from the mirror and cool it down by reducing thermal fluctuations. In general an anti-restoring force with a time lag is associated with damping while a restoring force with time lag is associated with anti-damping. In fact a mirror on the opposite side of the resonance will experience an amplification of the response to applied forces and thermal fluctuations. This optical damping cannot be neglected if

$$\tau_{cav} > T^2/\tau_{mech}$$

where τ_{cav} is the storage cavity time, T is the period of the mechanical oscillator and τ_{mech} its relaxation time, namely the time at which the amplitude of the

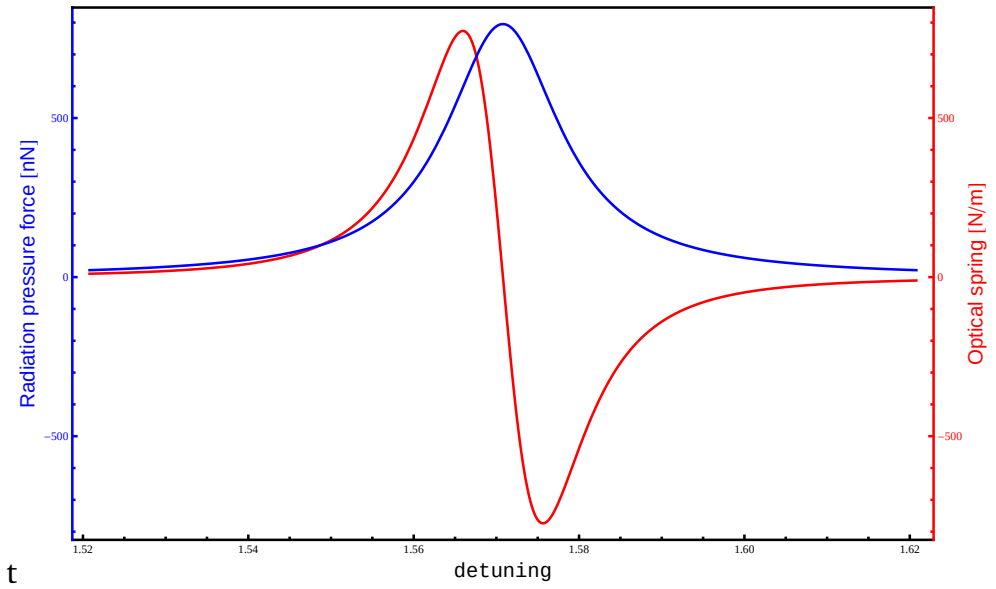

Figure 2.6: The spring constant and the radiation pressure force as functions of the detuning $2kx$ in a cavity with a Finesse of $\simeq 190$ and an input power of 1 Watt. (Note that with the parametrization used in the simulation the cavity is resonant when the detuning is $\frac{\pi}{2}$.)

oscillation is damped by a factor e^{-1} [14].

2.2 Quantization of the modes

So far we have given a classical description of some effects caused by the interaction of light with mechanical devices. However most of the relevant effects of such interaction affect quantum features of light and cannot be described without a quantum description of it. We will introduce a simplified model for the quantized electromagnetic field [15] that allows us to recover eventually the description in terms of HG modes.

We define the quantum electric field $\hat{E}$ as the quantum observable whose expectation values $\left\langle \psi \left| \hat{\mathrm{E}} \right| \psi \right\rangle$ correspond to the classical field $\vec{E}$ and we do the same for the other relevant electromagnetic field $\vec{D}$, $\vec{B}$, $\vec{H}$. We know they obey source free Maxwell equations (here in the presence of dielectric material)

$$\begin{aligned} \nabla \cdot B &= 0 \\ \nabla \cdot D &= 0 \\ \nabla \times E &= -\frac{\partial B}{\partial t} \\ \nabla \times H &= \frac{\partial D}{\partial t} \end{aligned}$$

It is easy to show that, because of their linearity, quantum electromagnetic operators obey Maxwell equations too. In other words from

$$\nabla \times E + \frac{\partial B}{\partial t} = 0 = 0$$

it follows

$$\nabla \times \left\langle \psi \left| \hat{\mathrm{E}} \right| \psi \right\rangle + \nabla \cdot \left\langle \psi \left| \frac{\partial \hat{\mathrm{B}}}{\partial \mathrm{t}} \right| \psi \right\rangle = 0 \Rightarrow \left\langle \psi \left| \nabla \times \hat{\mathrm{E}} + \frac{\partial \hat{\mathrm{B}}}{\partial \mathrm{t}} \right| \psi \right\rangle = 0$$

and

$$\left\langle \psi \left| \nabla \times \hat{\mathrm{E}} + \frac{\partial \hat{\mathrm{B}}}{\partial \mathrm{t}} \right| \psi \right\rangle = 0$$

The operator in the last equality has null expectation values for all $|\psi\rangle$, then also for its eigenvectors. Since expectation values of an operator on its eigen-

vectors correspond to their eigenvalues, they must be all zero and the operator itself must vanish.

We also assume a linear dependence between our fields, i.e $\vec{D} = \epsilon\vec{E}$, $\vec{B} = \mu\vec{H}$ that stands also for the correspondent quantum operators. We can give a description of our quantum fields in terms of vector potential as in classic electromagnetism. We define the quantum operator $\hat{A}$ associated with the vector potential as

$$\hat{E} = -\frac{\partial \hat{A}}{\partial t} \qquad \hat{B} = \nabla \times \hat{A}$$

with the Coulomb gauge condition

$$\nabla \cdot \epsilon\hat{A} = 0$$

We notice that with these definitions all Maxwell equations are automatically satisfied except for the last one that (assuming that μ and ϵ independent of space and time) becomes

$$\frac{1}{\mu}\nabla^2\hat{A} - \epsilon\frac{\partial^2\hat{A}}{\partial t^2} = 0 \tag{2.28}$$

Here we see that the vector potential operator obeys the wave equation like its associated classical field does. We also make the assumption that, in order to find the Hamiltonian, it suffices to replace the classical fields with their correspondent quantum operators in the expression for the classical energy of the electromagnetic field

$$\hat{H} = \frac{1}{2}\int \left(\hat{E}\cdot\hat{D} + \hat{B}\cdot\hat{H}\right) dV \tag{2.29}$$

which accounts for the total energy of the system and allows us to calculate the time evolution of the operators in the Heisenberg picture. We decided to use the vector potential to describe the field amplitudes at different points in space and time. Note that the displacement vector $\hat{D} = -\epsilon\frac{\partial\hat{A}}{\partial t}$ can be regarded as the momentum conjugate to the field $\hat{A}$ in a canonical quantization picture, so they must obey a canonical commutation relation

$$\left[\hat{D}(r,t), \hat{A}(r',t)\right] = i\hbar\delta(r-r') \tag{2.30}$$

In order to preserve causality in our theory, field amplitudes at the same time in different places should be independent and the correspondent observables $\hat{A}(r,t)$, $\hat{A}(r',t)$ should commute.

Our quantum operator $\hat{A}$ can be expanded in terms of classical functions A_k as

long as they form a complete set and are solutions for the wave equation. They can be complex but, since the wave equation is real, the complete set must then include also complex conjugate A_k^*. Since $\hat{A}$ is Hermitian we have

$$\hat{A}(r,t) = \sum_k \left(A_k(r,t)\,\hat{a}_k + A_k^*(r,t)\,\hat{a}_k^\dagger \right) \tag{2.31}$$

We see that operators $\hat{a}_k$ and $\hat{a}_k^\dagger$ account for the quantum properties of the field, while the temporal and spatial dependence are encoded in the classical waves (also referred to as modes of the field). We will show that, given two modes, it is possible to define a scalar product

$$(A_1, A_2) \equiv \frac{i\epsilon_o\epsilon}{\hbar} \int \left(A_1^* \cdot \frac{\partial A_2}{\partial t} - A_2 \cdot \frac{\partial A_1^*}{\partial t} \right) dV \tag{2.32}$$

which is non-positive definite but which is preserved by the time evolution and has the following properties: if we chose orthonormal modes, i.e $(A_k, A_{k'}) = \delta_{kk'}$ and $(A_k, A_{k'}^*) = 0$, we can write

$$\hat{a}_k = \left(A_k, \hat{A} \right) \qquad \hat{a}_k^\dagger = -\left(A_k^*, \hat{A} \right)$$

We can then use the scalar product we defined to work out the commutation relations for the mode operators

$$\begin{aligned}
\left[\hat{a}_k, \hat{a}_{k'}^\dagger \right] &= \left[\left(A_k, \hat{A} \right), -\left(A_k^*, \hat{A} \right) \right] \\
&= \frac{i}{\hbar^2} \int\int \left[A_k^* \cdot \hat{D} - \hat{A} \cdot D_k^*, A_{k'} \cdot \hat{D} - \hat{A} \cdot D_{k'} \right] dV\, dV' \\
&= \frac{i}{\hbar^2} \int A_k^* \cdot D_{k'} - A_{k'} \cdot D_k^* dV \\
&= (A_k, A_{k'}) = \delta_{kk'}
\end{aligned}$$

where we used the definition of scalar product, the fundamental commutator (2.30) and the orthonormality of the modes. In the same way we find that

$$\begin{aligned}
\left[\hat{a}_k, \hat{a}_{k'}^\dagger \right] &= \left[\left(A_k, \hat{A} \right), -\left(A_k^*, \hat{A} \right) \right] \\
&= \frac{i}{\hbar^2} \int\int \left[A_k^* \cdot \hat{D} - \hat{A} \cdot D_k^*, A_{k'} \cdot \hat{D} - \hat{A} \cdot D_{k'} \right] dV\, dV' \\
&= \frac{i}{\hbar^2} \int A_k^* \cdot D_{k'}^* - A_{k'}^* \cdot D_k^* dV
\end{aligned}$$

$$= \quad (A_k, A^*_{k'}) = 0$$

It's easy to see that positive frequency modes of the form

$$A(r,t) = \tilde{A}\,(r)\, e^{-i\omega t}$$

are solutions for the wave Equation (2.28) and so the Hamiltonian, if the modes are orthonormal with respect to (2.32), becomes

$$\hat{H} = \sum_k \hbar\omega \left(\hat{a}^\dagger_k \hat{a}_k + \frac{1}{2} \right) \tag{2.33}$$

This expression tells us that the electromagnetic field can be described as a sum of harmonic oscillators, one for each mode of the field, carrying an energy of $\hbar\omega$ times $\hat{a}^\dagger_k \hat{a}_k$ (analogous of the modulus squared of the quantum amplitude) plus $\frac{1}{2}$. The fact that mode operators associated with different modes commute tells us that $\hat{a}^\dagger_k \hat{a}_k$ can be regarded as creation and destruction operators for a Hilbert space and a quantum state of light will live in the space obtained as the tensor product of all these Hilbert spaces associated with different modes.

As for quantum harmonic oscillators we can introduce the quadrature operators $\hat{p}_k$ and $\hat{q}_k$, which are simply the momentum and the position of the k-th oscillator, usually defined as

$$\hat{p}_k = \frac{\hat{a}_k - \hat{a}^\dagger_k}{i\sqrt{2}} \quad \hat{q}_k \frac{\hat{a}_k + \hat{a}^\dagger_k}{\sqrt{2}}$$

whose commutation relations are

$$[\hat{p}_k, \hat{q}_{k'}] = i\delta_{kk'}$$

They are respectively proportional to the real and to the imaginary part of the complex amplitude $\hat{a}$

$$\hat{a} = \frac{1}{\sqrt{2}}(\hat{q} + i\hat{p}) \tag{2.34}$$

For a monochromatic wave, after fixing a phase-reference, they can be regarded as the in-phase and the out-of-phase components of the field amplitude. A rotation of an amount θ of these quadratures

$$\begin{aligned} \hat{q}'_k &= \hat{q}_k \cos\theta + \hat{p}_k \sin\theta \\ \hat{p}'_k &= -\hat{q}_k \sin\theta + \hat{p}_k \cos\theta \end{aligned}$$

is achievable by a "phase shifting" $\hat{a}_k \to e^{i\theta_k}\hat{a}_k$ which preserves the commutators and the form of the Hamiltonian, allowing us to change the phase reference of our mode as we prefer. We can define a general quadrature operator as

$$\hat{q}_\theta = \hat{q}\cos\theta + \hat{p}\sin\theta$$

2.3 Quantum states of light

In a quantized description of light in terms of mode superposition (2.31) the electromagnetic field is proportional to the mode amplitude $\hat{a}_k$ which fluctuates.

Quantization is responsible for the introduction of a quantum noise (ultimately connected with the uncertainty principle) which will be central in our discussion. We will present now some different representations of quantum light states paying special attention to their quantum noise features. It is possible to show (Pauli) that the condition of minimum uncertainty for a state results in its wave function to be Gaussian.

2.3.1 Fock states

Fock states, or number states, are defined as eigenstates of the Hamiltonian (2.33). In particular they are eigenstates of the number operator [16]

$$\hat{a}^\dagger\hat{a}\,|n\rangle = n\,|n\rangle$$

The vacuum state is defined by

$$\hat{a}\,|0\rangle = 0 \tag{2.35}$$

and the state vector for higher excited states can be created from it with a repeated application of the mode creation operators $\hat{a}_k^\dagger$. In fact

$$\hat{a}_k^\dagger\,|n_k\rangle = (n_k+1)^{\frac{1}{2}}\,|n_k+1\rangle$$

and thus

$$|n_k\rangle = \frac{\left(\hat{a}_k^\dagger\right)^{n_k}}{(n_k!)^{\frac{1}{2}}}\quad|0\rangle$$

while applying the destruction operator we have

$$\hat{a}_k\,|n_k\rangle = n_k^{\frac{1}{2}}\,|n_k-1\rangle$$

We are particularly interested in studying the vacuum state as we will show that other states of light we will present are created starting from it and will share its quantum noise features. We can easily work out the wave function $\psi(q)$ of the state $|0\rangle$ from its definition 2.35 and by using quadrature decomposition 2.34

$$\hat{a}\psi(q) = \frac{1}{\sqrt{2}}\left(q + \frac{\partial}{\partial q}\right)\psi(q) = 0$$

which is verified by

$$\psi(q) = \frac{1}{\pi^{\frac{1}{4}}}\exp\left(-\frac{q^2}{2}\right)$$

Similarly,using the in momentum representation we have

$$\psi(p) = \frac{1}{\pi^{\frac{1}{4}}}\exp\left(-\frac{p^2}{2}\right)$$

Such distributions centered in zero have a non-zero $\Delta^2 q$ and $\Delta^2 p$ in fact

$$\begin{aligned}
\Delta^2 q &= \left\langle\psi\left|(q-q_0)^2\right|\psi\right\rangle = \left\langle\psi\left|(q-q_0)^2\right|\psi\right\rangle = \int \frac{1}{\sqrt{\pi}} q^2 \exp\left(-q^2\right) dq = \frac{1}{2} \\
\Delta^2 p &= \left\langle\psi\left|(p-p_0)^2\right|\psi\right\rangle = \left\langle\psi\left|(p-p_0)^2\right|\psi\right\rangle = \int \frac{1}{\sqrt{\pi}} p^2 \exp\left(-p^2\right) dq = \frac{1}{2}
\end{aligned}$$

Here we see that even if we are in a zero-photon state, the are still quadrature fluctuations and thus the strength of the field fluctuates as well. However this fluctuation, which must exist because of Heisenberg's uncertainty principle, is the minimum possible. We have

$$\Delta q \Delta p = \frac{1}{2}$$

Quantum vacuum has much quantum noise as is unavoidable.

2.3.2 Coherent states

We introduce coherent states because they are are particularly suitable for a quantum description of laser light as their amplitude and phase are defined as precisely as possible[4]. As a matter of fact the product of their noises for every coherent state is the minimum allowed by Heisenberg's uncertainty principle. We start by defining a displacement operator

[4]It should be mentioned that the rigorous definition of a phase operator is problematic.

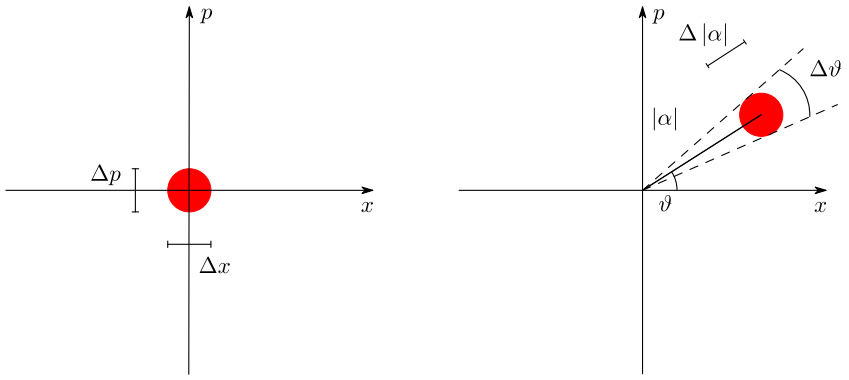

Figure 2.7: A coherent state in the optical phase space, obtained by means of a "displacement" of a vacuum state.

$$D(\alpha) = \exp\left(\alpha a^{\dagger} - \alpha^{*} a\right) \tag{2.36}$$

where α is a complex number which can be written as $|\alpha| e^{i\theta}$. The displacement operator has the following properties:

$$D^{\dagger}(\alpha) = D^{-1}(\alpha) = D(-\alpha) \quad D^{\dagger}(\alpha) a D(\alpha) = a + \alpha \tag{2.37}$$

The coherent state $|\alpha\rangle$ is created by applying to the vacuum state $|0\rangle$ the displacement operator

$$|\alpha\rangle = D(\alpha)|0\rangle = e^{\alpha a^{\dagger} - \alpha^{*} a}|0\rangle \tag{2.38}$$

This makes coherent state quantum noise similar to the vacuum state one: in particular it is the minimum possible allowed by Heisenberg's uncertainty principle.

We can represent the vacuum state as a "circle of error" centered in the origin of the x and the p axis and the coherent state $|\alpha\rangle$ as its translation by a vector with modulus $|\alpha|$ and phase θ. We will give a more precise definition of this error circle after introducing Wigner quasi-probability function. We know that it is a circle because the uncertainty area of the rotated quadrature

$$\Delta X_{\beta} \equiv \Delta\left(x \cos\beta + p \sin\beta\right)$$

does not depend on β. In Figure (2.7) it is natural to individuate two new quadratures one for the amplitude (in the direction parallel to α, X_{θ})and one for the phase (in the direction perpendicular to α, $X_{\theta+\pi/2}$). Identifying the mean

value of the field $\overline{E}$ with $|\alpha|$ we find an uncertainty relation between the new quadratures that reads

$$\Delta X_\theta = \Delta E, \quad \Delta X_{\theta+\pi/2} = \Delta\left(\overline{E}\theta\right) \tag{2.39}$$

and as we said before

$$\Delta X_\theta = \Delta X_{\theta+\pi/2} \tag{2.40}$$

Coherent states are also eigenvalues for the destruction operator $\hat{a}$

$$D^\dagger(\alpha)\, a\,|\alpha\rangle = D^\dagger(\alpha)\, aD(\alpha)\,|0\rangle = (a+\alpha)\,|0\rangle = \alpha\,|0\rangle \tag{2.41}$$

By multiplying both sides of the previous equation by $D(\alpha)$ we find

$$a\,|\alpha\rangle = \alpha\,|\alpha\rangle \tag{2.42}$$

From Heisenberg equation we deduce time evolution of $\hat{a}$ e $\hat{a}_t^\dagger$

$$\frac{d\hat{a}}{dt} = \frac{1}{i\hbar}\left[\hat{a}, \hat{H}\right] = \frac{1}{i\hbar}\hbar\omega\left[\hat{a}, \hat{a}^\dagger\hat{a}\right] = -i\omega\left[\hat{a}, \hat{a}^\dagger\right]\hat{a} = -i\omega\hat{a}$$

$$\frac{d\hat{a}^\dagger}{dt} = \frac{1}{i\hbar}\left[\hat{a}^\dagger, \hat{H}\right] = \frac{1}{i\hbar}\hbar\omega\left[\hat{a}^\dagger, \hat{a}^\dagger\hat{a}\right] = -i\omega\hat{a}^\dagger\left[\hat{a}^\dagger, \hat{a}\right] = i\omega\hat{a}^\dagger$$

so we have

$$\begin{aligned} \hat{a}_t &= e^{-i\omega t}\hat{a}_0 \\ \hat{a}_t^\dagger &= e^{i\omega t}\hat{a}_0^\dagger \end{aligned} \tag{2.43}$$

From that we can deduce time evolution of quadrature operators $\hat{x}$ and $\hat{p}$

$$\begin{aligned} \begin{pmatrix} \hat{x}_t \\ \hat{p}_t \end{pmatrix} &= \frac{1}{\sqrt{2}}\begin{pmatrix} 1 & 1 \\ -i & i \end{pmatrix}\begin{pmatrix} \hat{a}_t \\ \hat{a}_t^\dagger \end{pmatrix} \\ &= \frac{1}{\sqrt{2}}\begin{pmatrix} 1 & 1 \\ -i & i \end{pmatrix}\begin{pmatrix} e^{-i\omega t} & 0 \\ 0 & e^{i\omega t} \end{pmatrix}\begin{pmatrix} \hat{a}_0 \\ \hat{a}_0^\dagger \end{pmatrix} \\ &= \frac{1}{2}\begin{pmatrix} 1 & 1 \\ -i & i \end{pmatrix}\begin{pmatrix} e^{-i\omega t} & 0 \\ 0 & e^{i\omega t} \end{pmatrix}\begin{pmatrix} 1 & i \\ 1 & -i \end{pmatrix}\begin{pmatrix} \hat{x}_0 \\ \hat{p}_0 \end{pmatrix} \\ &= \begin{pmatrix} \cos\omega t & \sin\omega t \\ -\sin\omega t & \cos\omega t \end{pmatrix}\begin{pmatrix} \hat{x}_0 \\ \hat{p}_0 \end{pmatrix} \end{aligned}$$

and for their expectation values we have

$$\begin{aligned}
\begin{pmatrix} \langle \alpha | \hat{x}_t | \alpha \rangle \\ \langle \alpha | \hat{p}_t | \alpha \rangle \end{pmatrix} &= \left\langle \alpha \middle| \begin{pmatrix} \hat{x}_t \\ \hat{p}_t \end{pmatrix} \middle| \alpha \right\rangle \\
&= \frac{1}{\sqrt{2}} \begin{pmatrix} 1 & 1 \\ -i & i \end{pmatrix} \left\langle \alpha \middle| \begin{pmatrix} \hat{a}_t \\ \hat{a}_t^\dagger \end{pmatrix} \middle| \alpha \right\rangle \\
&= \frac{1}{\sqrt{2}} \begin{pmatrix} 1 & 1 \\ -i & i \end{pmatrix} \begin{pmatrix} \alpha e^{-i\omega t} \\ \alpha^* e^{i\omega t} \end{pmatrix} \\
&= \frac{1}{\sqrt{2}} \begin{pmatrix} \alpha e^{-i\omega t} + \alpha^* e^{i\omega t} \\ -i\alpha e^{-i\omega t} + i\alpha^* e^{i\omega t} \end{pmatrix}
\end{aligned}$$

We see that a coherent state $|\alpha\rangle$ represented in the x, p plane evolves in time rotating. For the time dependence of the variance we have

$$\left\langle \Delta \hat{p}^2 \right\rangle = \left\langle \hat{p}^2 \right\rangle - \left\langle \hat{p} \right\rangle^2 = \frac{1}{2} \tag{2.44}$$

$$\left\langle \Delta \hat{x}^2 \right\rangle = \left\langle \hat{x}^2 \right\rangle - \left\langle \hat{x} \right\rangle^2 = \frac{1}{2} \tag{2.45}$$

Since the variance is constant in time this means that a coherent state remains coherent during time evolution.

2.3.3 Squeezed states

Even though the condition of minimum uncertainty for a state implies its wave function to be a Gaussian as it happen for coherent states, quadrature uncertainties Δq can be different from Δp as long as their product is $\frac{1}{2}$. It is clear that a reduction of the noise in a quadrature will cause an enhancing of the noise in the other quadrature. This asymmetry of the quadrature uncertainty should result in a squeezing of the error circle we used to represent noise of a coherent state. Note that usually a squeezed state is defined as a state where fluctuations of a quadrature operator are lower than in coherent states and it does not necessarily mean that the uncertainty is the minimum possible but if that is the case we know that its wave function is a Gaussian.

Let us define a unitary squeezing operator for a single mode with squeezing parameter ε

$$S(\varepsilon) = \exp\left(\frac{1}{2} \varepsilon^* \hat{a}^2 - \frac{1}{2} \varepsilon \hat{a}^{\dagger 2} \right) \tag{2.46}$$

We obtain a squeezed state $|\alpha, \varepsilon\rangle$ by applying the squeezing operator to the vac-

uum state and later displacing it by means of the displacement operator (2.36)

$$|\alpha, \varepsilon\rangle = D(\alpha) S(\varepsilon) |0\rangle \tag{2.47}$$

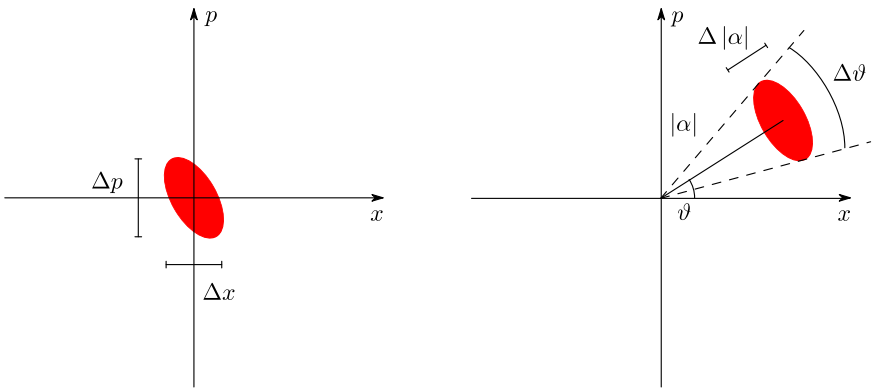

Figure 2.8: A squeezed state in the optical phase space obtained by "squeezing" and then displacing a vacuum state.

We can have different kinds of squeezed states depending on which quadrature noise we want to reduce. This corresponds to a different orientation of the axes in the error ellipse. In the more general case the quadrature with most reduced fluctuation is not q or p but a generic one q_θ (where the ellipse axes do not coincide with q and p). In this case the squeezing parameter ε is a complex number of the form

$$\varepsilon = r_s e^{2i\theta_s}$$

with r_s accounting for the degree of squeezing and θ_s for its direction. The expression for the variance of a generic quadrature is

$$\Delta q_\theta^2 = \langle \alpha, \varepsilon | q_\theta^2 | \alpha, \varepsilon \rangle - \langle \alpha, \varepsilon | q_\theta | \alpha, \varepsilon \rangle^2 = \cosh 2r_s - \sinh 2r_s \cos 2(\theta - \theta_s) \tag{2.48}$$

which gives the "noise" in each quadrature, located by the angle θ . It can be calculated on the squeezed vacuum $|0, \varepsilon\rangle$, since the displacement operator $D(\alpha)$ acts as a simple translation and doesn't change its value, knowing that

$$q_\beta = x \cos\beta + p \sin\beta = \frac{a + a^\dagger}{\sqrt{2}} \cos\beta + \frac{a - a^\dagger}{i\sqrt{2}} \sin\beta$$

from which

$$q_\beta^2 = \frac{1}{2}\left[aae^{-2i\beta} + a^\dagger a^\dagger e^{2i\beta} + aa^\dagger + a^\dagger a\right]$$

and

$$\begin{aligned} S^\dagger(\varepsilon)\, aS(\varepsilon) &= a\cosh r_s - a^\dagger e^{2i\theta_s}\sinh r_s \\ S^\dagger(\varepsilon)\, a^\dagger S(\varepsilon) &= a^\dagger\cosh r_s - ae^{-2i\theta_s}\sinh r_s \end{aligned}$$

In Figure 2.9 a polar plot of Eq. 2.48 is shown for $r_s = 0.7$ and $\theta_s = \frac{\pi}{4}$ and compared with the one of a coherent state $(r_s = 0)$.

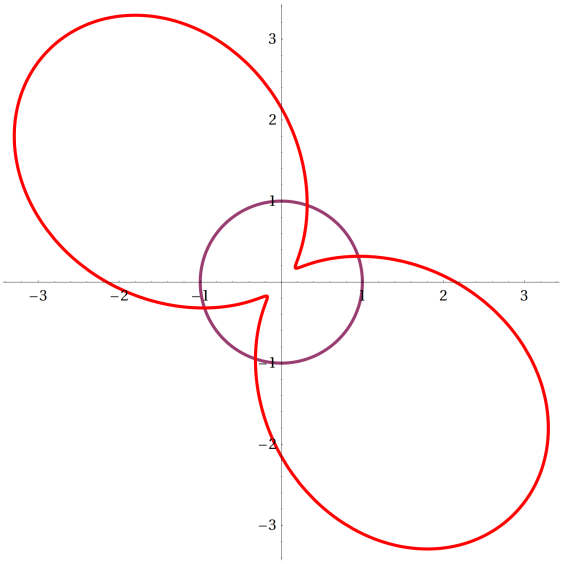

Figure 2.9: Polar plot for the quadrature variance of a squeezed state with $r_s = 0.7$, $\theta_s = \frac{\pi}{4}$ (in red) compared with the one of a coherent state $(r_s = 0)$.

2.4 The Wigner function

An extremely effective tool to describe light states and their quantum noise feature is the Wigner function[17]. It will also help to give a more formal definition of that circle/ellipse error we associated to quantum noise of our state. A quantum description for the motion of a particle which, for the sake of simplicity, will be thought to be one-dimensional, can be described by means of a position

operator $\hat{q}$ and a momentum operator $\hat{p}$ but it is clearly impossible to define a genuine distribution in the phase space as the operators $\hat{q}$ and $\hat{p}$ do not commute. However it is possible to define functions, as the Wigner function, also known as quasi-probability distributions, which can be used to derive separately the probability distributions of both the position and the momentum, or more generally of any linear combination of the two.

The fact that these function do not constitute a proper probability distributions can be confirmed observing that it is not always positive (especially for those state with strong quantum features as Fock states). The Wigner function of a state described by the density operator $\hat{\rho}$ is given by

$$W(p,q,t) = \frac{1}{2\pi}\int_{-\infty}^{\infty} e^{-ipx}\left\langle q+\frac{x}{2}\right|\hat{\rho}(t)\left|q-\frac{x}{2}\right\rangle dx \tag{2.49}$$

Integration with respect to the variable p yields the probability distribution for the position while integration with respect to the variable q yields the probability distribution for the momentum. Let's check the first case:

$$\int_{-\infty}^{\infty} W(p,q,t)\,dp = \frac{1}{2\pi}\int_{-\infty}^{\infty}\left\langle q+\frac{x}{2}\right|\hat{\rho}(t)\left|q-\frac{x}{2}\right\rangle dx\int_{-\infty}^{\infty} e^{-ipx}dp \tag{2.50}$$

Using the relation

$$\frac{1}{2\pi}\int_{-\infty}^{\infty} e^{-ipx}dp = \delta(x) \tag{2.51}$$

we get

$$\int_{-\infty}^{\infty} W(p,q,t)\,dp = \int_{-\infty}^{\infty} dx\left\langle q+\frac{x}{2}\right|\hat{\rho}(t)\left|q-\frac{x}{2}\right\rangle \delta(x) \tag{2.52}$$

and therefore

$$\int_{-\infty}^{\infty} W(p,q,t)\,dp = \langle q|\,\hat{\rho}(t)\,|q\rangle \equiv W(q,t) \tag{2.53}$$

We have thus shown that by integrating the Wigner function with respect to the variable p we get the probability distribution of the position $W(q,t)$.

Figure 2.10 shows the representation in the quadrature space of the Wigner function for both coherent and squeezed states of radiation. A two-dimensional representation which gives intuition of the properties of these states is obtained by cutting the graphic of the Wigner function with an horizontal plane at a half of the maximal height. We obtain circles for coherent states and ellipses for squeezed states. We stress the fact that, although these representation are useful to picture intuitively the noise properties of these states, only the marginal dis-

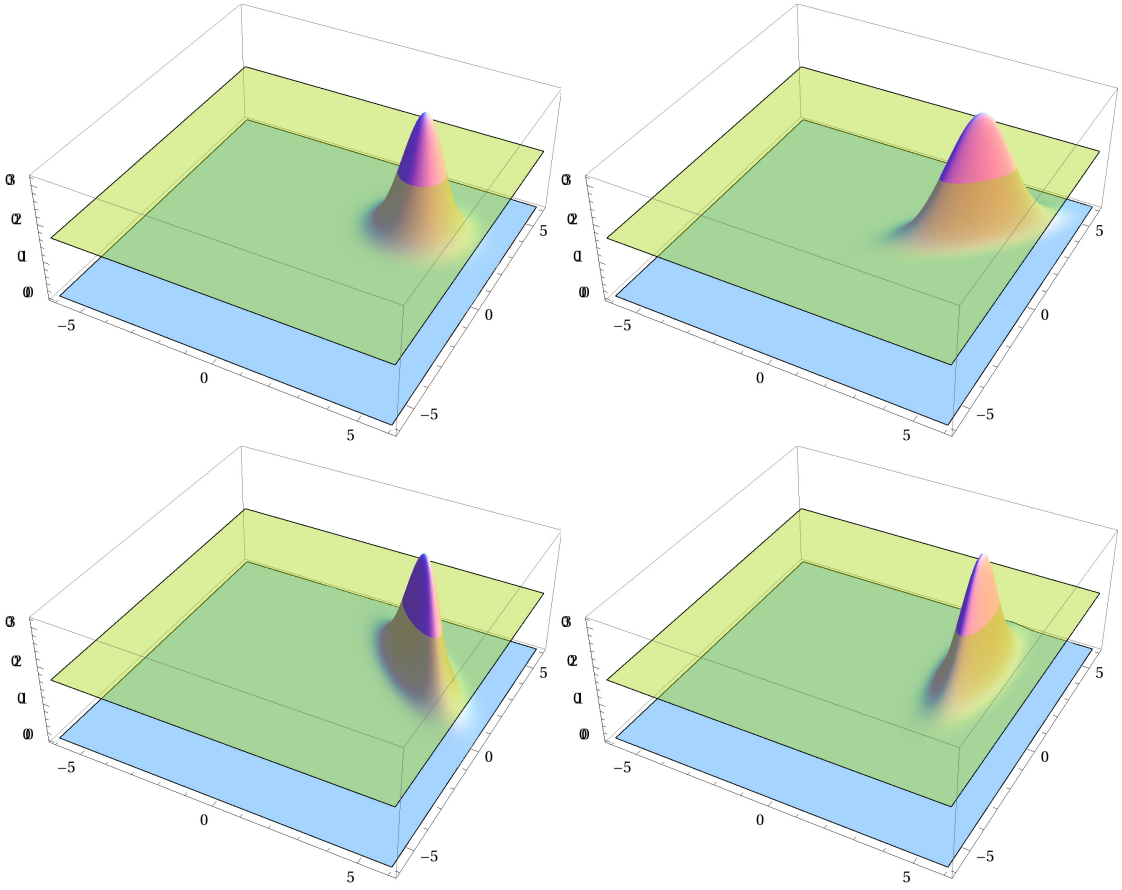

Figure 2.10: Wigner function of a coherent state (top left) and of squeezed states with different squeezing angles.

tributions obtained by integration with respect to one of the two variables can be interpreted as a probability distributions.

The evolution of the Wigner function in the case of a quadratic Hamiltonian like the ones we are interested in is given by

$$\begin{aligned}\frac{\partial W}{\partial t}(p,q,t) &= \omega\left[-p\frac{\partial W(q,p,t)}{\partial q}+q\frac{\partial W(q,p,t)}{\partial p}\right]\\ &= \left[-\frac{\partial H}{\partial p}\frac{\partial W(q,p,t)}{\partial q}+\frac{\partial H}{\partial q}\frac{\partial W(q,p,t)}{\partial p}\right]\\ &= -\left\{W(p,q,t),H\right\}_{PB}\end{aligned} \tag{2.54}$$

where $\{\}_{PB}$ are the Poisson brackets. Hence $W(p,q,t)$ evolves according to the classical Liouville equation. The solution is obtained by observing that we have

$$\begin{aligned}\frac{d}{dt}W(q_{cl}(t),p_{cl}(t),t) &= \frac{\partial W}{\partial t}-\frac{\partial W}{\partial q}\dot{q}_{cl}-\frac{\partial W}{\partial p}\dot{p}_{cl}\\ &= \frac{\partial W}{\partial t}-\frac{\partial W}{\partial q}\frac{\partial H}{\partial p}+\frac{\partial W}{\partial p}\frac{\partial H}{\partial q}\\ &= \frac{\partial W}{\partial t}+\left\{W,H\right\}_{PB}=0\end{aligned}$$

where the last equality follows from equation (2.54). Therefore the total derivative of $W(q,p,t)$ evaluated along the classical trajectory vanishes, i.e. the Wigner function is "dragged" by the classical evolution in the phase space. Thus we have

$$W(q_{cl}(t+\tau),p_{cl}(t+\tau),t'+\tau)=W(q_{cl}(t),p_{cl}(t),t') \tag{2.55}$$

for an arbitrary trajectory q_{cl}, p_{cl} in the phase space and for arbitrary t, t', τ. In the particular case of a coherent state the Wigner function is

$$W_\alpha(q,p,t)=\frac{1}{\pi}\exp\left[-\left(q-\overline{q}(t)\right)^2-\left(p-\overline{p}(t)\right)^2\right]$$

where $\bar{q}\left(0\right)=\sqrt{2}\mathrm{Re}\alpha\left(0\right)$ and $\bar{p}\left(0\right)=\sqrt{2}\mathrm{Im}\alpha\left(0\right)$. We know from what was previously observed that the evolution satisfies Eq. (2.55), and therefore

$$W_\alpha(q,p,t)=\frac{1}{\pi}\exp\left[-\left(q-q_{cl}(t)\right)^2-\left(p-p_{cl}(t)\right)^2\right]$$

For a coherent state what matters is just the position of the mean value of the Gaussian, as it is invariant under rotations around its mean value. For a squeezed state we loose this rotational invariance, and we can ask ourselves how does the

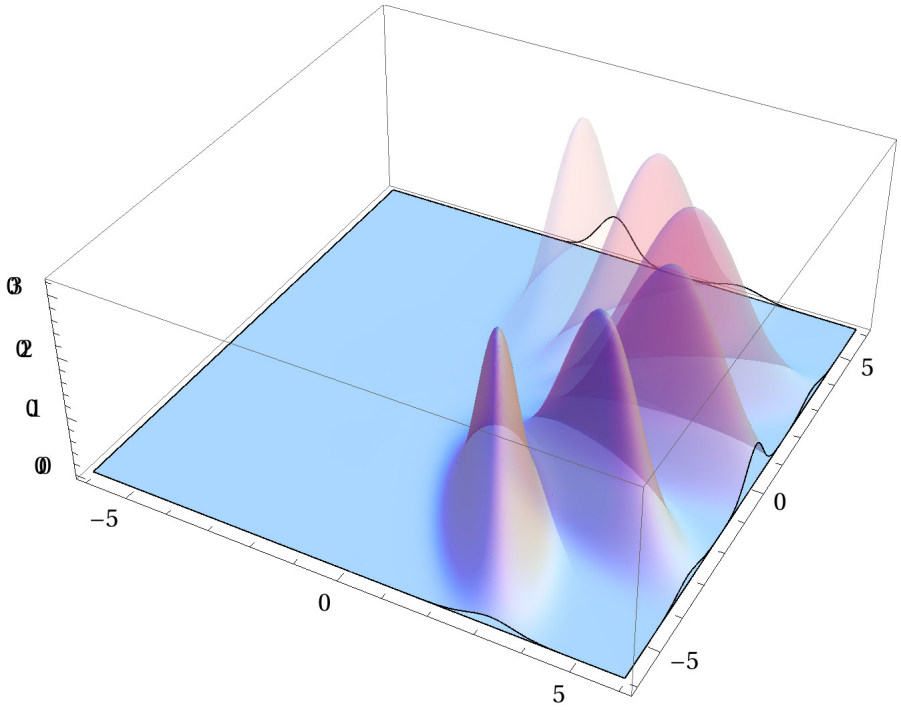

Figure 2.11: The time evolution in the phase space of the Wigner function for a squeezed state.

Gaussian change with respect to its mean value as time passes. The answer is readily obtained by observing that the evolution determined by Liouville's equation is equivalent to a rigid rotation of the whole phase space. Indeed if we set $t' = 0$ and $t = -\tau$ in Eq. (2.55) we get

$$W(q_{cl}(0), p_{cl}(0), \tau) = W(q_{cl}(-\tau), p_{cl}(-\tau), 0) \tag{2.56}$$

which gives

$$W(q, p, t) = W\left(q_0 \cos\omega t - p_0 \sin\omega t, q_0 \sin\omega t + p_0 \cos\omega t, 0\right)$$

Therefore the outline of the Gaussian (and hence the error ellipsis) is rotated. An example of temporal evolution, for a state with phase squeezing, is represented in Figure 2.11.

2.5 Quantum description of a laser beam and two-photons formalism

As we said, coherent states are the light states best suited to describe a laser beam. A coherent state $|\alpha\rangle$ characterized by the complex parameter α corresponds to a classical wave with amplitude $|\alpha|$ and phases $\arg\alpha$. We describe it as a classical carrier rotating with a frequency ω_o, surrounded by a continuum of small quantum fluctuations.

The positive frequency part, neglecting the contribution of spatial dependence and polarization (appropriately normalized to get the right dimension) is

$$E^{+}(t) = \sqrt{\frac{2\pi\hbar\omega}{Ac}}\alpha e^{-i\omega_o t} + \int_0^\infty \sqrt{\frac{2\pi\hbar\omega}{Ac}}\hat{a}_\omega e^{-i\omega t}\frac{d\omega}{2\pi} \tag{2.57}$$

where A is the effective cross sectional area of the beam and $\hat{a}_\omega$, $\hat{a}^\dagger_\omega$ are the annihilation and creation operators of each mode, whose commutation relations are

$$[\hat{a}_\omega, \hat{a}_{\omega'}] = 0 \qquad \left[\hat{a}_\omega, \hat{a}^\dagger_{\omega'}\right] = 2\pi\delta(\omega - \omega')$$

To understand these fluctuation as sidebands, separated from the carrier frequency ω_o by a frequency Ω (usually much smaller than ω_o) we define

$$\hat{a}_+ \equiv \hat{a}_{\omega_0+\Omega} \qquad \hat{a}_- \equiv \hat{a}_{\omega_0-\Omega}$$

and the relative commutation relations are

$$\left[\hat{a}_+, \hat{a}^\dagger_{+'}\right] = 2\pi\delta(\Omega - \Omega') \qquad \left[\hat{a}_-, \hat{a}^\dagger_{-'}\right] = 2\pi\delta(\Omega - \Omega') \tag{2.58}$$

Therefore, after the change of variables $\omega = \omega_o + \Omega$ and the approximation $\omega_0 \pm \Omega \simeq \omega_0$ inside the square root, since $\Omega \ll \omega_0$ Eq. 2.57 becomes

$$\hat{E}^{+}(t) = \sqrt{\frac{2\pi\hbar\omega}{Ac}}e^{-i\omega_o t}\left[\alpha + \int_0^\infty \hat{a}_+ e^{-i\Omega t}\frac{d\Omega}{2\pi} + \int_{-\omega_o}^0 \hat{a}_+ e^{-i\Omega t}\frac{d\Omega}{2\pi}\right]$$

Then a change of variables in the second integral gives

$$\begin{aligned}\hat{E}^{+}(t) &= \sqrt{\frac{2\pi\hbar\omega}{Ac}}e^{-i\omega_o t}\left[\alpha + \int_0^\infty \hat{a}_+ e^{-i\Omega t}\frac{d\Omega}{2\pi} - \int_{\omega_o}^0 \hat{a}_- e^{+i\Omega t}\frac{d\Omega}{2\pi}\right] \\ &= \sqrt{\frac{2\pi\hbar\omega}{Ac}}e^{-i\omega_o t}\left[\alpha + \int_0^\infty \hat{a}_+ e^{-i\Omega t}\frac{d\Omega}{2\pi} + \int_0^{\omega_o} \hat{a}_- e^{+i\Omega t}\frac{d\Omega}{2\pi}\right]\end{aligned}$$

and extending, for ease of notation, the last integral to infinity, we have

$$\hat{E}^{+}(t) = \sqrt{\frac{2\pi\hbar\omega}{Ac}} e^{-i\omega_o t} \left[\alpha + \int_0^{\infty} \hat{a}_{+} e^{-i\Omega t} + \hat{a}_{-} e^{+i\Omega t} \frac{d\Omega}{2\pi} \right]$$

and

$$\hat{E}^{-}(t) = \left(\hat{E}^{+}(t)\right)^{\dagger} = \sqrt{\frac{2\pi\hbar\omega}{Ac}} e^{i\omega_o t} \left[\alpha^{*} + \int_0^{\infty} \hat{a}_{+}^{\dagger} e^{i\Omega t} \frac{d\Omega}{2\pi} + \hat{a}_{-}^{\dagger} e^{-i\Omega t} \frac{d\Omega}{2\pi} \right]$$

For our purpose it will be convenient to regard the field not in terms of single-photon modes whose annihilation and creation operators are $\hat{a}$ and $\hat{a}^{\dagger}$, but in terms of correlated two-photon modes. As we will see, this provides a more effective way to describe correlations between fluctuations due to the interaction of the field with optical elements like movable mirror, by means of radiation pressure. It also allows us to understand this fluctuations in terms of phase and amplitude quadratures uncertainty. The annihilation and creation operators of these two-photon modes are defined as

$$\hat{a}_1 = \frac{\hat{a}_{+} + \hat{a}_{-}^{\dagger}}{\sqrt{2}} \quad \hat{a}_2 = \frac{\hat{a}_{+} - \hat{a}_{-}^{\dagger}}{\sqrt{2}i} \tag{2.59}$$

with

$$\left[\hat{a}_1, \hat{a}_{2'}^{\dagger}\right] = -\left[\hat{a}_2, \hat{a}_{1'}^{\dagger}\right] = i2\pi\delta(\Omega - \Omega')$$

$$[\hat{a}_1, \hat{a}_{1'}] = \left[\hat{a}_1, \hat{a}_{1'}^{\dagger}\right] = \left[\hat{a}_1^{\dagger}, \hat{a}_{1'}^{\dagger}\right] = [\hat{a}_1, \hat{a}_{2'}] = \left[\hat{a}_1^{\dagger}, \hat{a}_{2'}^{\dagger}\right] = 0$$

where we neglect quantities of the order Ω/ω_0. We also define

$$D_{1,cl} = \frac{\alpha + \alpha^{*}}{\sqrt{2}} \qquad D_{2,cl} = \frac{\alpha - \alpha^{*}}{i\sqrt{2}}$$

Now we can express $\hat{E} = \hat{E}^{+} + \hat{E}^{-}$ in terms of these two-photon operators

$$\hat{E} = \sqrt{\frac{4\pi\hbar\omega_0}{Ac}} \Bigg[\cos(\omega_o t) \left(\sqrt{2} D_{1,cl} + \int \left(\hat{a}_1 e^{-i\Omega t} + \hat{a}_1^{\dagger} e^{+i\Omega t} \right) \frac{d\Omega}{2\pi} \right) + \sin(\omega_o t) \left(\sqrt{2} D_{2,cl} + \int \left(\hat{a}_2 e^{-i\Omega t} + \hat{a}_2^{\dagger} e^{+i\Omega t} \right) \frac{d\Omega}{2\pi} \right) \Bigg]$$

By defining

$$E_{cl} = \sqrt{\frac{8\pi\hbar\omega_0}{Ac}} \begin{pmatrix} D_{1,cl} \\ D_{2,cl} \end{pmatrix}$$
$$\hat{E}_{1,2}(t) = \sqrt{\frac{4\pi\hbar\omega_0}{Ac}} \int \left(\hat{a}_{1,2} e^{-i\Omega t} + \hat{a}_{1,2}^{\dagger} e^{+i\Omega t} \right) \frac{d\Omega}{2\pi} \tag{2.60}$$

we get the interpretation in term of sine and cosine quadrature of our field

$$\hat{E} = \left(E_{1,cl} + \hat{E}_1(t) \right) \cos(\omega_o t) + \left(E_{2,cl} + \hat{E}_2(t) \right) \sin(\omega_o t) \tag{2.61}$$

Note that if we assume α to be real we have $E_{2,cl} = 0$ and Eq. (2.61) becomes

$$\hat{E} = \left(E_{1,cl} + \hat{E}_1(t) \right) \cos(\omega_o t) + \hat{E}_2(t) \sin(\omega_o t) \tag{2.62}$$

and we can now understand $\hat{E}_1(t)$ and $\hat{E}_2(t)$ as amplitude and phase modulation of our field.

We can define a two-mode squeezed state as

$$|\alpha_+, \alpha_-\rangle = D_+(\alpha_+) D_-(\alpha_-) S(\eta) |0\rangle \tag{2.63}$$

where the displacement operators $D_{\pm}(\alpha)$ are

$$D_{\pm}(\alpha) = \exp\left(\alpha a_{\pm}^{\dagger} - \alpha^* a_{\pm} \right)$$

and the two-mode squeezing operator is

$$S(\eta) = \exp\left(\eta^* \hat{a}_+ \hat{a}_- - \eta \hat{a}_+^{\dagger} \hat{a}_-^{\dagger} \right) \tag{2.64}$$

with $\eta = re^{2i\phi}$. When applied to $a_{\pm}$ it gives

$$S(r,\phi)\, \hat{a}_{\pm} S^{\dagger}(r,\phi) = \hat{a}_{\pm} \cosh r + \hat{a}_{\mp}^{\dagger} e^{2i\phi} \sinh r \tag{2.65}$$

From this and from Eq. 2.59 which defines $\hat{a}_1$ e $\hat{a}_2$ (the operators that quantize the amplitudes of the electric field quadratures) we deduce the effect of $S(r,\phi)$ on $\hat{a}_1$and $\hat{a}_2$

$$\hat{b}_1 \equiv S(r,\phi)\, \hat{a}_1 S^{\dagger}(r,\phi) = \hat{a}_1 (\cosh r + \sinh r \cos 2\phi) + \hat{a}_2 \sinh r \sin 2\phi \tag{2.66}$$
$$\hat{b}_2 \equiv S(r,\phi)\, \hat{a}_2 S^{\dagger}(r,\phi) = \hat{a}_2 (\cosh r - \sinh r \cos 2\phi) + \hat{a}_1 \sinh r \sin 2\phi \tag{2.67}$$

that is

$$\begin{pmatrix} \hat{b}_1 \\ \hat{b}_2 \end{pmatrix} = \begin{pmatrix} \cosh r + \sinh r \cos 2\phi & \sinh r \sin 2\phi \\ \sinh r \sin 2\phi & \cosh r - \sinh r \cos 2\phi \end{pmatrix} \begin{pmatrix} \hat{a}_1 \\ \hat{a}_2 \end{pmatrix} \tag{2.68}$$

It will be useful to study the effects of it when combined with a rotation of the quadrature

$$\hat{b}_1 \equiv R(\theta)\,\hat{a}_1 R^{\dagger}(\theta) = \hat{a}_1 \cos\theta - \hat{a}_2 \sin\theta \tag{2.69}$$

$$\hat{b}_2 \equiv R(\theta)\,\hat{a}_2 R^{\dagger}(\theta) = \hat{a}_1 \sin\theta + \hat{a}_2 \cos\theta \tag{2.70}$$

$$\begin{pmatrix} \hat{b}_1 \\ \hat{b}_2 \end{pmatrix} = \begin{pmatrix} \cos\theta & -\sin\theta \\ \sin\theta & \cos\theta \end{pmatrix} \begin{pmatrix} \hat{a}_1 \\ \hat{a}_2 \end{pmatrix} \tag{2.71}$$

Applying both $R(\theta)$ and $S(r,\phi)$ we have

$$\hat{b}_i \equiv S(r,\phi)\,R(\theta)\,\hat{a}_i R^{\dagger}(\theta)\,S^{\dagger}(r,\phi) \tag{2.72}$$

that corresponds to a multiplication in sequence of the matrices (2.68) and (2.71). For a particular choice of the squeezing parameters

$$\theta = \arctan\left(\frac{K}{2}\right) \qquad \phi = \frac{1}{2}\text{arccot}\left(\frac{K}{2}\right) \qquad r = \text{arcsinh}\left(\frac{K}{2}\right)$$

the matrix representing the transformation (2.72) assumes the simple form

$$\begin{pmatrix} b_1 \\ b_2 \end{pmatrix} = \begin{pmatrix} 1 & 0 \\ -K & 1 \end{pmatrix} \begin{pmatrix} a_1 \\ a_2 \end{pmatrix} \tag{2.73}$$

Ponderomotive squeezed states will turn out to be of this form consistently with the fact that they are two-mode squeezed states.

2.6 Hamiltonian description of opto-mechanical systems

Here we present the Hamiltonian which describes the opto-mecanical system of a cavity with a movable end mirror. Then we use it to deduce the relations which connect the outgoing fields to the incoming ones. We won't use directly this approach in our simulation but we will present it anyway as it allows to deduce many rules we are going to use and enlightens some important details and issues about opto-mechanical coupling.

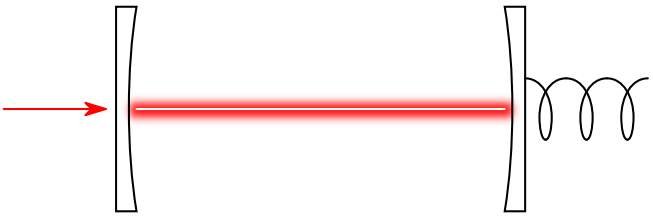

Figure 2.12: Cavity with movable end mirror.

2.6.1 The Hamiltonian of a driven optical cavity with a movable end mirror

In order to give an Hamiltonian description of the dynamics of an optical cavity it is necessary to take into account the coupling of its excited modes with the external vacuum field, containing an infinite number of degree of freedom [18]. Such weak interaction is provided, in our case, by a partially transmitting mirror. Therefore, the total Hamiltonian will be composed of the Hamiltonian of the system H_S (the cavity), the one of the reservoir H_R (the external field) and a third part describing their weak interaction V

$$H_{TOT} = H_S + H_R + V$$

Let us start from the Hamiltonian of the cavity H_S, that reads

$$H_s = \hbar\omega_m \hat{B}^\dagger \hat{B} - F\hat{x} + \hbar\left(\omega_0 + \Delta\right)\hat{A}^\dagger\hat{A} - \hbar\frac{\omega_0}{L}\hat{x}\hat{A}^\dagger\hat{A} \tag{2.74}$$

The first term refers to the movable end mirror that is treated as an harmonic oscillator, with mechanical resonant frequency ω_m, $\hat{B}^\dagger$and $\hat{B}$ creation and annihilation operators, and $\hat{x}$ position operator. In the second term, F is an external driving force acting on the end mirror. Given the pumping frequency ω_0, we assumed that the only intracavity mode to be excited is the one at the nearest resonant frequency $\omega_0 + \Delta$, where Δ is the cavity detaining. That single cavity mode is described by the third term of H_S (with $\hat{A}^\dagger$ and $\hat{A}$ creation and annihilation operators). The last term describes the coupling of the cavity mode to the end mirror motion resulting from the radiation pressure force of the circulating light. It can be derived directly from the equation of motion of the moving mirror and the wave equation with time-vary boundary conditions [19]. The Hamiltonian of the external field H_R is simply

$$H_R = \int_0^{+\infty} \frac{d\omega}{2\pi}\hbar\omega\hat{c}_\omega^\dagger\hat{c}_\omega \tag{2.75}$$

where $\hat{c}_\omega^\dagger$ and $\hat{c}_\omega$ are the creation and annihilation operators for the field at each frequency ω.

The interaction Hamiltonian V between the cavity mode and the external field is given by

$$V = i\hbar\sqrt{2\gamma}\int_0^{+\infty}\frac{d\omega}{2\pi}\left[\hat{A}^\dagger\hat{c}_\omega - \hat{A}\hat{c}_\omega^\dagger\right] \tag{2.76}$$

Where γ in the opto-mechanical coupling constant is the decay rate of the cavity mode.

2.6.2 Input-output relations

We can use this Hamiltonian to obtain the so-called input-output relations for the cavity. These relations link together the incoming and the outgoing fields, removing the explicit dependence on the intracavity modes and they provide a generally valid result that can be used every time we have that sort of cavity in a more complex optical system (e.g. laser interferometers).

To simplify our Hamiltonian firstly we can switch to an interaction picture that allows us to remove $\hbar\omega_0\hat{A}^\dagger\hat{A}$ from H_S and $\hbar\omega_0\hat{c}_\omega^\dagger\hat{c}_\omega$ from H_R. Then, assuming a high pumping level (that means a large number of photon in the cavity) we can linearize the cavity mode around its stationary state: from $\hat{A}$ we define a fluctuation operator $\delta\hat{A}$ such that $\hat{A} = \bar{A} + \delta\hat{A}$, where $\bar{A}$ is the expectation value of $\hat{A}$ at a steady state. The arbitrary phase reference is fixed if we assume $\bar{A}$ to be real. According to that, the linearized radiation pressure term becomes

$$\hbar\frac{\omega_0}{L}\hat{x}\hat{A}^\dagger\hat{A} \to \hbar\frac{\omega_0}{L}\bar{A}\hat{x}\left(\delta\hat{A} + \delta\hat{A}^\dagger\right)$$

where we have neglected second-order terms of the fluctuation and the term proportional to $\bar{A}^2$ that is constant. We can also assume that all the excited modes of the external field have frequencies centered on ω_0 and then we can make the substitution $\omega \to \omega_0 + \Omega$ and integrate over the sidebands frequency Ω. Since $\Omega \ll \omega_0$ we can set the integration bound to $\pm\infty$. We find

$$\begin{aligned} H_{TOT} = {} & \hbar\omega_m\hat{B}^\dagger\hat{B} - F\hat{x} + \hbar\Delta\hat{A}^\dagger\hat{A} + \hbar\frac{\omega_0}{L}\bar{A}\hat{x}\left(\hat{A} + \hat{A}^\dagger\right) \\ & + \int_{-\infty}^{+\infty}\frac{d\Omega}{2\pi}\hbar\Omega\hat{c}_{\omega_0+\Omega}^\dagger\hat{c}_{\omega_0+\Omega} \end{aligned} \tag{2.77}$$

$$+ i\hbar\sqrt{2\gamma}\int_{-\infty}^{+\infty}\frac{d\Omega}{2\pi}\left[\hat{A}^{\dagger}\hat{c}_{\omega_0+\Omega} - \hat{A}\hat{c}^{\dagger}_{\omega_0+\Omega}\right]$$

where we now used $\hat{A}$ to indicate just the fluctuation operator $\delta\hat{A}$. To give a spatial description of the external field we define

$$\hat{c}_z = \int_{-\infty}^{+\infty}\frac{d\omega}{2\pi}\hat{c}_{\omega_0+\Omega}e^{+i\Omega z}$$

whose relative commutation relations are:

$$\left[[\hat{c}_z, \hat{c}_{z'}] = \left[\hat{c}^{\dagger}_z, \hat{c}^{\dagger}_{z'}\right] = 0, \qquad \left[\hat{c}_z, \hat{c}^{\dagger}_{z'}\right] = \delta\left(z - z'\right)\right]$$

We can now redefine H_R and V in terms of $\hat{c}_z$

$$H_R = i\hbar\sqrt{2\gamma}\left[\hat{A}^{\dagger}\hat{c}_{z=0} - \hat{A}\hat{c}^{\dagger}_{z=0}\right]$$

$$V = -i\hbar\int_{-\infty}^{+\infty}\hat{c}^{\dagger}_z\left(\partial_z\hat{c}_z\right)dz$$

From this Hamiltonian we work out the Heisenberg equations for $\hat{c}_z$ and $\hat{A}$

$$\frac{d\hat{c}_z}{dt} = \frac{1}{ih}\left([\hat{c}_z, H_R] + [\hat{c}_z, V]\right) = -\sqrt{2\gamma}\hat{A}\delta\left(z\right) - \partial_z\hat{c}_z \tag{2.78}$$

$$\frac{d\hat{A}}{dt} = \frac{1}{ih}\left(\left[\hat{A}, H_s\right] + \left[\hat{A}, V\right]\right) = \frac{1}{ih}\left[\hat{A}, H_s\right] + \sqrt{2\gamma}\hat{c}_{z=0} \tag{2.79}$$

From Eq. (2.78) we note that $\hat{c}_z$ has a discontinuity in $z = 0$. Physically this corresponds to the mirror position where the cavity mode $\hat{A}$ interacts with $\hat{c}_z$ which is not well-defined. Then the value of $\hat{c}_{z=0-}$ just before the interaction will be understood as the incoming field while $\hat{c}_{z=0+}$ will be the outgoing field and from now on they will be referred to as $\hat{a}^{in}$ and $\hat{a}^{out}$. Integrating the equation along $z = 0$ we find the relation

$$\hat{a}^{out} = \hat{a}^{in} - \sqrt{2\gamma}\hat{A} \tag{2.80}$$

Then we can arbitrarily define $\hat{c}_{z=0}$ as the average of $\hat{a}^{in}$ and $\hat{a}^{out}$ and, using the previous equation, we find

$$\hat{c}_{z=0} = \hat{a}^{in} - \sqrt{\frac{\gamma}{2}}\hat{A} = \hat{a}^{out} + \sqrt{\frac{\gamma}{2}}\hat{A} \tag{2.81}$$

which can be put in Eq. (2.79) leading to

$$\frac{d\hat{A}}{dt} = -\gamma\hat{A} + \sqrt{2\gamma}\hat{a}^{in} + \frac{1}{ih}\left[\hat{A}, H_s\right] \tag{2.82}$$

Such substitution brings a damping to $\hat{A}$ which, in case $\hat{a}^{in}$ is switched off, will eventually extinguish the intracavity field, as expected.

From (2.74) we find Heisenberg equations for $\hat{x}$ and $\hat{p}$ of the mirror. In the frequency domain we have

$$-i\Omega\hat{x}_\Omega = \frac{\hat{p}_\Omega}{M} \tag{2.83}$$

$$-i\Omega\hat{p}_\Omega = -M\omega^2\hat{x}_\Omega + \frac{\omega_0}{L}\bar{A}\left(\hat{A}_\Omega + \hat{A}^\dagger_\Omega\right) \tag{2.84}$$

and then

$$\hat{x}_\Omega = \frac{G\left(\hat{A}_\Omega + \hat{A}^\dagger_\Omega\right)}{M\left(\omega^2 - \Omega^2\right)} \tag{2.85}$$

where $G = \frac{\omega_0}{L}\bar{A}$. Evaluating the commutator in Eq. (2.82) and switching to the frequency domain we find

$$-i\Omega\hat{A}_\Omega = \sqrt{2\gamma}\hat{a}^{in}_{\omega_0+\Omega} + \left(-i\Delta - \gamma\right)\hat{A} + iG\hat{x}_\Omega \tag{2.86}$$

$$-i\Omega\hat{A}^\dagger = \sqrt{2\gamma}\hat{a}^{in\dagger}_{\omega_0-\Omega} + \left(+i\Delta - \gamma\right)\hat{A}^\dagger - iG\hat{x}_\Omega \tag{2.87}$$

We can also re-express (2.80) and its Hermitian conjugate in the frequency domain

$$\hat{a}^{out}_{\omega_0+\Omega} = \hat{a}^{in}_{\omega_0+\Omega} - \sqrt{2\gamma}\hat{A}_\Omega \tag{2.88}$$

$$\hat{a}^{out}_{\omega_0-\Omega} = \hat{a}^{in}_{\omega_0-\Omega} - \sqrt{2\gamma}\hat{A}^\dagger_\Omega \tag{2.89}$$

and, using the two-photon formalism we defined in Eq. (2.59), we can rearrange the previous equations and find

$$\hat{a}_1^{out} = \hat{a}_1^{in} - \sqrt{\gamma}\left(\hat{A}_\Omega + \hat{A}_\Omega^\dagger\right)$$
$$\hat{a}_2^{out} = \hat{a}_2^{in} + i\sqrt{\gamma}\left(\hat{A}_\Omega - \hat{A}_\Omega^\dagger\right)$$

In the simplified case of zero detaining using (2.86) and (2.87) we obtain

$$\left(\hat{A}_\Omega + \hat{A}_\Omega^\dagger\right) = \hat{a}_1^{in}\frac{2\sqrt{\gamma}}{\gamma - i\Omega}$$
$$\left(\hat{A}_\Omega + \hat{A}_\Omega^\dagger\right) = \left(\hat{a}_2^{in} + \frac{G}{\sqrt{\gamma}}\hat{x}_\Omega\right)\frac{i2\sqrt{\gamma}}{\gamma - i\Omega}$$

Finally, using (2.85) we find the input-output relations

$$\begin{aligned}\hat{a}_1^{out} &= \frac{\Omega - i\gamma}{\Omega + i\gamma}\hat{a}_1^{in} \\ \hat{a}_2^{out} &= \frac{\Omega - i\gamma}{\Omega + i\gamma}\left[\hat{a}_2^{in} - K\hat{a}_1^{in}\right]\end{aligned}$$

with $K = \frac{4G^2\gamma}{M(\Omega^2-\omega^2)(\Omega^2+\gamma^2)}$

2.6.3 Quantum noise evaluation: the covariance matrix

A useful tool to characterize quantum noise of a two-photon light state is the spectral density matrix , which can be defined as

$$\Sigma\left(\hat{a}\right) = \left\langle \hat{a}\hat{a}^\dagger \right\rangle_{sym} = \begin{pmatrix} \left\langle \hat{a}_1\hat{a}_1^\dagger \right\rangle_{sym} & \left\langle \hat{a}_1\hat{a}_2^\dagger \right\rangle_{sym} \\ \left\langle \hat{a}_2\hat{a}_1^\dagger \right\rangle_{sym} & \left\langle \hat{a}_2\hat{a}_2^\dagger \right\rangle_{sym} \end{pmatrix}$$

where

$$\left\langle \hat{a}_1\hat{a}_2^\dagger \right\rangle_{sym} = \frac{1}{2}\left\langle \hat{a}_1\hat{a}_2^\dagger + \hat{a}_2^\dagger\hat{a}_1 \right\rangle$$

The matrix elements can be evaluated recalling definition of quadrature operators (2.59) in terms of $\hat{a}_+$,$\hat{a}_-^\dagger$ operators and their commutation relations (2.58). For a coherent state we have

$$\begin{aligned}\left\langle \hat{a}_1\hat{a}_2^\dagger \right\rangle_{sym} &= \frac{1}{2}\left\langle \hat{a}_1\hat{a}_2^\dagger + \hat{a}_2^\dagger\hat{a}_1 \right\rangle \\ &= \frac{1}{4}\left\langle \left(\hat{a}_+ + \hat{a}_-^\dagger\right)\left(i\hat{a}_+^\dagger - i\hat{a}_-\right) + \left(i\hat{a}_+^\dagger - i\hat{a}_-\right)\left(\hat{a}_+ + \hat{a}_-^\dagger\right) \right\rangle \\ &= \frac{i}{4}\left\langle \left(\hat{a}_+ + \hat{a}_-^\dagger\right)\hat{a}_+^\dagger + \left(\hat{a}_+^\dagger - \hat{a}_-\right)\hat{a}_-^\dagger \right\rangle \\ &= \frac{i}{4}\left\langle \left(\hat{a}_+ + \hat{a}_-^\dagger\right)\hat{a}_+^\dagger + \left(\hat{a}_+^\dagger - \hat{a}_-\right)\hat{a}_-^\dagger \right\rangle \\ &= \frac{i}{4}\left\langle \hat{a}_+\hat{a}_+^\dagger - \hat{a}_-\hat{a}_-^\dagger \right\rangle = 0\end{aligned}$$

while

$$\begin{aligned}\left\langle \hat{a}_1\hat{a}_1^\dagger \right\rangle_{sym} &= \frac{1}{2}\left\langle \hat{a}_1\hat{a}_1^\dagger + \hat{a}_1^\dagger\hat{a}_1 \right\rangle \\ &= \frac{1}{4}\left\langle \left(\hat{a}_+ + \hat{a}_-^\dagger\right)\left(\hat{a}_+^\dagger + \hat{a}_-\right) + \left(\hat{a}_+^\dagger + \hat{a}_-\right)\left(\hat{a}_+ + \hat{a}_-^\dagger\right) \right\rangle \\ &= \frac{1}{4}\left\langle \hat{a}_+\hat{a}_+^\dagger + \hat{a}_-\hat{a}_-^\dagger \right\rangle = \frac{\pi}{2}\delta\left(\Omega - \Omega'\right)\end{aligned} \tag{2.90}$$

$$\begin{aligned}\left\langle \hat{a}_2\hat{a}_2^\dagger \right\rangle_{sym} &= \frac{1}{2}\left\langle \hat{a}_2\hat{a}_2^\dagger + \hat{a}_2^\dagger\hat{a}_2 \right\rangle \\ &= -\frac{1}{4}\left\langle \left(\hat{a}_-^\dagger - \hat{a}_+\right)\left(\hat{a}_+^\dagger - \hat{a}_-\right) + \left(\hat{a}_+^\dagger - \hat{a}_-\right)\left(\hat{a}_-^\dagger - \hat{a}_+\right) \right\rangle \\ &= \frac{1}{4}\left\langle \hat{a}_+\hat{a}_+^\dagger + \hat{a}_-\hat{a}_-^\dagger \right\rangle = \frac{\pi}{2}\delta\left(\Omega - \Omega'\right)\end{aligned} \tag{2.91}$$

The spectral density matrix determines the autocorrelation function of the quadrature field[20], defined as

$$\left\langle \hat{E}_i\left(t\right)\hat{E}_j\left(t+\tau\right) \right\rangle_{sym} = \frac{4\pi\hbar\omega_0}{Ac}\int \frac{d\Omega}{2\pi}\mathrm{Re}\left(\Sigma_{ij}\left(\Omega\right)e^{-i\Omega\tau}\right) \tag{2.92}$$

where

$$\mathrm{Re}\left(\Sigma_{ij}\left(\Omega\right)e^{-i\Omega\tau}\right) = \frac{1}{2}\left(\Sigma_{ij}\left(\Omega\right)e^{-i\Omega\tau} + \Sigma_{ij}^\dagger\left(\Omega\right)e^{i\Omega\tau}\right)$$

From Eq. (2.92) and Eq. (2.61) we find the variance of the electric field

$$\left\langle \left[\Delta\hat{E}\left(t\right)\right]^{2}\right\rangle = \frac{4\pi\hbar\omega_{0}}{Ac}\int\frac{d\Omega}{2\pi}\left[\Sigma_{11}+\Sigma_{22}\right.$$
$$\left.+\left(\Sigma_{11}-\Sigma_{22}\right)\cos\left(2\omega_{0}t\right)+2\mathrm{Re}\left(\Sigma_{12}\right)\sin\left(2\omega_{0}t\right)\right]$$

Its time-dependence is determined by the real part of the spectral density matrix referred to as covariance matrix $\boldsymbol{C}=\mathrm{Re}\boldsymbol{\Sigma}$ and from (2.90) and (2.91) we see that the variance is time-independent for coherent state since $\Sigma_{11}-\Sigma_{22}=\Sigma_{12}=0$.

The elements of the covariance matrix are also connected to the autocorrelation functions of the quadrature fields (2.92) when calculated at the same time:

$$\left\langle \left[\hat{E}_{i}\left(t\right)\right]^{2}\right\rangle_{sym} = \frac{4\pi\hbar\omega_{0}}{Ac}\int\frac{d\Omega}{2\pi}\Sigma_{ii}\left(\Omega\right)$$
$$\left\langle \hat{E}_{i}\left(t\right)\hat{E}_{j}\left(t\right)\right\rangle_{sym} = \frac{4\pi\hbar\omega_{0}}{Ac}\int\frac{d\Omega}{2\pi}\mathrm{Re}\left(\Sigma_{ij}\left(\Omega\right)\right)$$

We can associate the 2×2 covariance matrix to an error ellipse for our state, defined by

$$\vec{a}^{T}\boldsymbol{C}^{-1}\vec{a}=1$$

It will be centered on the point $\left(\mathrm{Re}\left(\alpha\right),\mathrm{Im}\left(\alpha\right)\right)$ where α is the complex amplitude associated with the carrier. The eigenvectors of $\boldsymbol{C}$ locate the axes and the square root of their eigenvalues gives their length. In the case of a coherent state the covariance matrix is the identity matrix and the ellipse reduce to a circle. For a squeezed state as the one we present in (2.73) we have

$$\hat{b}=\begin{pmatrix}1 & 0\\ k & 1\end{pmatrix}\hat{a}$$

so that

$$\boldsymbol{\Sigma}=\begin{pmatrix}1 & 0\\ k & 1\end{pmatrix}\left\langle \hat{a}\,\hat{a}^{\dagger}\right\rangle \begin{pmatrix}1 & k^{*}\\ 0 & 1\end{pmatrix}$$
$$=\begin{pmatrix}1 & k\\ k^{*} & 1+\left|k\right|^{2}\end{pmatrix}$$

and

$$\boldsymbol{C} = \mathrm{Re}\boldsymbol{\Sigma} = \begin{pmatrix} 1 & \mathrm{Re}\,(k) \\ \mathrm{Re}\,(k) & 1+|k|^2 \end{pmatrix}$$

The imaginary part of the spectral density matrix gives information about the retarded correlation between different quadrature. Eq. (2.92) with $\Omega\tau = \pi/2)$ becomes

$$\left\langle \hat{E}_i\,(t)\,\hat{E}_j\left(t+\frac{\pi}{2\Omega}\right)\right\rangle_{sym} = \frac{4\pi\hbar\omega_0}{Ac}\int\frac{d\Omega}{2\pi}\mathrm{Im}\,(\Sigma_{ij}\,(\Omega))$$

This informations is lost in the covariance matrix and cannot be represented in the error ellipse.

Even though the error ellipse provide an intuitive representation of noise correlations of a light state, we cannot simply use it to infer the noise in a particular direction θ. The noise spectrum in the quadrature $X_{\hat{n}} = \hat{n}\cdot\vec{b}$, where $\hat{n} \equiv \begin{pmatrix} \cos\theta \\ \sin\theta \end{pmatrix}$, can be found correctly starting from the spectral density of $X_{\hat{n}}$

$$\left\langle X_{\hat{n}}\,(\Omega)\,X^{\dagger}_{\hat{n}}\,(\Omega')\right\rangle_{symm} = 2\pi\delta\,(\Omega-\Omega')\,S_{X_{\hat{n}}}(\Omega) \tag{2.93}$$

which becomes

$$2\pi\delta\,(\Omega-\Omega')\,S_{X_{\hat{n}}} = \hat{n}\begin{pmatrix} 1 & 0 \\ k & 1 \end{pmatrix}\left\langle\vec{a}\,\vec{a}^{\,\dagger}\right\rangle\begin{pmatrix} 1 & k \\ 0 & 1 \end{pmatrix}\hat{n} \tag{2.94}$$

and since $\left\langle\vec{a}\,\vec{a}^{\dagger}\right\rangle = 2\pi\delta\,(\Omega-\Omega')$ we find

$$\begin{aligned} S_{X_{\hat{n}}} &= \begin{pmatrix} \cos\theta & \sin\theta \end{pmatrix}\begin{pmatrix} 1 & k \\ k & 1+k_I^2 \end{pmatrix}\begin{pmatrix} \cos\theta \\ \sin\theta \end{pmatrix} \\ &= \cos^2\theta + \left(1+k_I^2\right)\sin^2\theta - 2k_I\cos\theta\sin\theta \end{aligned} \tag{2.95}$$

We will refer to it as (noise) polar plot and it represents the variance for a squeezed state which we defined in 2.48. In Figure 2.13 the noise polar plot and the noise ellipse for the same squeezed state are shown together. Even if the maximum and minimum have the same values at the same angles, the "noise predicted" is different in all the other directions.

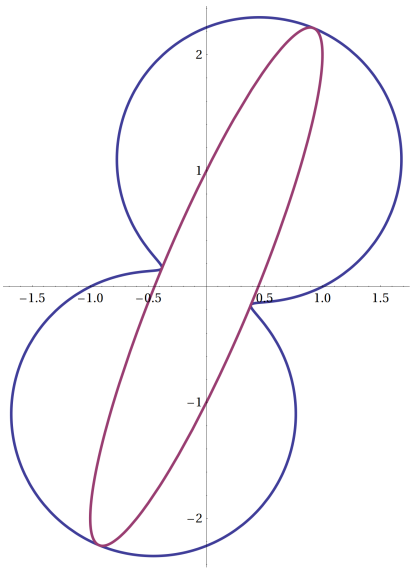

Figure 2.13: The error ellipse (purple) compared with the noise polar plot (blue) for the same squeezed state.

3 Simulation of opto-mechanical interactions

3.1 Quantum description of a linearized opto-mechanical system

The goal of this work is the implementation of a code able to simulate optical systems with particular regard to the opto-mechanical effects caused by the interaction of light modes with mechanical modes of the movable mirrors, by means of light radiation pressure. As we have seen before the best choice to describe these effects it to use the two-photon formalism we introduced in the previous chapter. We will use a linearized description for the fields in our cavity.

They will be associated with a zero-order vector, which represents the real and the imaginary part of the carrier

$$\vec{\Lambda} = \begin{pmatrix} \Lambda_1 \\ \Lambda_2 \end{pmatrix} \tag{3.1}$$

and a first order vector which accounts for quantum fluctuations of our field at a frequency Ω, where Ω is the distance from the carrier frequency ω_o,

$$\hat{a}(\Omega) = \begin{pmatrix} \hat{a}_1(\Omega) \\ \hat{a}_2(\Omega) \end{pmatrix} \tag{3.2}$$

The first and the second component of this vector can be interpreted respectively as amplitude and phase quadrature if we choose for the carrier

$$\vec{\Lambda} = \alpha \begin{pmatrix} 1 \\ 0 \end{pmatrix}$$

We want to give a description of our cavity fields as a superposition of matched Hermite Gauss modes in order to point out those effect of mode coupling we described in 2.1.4 and at the same time we are interested in a quantum description of our fields and relative fluctuations. We will associate with every HG mode a zero-order vector as (3.1) and relative fluctuations (3.2).

A generic expression for an electric field in a cavity will be

$$E(t) = \sqrt{\frac{4\pi\hbar\omega_0}{c}} \left[\sum_{m,n} E_0 \, \phi_{mn;\omega_0}(x,y) e^{i\omega_0 t} + E_0^* \, \phi^*_{mn;\omega_0}(x,y) e^{-i\omega_0 t} \right.$$
$$\left. + \int_0^\infty d\omega \sum_{m,n} \hat{a}_{mn}(\omega) \phi_{mn;\omega}(x,y) e^{i\omega t} + \hat{a}^\dagger_{mn}(\omega) \phi^*_{mn;\omega}(x,y) e^{-i\omega t} \right] \tag{3.3}$$

where

$$\phi_{mn} = c_{mn} e^{\frac{ikr^2}{2q(z)}} H_m \left(\frac{\sqrt{2}x}{w(z)} \right) H_n \left(\frac{\sqrt{2}y}{w(z)} \right)$$

The variables related to our system we want to obtain by means of this simulation are

- the values of the classical field (3.1) for each mode, in any relevant point of the cavity;
- the values of quadrature fluctuation (3.2) as functions of Ω for each mode, in any relevant point of the cavity;
- the motion of the mirrors caused by radiation pressure forces and torques.

3.2 Implementation of the simulation: input-output relations

Since an optical system is generally composed by a set of optical devices (mirrors, beam splitter, sources, detectors etc), a first step for our simulation will be to understand how light states are modified by the interaction with these instruments. We now present the so-call input-output relations for the objects that represent the building blocks of our optical system [21]. We start considering plane waves and then specialize the results to HG modes.

3.2.1 Free propagation

It is well known that the free propagation of the carrier component of a plane wave over a length ℓ can be written as a rotation of the vector (3.1) representing it:

$$\begin{pmatrix} \Lambda_1(\ell) \\ \Lambda_2(\ell) \end{pmatrix} = \begin{pmatrix} \cos\frac{\omega_0\ell}{c} & -\sin\frac{\omega_0\ell}{c} \\ \sin\frac{\omega_0\ell}{c} & \cos\frac{\omega_0\ell}{c} \end{pmatrix} \begin{pmatrix} \Lambda_1(0) \\ \Lambda_2(0) \end{pmatrix} \equiv \mathbf{R}\left(\frac{\omega_0\ell}{c}\right) \begin{pmatrix} \Lambda_1(0) \\ \Lambda_2(0) \end{pmatrix}$$

where ω_o is the carrier frequency. For the quadrature vectors (3.2) we have

$$\begin{aligned}
\begin{pmatrix} a_1(\ell) \\ a_2(\ell) \end{pmatrix} &= \frac{1}{\sqrt{2}} \begin{pmatrix} a_+(\ell) + a_-^\dagger(\ell) \\ -ia_+(\ell) + ia_-^\dagger(\ell) \end{pmatrix} \\
&= \frac{1}{\sqrt{2}} \begin{pmatrix} e^{i(\omega_0+\Omega)\ell/c} a_+(0) + e^{-i(\omega_0-\Omega)\ell/c} a_-^\dagger(0) \\ -ie^{i(\omega_0+\Omega)\ell/c} a_+(0) + ie^{-i(\omega_0-\Omega)\ell/c} a_-^\dagger(\ell) \end{pmatrix} \\
&= e^{i\Omega\ell/c} \frac{1}{\sqrt{2}} \begin{pmatrix} e^{i\omega_0\ell/c} a_+(0) + e^{-i\omega_0\ell/c} a_-^\dagger(0) \\ -ie^{i\omega_0\ell/c} a_+(0) + ie^{-i\omega_0\ell/c} a_-^\dagger(0) \end{pmatrix} \\
&= e^{i\frac{\Omega\ell}{c}} \begin{pmatrix} \cos\frac{\omega_0\ell}{c} & -\sin\frac{\omega_0\ell}{c} \\ \sin\frac{\omega_0\ell}{c} & \cos\frac{\omega_0\ell}{c} \end{pmatrix} \begin{pmatrix} a_1(0) \\ a_2(0) \end{pmatrix} \\
&= e^{i\frac{\Omega\ell}{c}} \mathbf{R}\left(\frac{\omega_0\ell}{c}\right) \begin{pmatrix} a_1(0) \\ a_2(0) \end{pmatrix}
\end{aligned} \tag{3.4}$$

We see that quadratures undergo the same rotation of the carrier but they gain a phase $e^{i\Omega\ell/c}$ depending on their distance Ω from carrier frequency ω_o. This effect is normally small since parameters of our system are such that $\Omega\ell/c \ll 1$.

Naively we could estimate an upper limit for the sidebands frequencies which are not affected by this phase: in a cavity long 4000m (LIGO) this upper limit would be $\Omega < 10^5 \mathrm{rad\,s^{-1}}$. However it should be noted that when resonating cavities are present the real "small" expansion parameter can be $F\Omega\ell/c$, where F is the finesse of the cavity. This quantity accounts for the multiple round trips of the mode in the cavity and represents the phase delay cumulated by the quadratures during them.

Free propagation of HG mode is basically the same of a plane wave except for an extra mode dependent factor usually referred to as Gouy phase. We will have

$$\begin{pmatrix} \Lambda_1^{mn}(z_2) \\ \Lambda_2^{mn}(z_2) \end{pmatrix} = \mathbf{R}\left(\frac{\omega_0\ell}{c} + \eta_{mn}\right) \begin{pmatrix} \Lambda_1^{mn}(z_1) \\ \Lambda_2^{mn}(z_1) \end{pmatrix} \tag{3.5}$$

where

$$\eta_{mn} = (m+n+1)\left(\arctan\frac{z_2}{b} - \arctan\frac{z_1}{b}\right)$$

The same happens to the quadrature vectors

$$\begin{pmatrix} a_1^{mn}(z_2) \\ a_2^{mn}(z_2) \end{pmatrix} = e^{i\Omega\ell/c} \mathbf{R}\left(\frac{\omega_0\ell}{c} + \eta\right) \begin{pmatrix} a_1^{mn}(z_1) \\ a_2^{mn}(z_1) \end{pmatrix}$$

Here we supposed the waist located at the $z = 0$ position along the optical axis, the general case can easily be obtained with a simple translation.

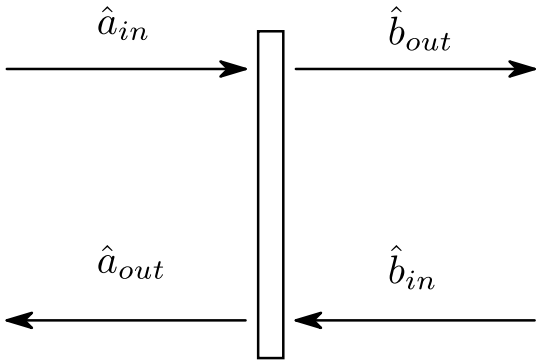

Figure 3.1: Input-Output relations for a mirror.

3.2.2 Mirrors

Input-output relations for a static mirror of reflectivity R and transmissivity T such that $R^2 + T^2 = 1$ are (with reference to Figure 3.1)

$$\begin{pmatrix} \hat{a}_{out} \\ \hat{b}_{out} \end{pmatrix} = \begin{pmatrix} -R\mathbf{1}_2 & T\mathbf{1}_2 \\ T\mathbf{1}_2 & R\mathbf{1}_2 \end{pmatrix} \begin{pmatrix} \hat{a}_{in} \\ \hat{b}_{in} \end{pmatrix} \equiv \mathbf{M}(R) \begin{pmatrix} \hat{a}_{in} \\ \hat{b}_{in} \end{pmatrix} \tag{3.6}$$

where, since $\hat{a}$ and $\hat{b}$ are two-component vectors representing modulation, $\mathbf{M}$ is actually 4×4 matrix and we represented with $\mathbf{1}_2$ the 2×2 identity matrix. We see that a mirror does not mix quadrature components. The same relation holds for HG modes, provided that they are matched with the mirror profile, namely that the mirror curvature radius is equal to the $R(z)$ of the beam at the mirror. The reflection by a static mirror of matched modes does not mix them[1], therefore the input-output relation can be immediately generalized to

$$\begin{pmatrix} \hat{a}^{mn}_{out} \\ \hat{b}^{mn}_{out} \end{pmatrix} = \mathbf{M}(R) \begin{pmatrix} \hat{a}^{mn}_{in} \\ \hat{b}^{mn}_{in} \end{pmatrix}$$

As we said many times before, fluctuations are not only associated to a non-zero carrier but they exist for the vacuum state. We see that it would be impossible not to take into account an incoming fluctuation field (even if it is just vacuum fluctuation) and preserve the correct commutation relations for outgoing operators. From

$$\hat{a}_{out} = T\hat{b}_{in} - R\hat{a}_{in}$$
$$\hat{b}_{out} = R\hat{b}_{in} + T\hat{a}_{in}$$

[1]This can be easily shown using the ABCD formalism described in Section 2.1.2

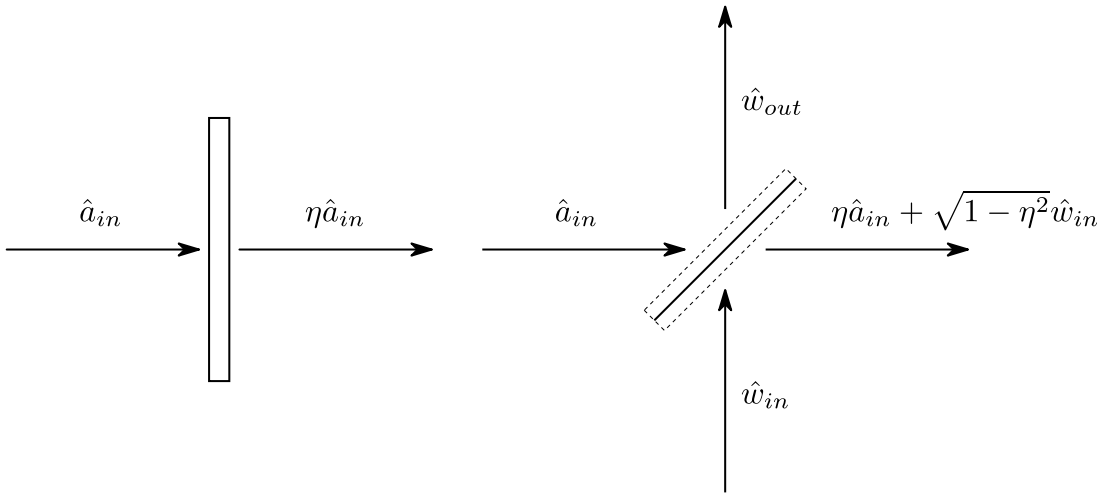

Figure 3.2: A loss is equivalent to a coupling with additional fluctuations. Here we see a schematization of a beam splitter where vacuum fluctuation are mixed to the incoming field in order to preserve the commutation relations.

we get

$$\left[\hat{a}_{out}, \hat{a}^{\dagger}_{out}\right] = R^2 \left[\hat{a}_{in}, \hat{a}^{\dagger}_{in}\right] + T^2 \left[\hat{b}_{in}, \hat{b}^{\dagger}_{in}\right] = T^2 + R^2 = 1$$

and we could not have found the same result ignoring one of the incoming fluctuation fields.

Note that proper commutation relations cannot be obtained if we assume to have losses L such that $T^2 + R^2 = 1 - L$. In order to restore them, vacuum fluctuations need to be introduced again.

We can regard an incoming field $\hat{a}_{in}$ subject to a loss, such that the field intensity is reduced by a factor η, as it passed through a beam splitter which in order to preserve the correct commutation relations will mix the incoming field with a vacuum (Figure 3.2). This is described by

$$\begin{pmatrix} \hat{a}_{out} \\ \hat{w}_{out} \end{pmatrix} = \begin{pmatrix} \eta & \sqrt{1-\eta^2} \\ -\sqrt{1-\eta^2} & \eta \end{pmatrix} \begin{pmatrix} \hat{a}_{in} \\ \hat{w}_{in} \end{pmatrix}$$

We saw in 2.1.4 a classical description of what happens if the mirror can move (in response to the radiation pressure of incident light or because of an external force). In the case of a plane wave we will have a phase modulation for the reflected beam which we are going to describe by means of two-photon formalism. Switching to HG modes description things become more complicated: a torque

induced by radiation pressure can rotate the mirror, which, once displaced, generate a coupling of different HG modes. We are going to investigate input-output relations for quantum fluctuations.

3.2.2.1 Radiation pressure modulation for a plane wave

Let us start with the simple example of an incoming plane wave or a laser beam described as usual as a classical carrier with amplitude α rotating with a frequency ω_o, surrounded by a continuum of small quantum fluctuations

$$\begin{aligned}\hat{E}(t) = \sqrt{\frac{4\pi\hbar\omega_0}{Ac}}\Bigg[\cos(\omega_o t)\left(\sqrt{2}D_{1,cl} + \int\left(\hat{a}_1 e^{-i\Omega t} + \hat{a}_1^\dagger e^{+i\Omega t}\right)\frac{d\Omega}{2\pi}\right) \\ + \sin(\omega_o t)\left(\sqrt{2}D_{2,cl} + \int\left(\hat{a}_2 e^{-i\Omega t} + \hat{a}_2^\dagger e^{+i\Omega t}\right)\frac{d\Omega}{2\pi}\right]\Bigg)\end{aligned} \tag{3.7}$$

By defining

$$E_{cl} = \begin{pmatrix} E_{1,cl} \\ E_{2,cl}\end{pmatrix} = \sqrt{\frac{8\pi\hbar\omega_0}{Ac}}\begin{pmatrix} D_{1,cl} \\ D_{2,cl}\end{pmatrix}$$
$$\hat{E}_{1,2}(t) = \sqrt{\frac{4\pi\hbar\omega_0}{Ac}}\int\left(\hat{a}_{1,2}e^{-i\Omega t} + \hat{a}_{1,2}^\dagger e^{+i\Omega t}\right)\frac{d\Omega}{2\pi}$$

Eq. (3.7) becomes

$$\hat{E}(t) = \left[E_{1,cl} + \hat{E}_1(t)\right]\cos(\omega_o t) + \left[E_{2,cl} + \hat{E}_2(t)\right]\sin(\omega_o t)$$

The effect of reflection results in a phase-shift $\Phi = \frac{2\omega_o z}{c}$. Being $z(t)$ the displacement of the mirror which can be decomposed in a constant part and a fluctuation $\bar{z}(t) = \bar{z} + \tilde{z}(t)$, we can decompose the phase shift in the same way: $\bar{\Phi}(t) = \bar{\Phi} + \tilde{\Phi}(t)$ with $\bar{\Phi} = \frac{2\omega_o\bar{z}}{c}$ and $\tilde{\Phi} = \frac{2\omega_o\tilde{z}}{c}$ [12]. The reflected beam reads

$$\begin{aligned}\hat{E}^r(t) &= r\left[E_1^{cl} + \hat{E}_1(t)\right]\cos(\omega_o t + \Phi) + r\left[E_2^{cl} + \hat{E}_1(t)\right]\sin(\omega_o t + \Phi) \\ &= r\left[E_1^{cl} + \hat{E}_1(t)\right]\cos\left(\Theta + \tilde{\Phi}\right) + r\left[E_2^{cl} + \hat{E}_1(t)\right]\sin\left(\Theta + \tilde{\Phi}\right)\end{aligned}$$

with $\Theta = \omega_o t + \bar{\Phi}$. We can carry out the calculations

$$\hat{E}^r(t) = r\left[E_1^{cl} + \hat{E}_1(t)\right]\cos\left(\Theta + \tilde{\Phi}\right) + r\left[E_2^{cl} + \hat{E}_2(t)\right]\sin\left(\Theta + \tilde{\Phi}\right)$$

$$
\begin{aligned}
&= r\left[E_1^{cl} + \hat{E}_1(t)\right]\left(\cos\Theta\cos\tilde{\Phi} - \sin\Theta\sin\tilde{\Phi}\right) \\
&+ r\left[E_2^{cl} + \hat{E}_2(t)\right]\left(\sin\Theta\cos\tilde{\Phi} + \cos\Theta\sin\tilde{\Phi}\right) \\
&= r\left[E_1^{cl} + \hat{E}_1(t)\right]\left(\cos\Theta - \tilde{\Phi}\sin\Theta\right) + r\left[E_2^{cl} + \hat{E}_2(t)\right]\left(\sin\Theta + \tilde{\Phi}\cos\Theta\right)
\end{aligned}
$$

and neglecting second order fluctuations we find

$$
\begin{aligned}
\hat{E}^r(t) &= r\left[E_1^{cl} + \hat{E}_1(t)\right]\cos\Theta - E_1^{cl}\tilde{\Phi}\sin\Theta + r\left[E_2^{cl} + \hat{E}_2(t)\right]\sin\Theta + E_2^{cl}\tilde{\Phi}\cos\Theta \\
&= r\left[E_1^{cl} + \hat{E}_1(t) + E_2^{cl}\tilde{\Phi}\right]\cos\Theta + r\left[E_2^{cl} + \hat{E}_2(t) - E_1^{cl}\tilde{\Phi}\right]\sin\Theta
\end{aligned}
$$

If we confront this with the standard expression for the reflected field

$$
\hat{E}^r(t) \;=\; \left[E_1^{cl} + \hat{E}_1^r(t)\right]\cos\left(\omega_o t + \bar{\Phi}\right) + \left[E_2^{cl} + \hat{E}_2^r(t)\right]\sin\left(\omega_o t + \bar{\Phi}\right)
$$

we find the following relation between fluctuation quadratures

$$
\begin{aligned}
\hat{E}_1^r(t) &= r\hat{E}_1(t) + rE_2^{cl}\tilde{\Phi} = r\hat{E}_1(t) + \frac{2r\omega_o\tilde{z}}{c}E_2^{cl} \\
\hat{E}_2^r(t) &= r\hat{E}_2(t) - rE_1^{cl}\tilde{\Phi} = r\hat{E}_2(t) - \frac{2r\omega_o\tilde{z}}{c}E_1^{cl}
\end{aligned}
$$

that is

$$
\hat{E}^r(t) = r\hat{E}(t) + \frac{2r\omega_0}{c}\tilde{z}(t)\begin{pmatrix} 0 & 1 \\ -1 & 0 \end{pmatrix}E^{cl}
$$

Switching to frequency domain this can be written as

$$
\hat{E}(\Omega) = r\hat{E}(\Omega) + \frac{2r\omega_0}{c}\tilde{z}(\Omega)\begin{pmatrix} 0 & 1 \\ -1 & 0 \end{pmatrix}E^{cl}
$$

and for $\hat{a}$

$$
\hat{a}(\Omega) = r\hat{a}(\Omega) + \frac{2r\omega_0}{c}\tilde{z}(\Omega)\begin{pmatrix} 0 & 1 \\ -1 & 0 \end{pmatrix}E^{cl} \tag{3.8}
$$

3.2.2.2 Radiation pressure and torque of HG modes

We will now recover the description in terms of HG modes and we will look for an expression for the fluctuating part of radiation pressure force and torque.

In Eq. (3.3) we wrote the field as the sum of a "classical" part and a fluctuating part

$$E(t) = E_{cl}(t) + \delta E(t)$$

since radiation pressure is given by $(4\pi)^{-1}E(t)^2$, the fluctuating part of the radiation pressure, at the first order, will be

$$P(x, y, t) = \frac{1}{4\pi} 2\overline{E_{cl}(t)\delta E(t)} \tag{3.9}$$

The average is over the fast oscillations of the field. Now we recall Eq. (3.3)

$$\begin{aligned} E_{cl}(t) &= \sum_{m,n} E_{0;mn}\phi_{mn;\omega_0}(x, y)e^{i\omega_0 t} + E^*_{0;mn}\phi^*_{mn;\omega_0}(x, y)e^{-i\omega_0 t} \\ \delta E(t) &= N\int_0^\infty d\omega \sum_{m,n} \hat{a}_{mn}(\omega)\phi_{mn;\omega}(x, y)e^{i\omega t} + \hat{a}^\dagger_{mn}(\omega)\phi^*_{mn;\omega}(x, y)e^{-i\omega t} \end{aligned}$$

where we set for brevity $N = \sqrt{4\pi\hbar\omega_0/c}$. After a Fourier transform this correspond to

$$\begin{aligned} \tilde{E}_{cl}(\omega) &= \sum_{m,n} E_{0;mn}\phi_{mn;\omega_0}(x, y)\delta(\omega - \omega_0) + E^*_{0;mn}\phi^*_{mn;\omega_0}(x, y)\delta(\omega + \omega_0) \\ \delta\tilde{E}(\omega) &= N\sum_{m,n} \hat{a}_{mn}(\omega)\,\phi_{mn;\omega}(x, y) \end{aligned} \tag{3.10}$$

where

$$\begin{aligned} \hat{a}_{mn}(-\omega) &= \hat{a}^\dagger_{mn}(\omega) \\ \phi_{mn;-\omega} &= \phi^*_{mn;\omega} \end{aligned}$$

The Fourier transform of the first order fluctuating part of the field is given by the convolution

$$\begin{aligned} \widetilde{E_{cl}\delta E}(\omega) &= N\sum_{mn}\sum_{m'n'}\int d\omega' \hat{a}_{m'n'}(\omega')\,\phi_{m'n';\omega'}(x, y) \\ &\quad\times\left[E_{0;mn}\phi_{mn;\omega_0}(x, y)\delta(\omega - \omega' - \omega_0) + E^*_{0;mn}\phi^*_{mn;\omega_0}(x, y)\delta(\omega - \omega' + \omega_0)\right] \\ &= N\sum_{mn} E_{0;mn}\sum_{m'n'} \hat{a}_{m'n'}(\omega - \omega_0)\,\phi_{m'n';\omega-\omega_0}(x, y)\phi_{mn;\omega_0}(x, y) \end{aligned}$$

$$+ N \sum_{mn} E^*_{0;mn} \sum_{m'n'} \hat{a}_{m'n'}\left(\omega+\omega_0\right) \phi_{m'n';\omega+\omega_0}(x,y)\phi^*_{mn;\omega_0}(x,y)$$

The average over the oscillatory modes means that this quantity is different from zero only when $|\omega| \ll \omega_0$. In order to remember that, we will indicate this "small" frequency with Ω. Also, we will approximate

$$\phi_{m'n';\Omega-\omega_0}(x,y) \simeq \phi_{m'n';-\omega_0}(x,y) = \phi^*_{m'n';\omega_0}(x,y)$$

and

$$\phi_{m'n';\Omega+\omega_0}(x,y) \simeq \phi_{m'n';\omega_0}(x,y)$$

Fluctuating radiation pressure at first order in the frequency domain becomes:

$$\begin{aligned}\widetilde{P}(\Omega) = &\frac{N}{2\pi} \sum_{mn} E_{0;mn} \sum_{m'n'} \hat{a}_{m'n'}\left(\Omega-\omega_0\right) \phi^*_{m'n';\omega_0}(x,y)\phi_{mn;\omega_0}(x,y) \\ &+ \frac{N}{2\pi} \sum_{mn} E^*_{0;mn} \sum_{m'n'} \hat{a}_{m'n'}\left(\Omega+\omega_0\right) \phi_{m'n';\omega_0}(x,y)\phi^*_{mn;\omega_0}(x,y) \end{aligned} \tag{3.11}$$

Now we can rewrite this in term of quadratures, by defining

$$\hat{a}_{mn} \equiv \begin{pmatrix} \hat{a}_{mn,1} \\ \hat{a}_{mn,2} \end{pmatrix} = \begin{pmatrix} \frac{\hat{a}_{mn}(\omega_0+\Omega)+\hat{a}^\dagger_{mn}(\omega_0-\Omega)}{\sqrt{2}} \\ \frac{\hat{a}_{mn}(\omega_0+\Omega)-\hat{a}^\dagger_{mn}(\omega_0-\Omega)}{i\sqrt{2}} \end{pmatrix} = \mathbf{\Sigma} \begin{pmatrix} \hat{a}_{mn}(\omega_0+\Omega) \\ \hat{a}^\dagger_{mn}(\omega_0-\Omega) \end{pmatrix}$$

where the unitary matrix $\mathbf{\Sigma}$ is defined as

$$\mathbf{\Sigma} = \frac{1}{\sqrt{2}} \begin{pmatrix} 1 & 1 \\ -i & i \end{pmatrix}$$

and

$$\alpha_{mn} \equiv \mathbf{\Sigma} \begin{pmatrix} E_{0;mn} \\ E^*_{0;mn} \end{pmatrix}$$

Equation (3.11) can be rewritten now as

$$\begin{aligned}\widetilde{P}(\Omega) &= \frac{N}{2\pi} \sum_{mn} \sum_{m'n'} \begin{pmatrix} \hat{a}_{m'n'}(\omega_0+\Omega) \\ \hat{a}^\dagger_{m'n'}(\omega_0-\Omega) \end{pmatrix}^T \begin{pmatrix} 0 & \phi^*_{m'n';\omega_0}\phi_{mn;\omega_0} \\ \phi_{m'n';\omega_0}\phi^*_{mn;\omega_0} & 0 \end{pmatrix} \begin{pmatrix} E_{0;mn} \\ E^*_{0;mn} \end{pmatrix} \\ &= \frac{N}{2\pi} \sum_{mn} \sum_{m'n'} \hat{a}^T_{m'n'} \left(\mathbf{\Sigma}^T\right)^{-1} \begin{pmatrix} 0 & \phi^*_{m'n';\omega_0}\phi_{mn;\omega_0} \\ \phi_{m'n';\omega_0}\phi^*_{mn;\omega_0} & 0 \end{pmatrix} \mathbf{\Sigma}^{-1} \alpha_{mn}\end{aligned}$$

$$= \frac{N}{2\pi} \sum_{mn} \sum_{m'n'} \alpha_{mn}^{T} \begin{pmatrix} \mathrm{Re}\left(\phi^{*}_{m'n';\omega_0}\phi_{mn;\omega_0}\right) & -\mathrm{Im}\left(\phi^{*}_{m'n';\omega_0}\phi_{mn;\omega_0}\right) \\ \mathrm{Im}\left(\phi^{*}_{m'n';\omega_0}\phi_{mn;\omega_0}\right) & \mathrm{Re}\left(\phi^{*}_{m'n';\omega_0}\phi_{mn;\omega_0}\right) \end{pmatrix} \hat{a}_{m'n'} \tag{3.12}$$

If we integrate over the mirror we get, taking into account the orthogonality of the modes,

$$\tilde{F}_z\left(\Omega\right) = \frac{N}{2\pi} \sum_{mn} \alpha_{mn}^{T} \hat{a}_{mn} \tag{3.13}$$

The equation for the harmonic oscillator associated with the longitudinal displacement δZ becomes

$$-M\left(\Omega^2 - \omega_z^2\right)\delta\tilde{Z}(\Omega) = \tilde{F}_z\left(\Omega\right) = \frac{N}{2\pi} \sum_{mn} \alpha_{mn}^{T} \hat{a}_{mn} \tag{3.14}$$

Now we look for an expression for the torque induced by radiation pressure. We will use a slightly different approach, which could be useful if we are interested in the study of the effect of a general deformation of the mirror. The work done by the component of angular frequency Ω of the radiation pressure on the mirror can be written as

$$\delta\tilde{L} = \int \tilde{P}(x,y)\delta\tilde{Z}(x,y)^{*}dxdy$$

where $\delta\tilde{Z}(x,y)$ is the longitudinal displacement of a region of the mirror from his reference position. Using Equation (3.12) we find

$$\delta\tilde{L} \equiv \frac{N}{2\pi} \sum_{mn} \sum_{m'n'} \alpha_{mn}^{T} \Gamma\left[\delta\tilde{Z}\right]^{mn;m'n'} \hat{a}_{m'n'} \tag{3.15}$$

where

$$\Gamma\left[\delta\tilde{Z}\right]^{mn;m'n'} = \begin{pmatrix} \frac{\langle mn|\delta\tilde{Z}|m'n'\rangle + \langle m'n'|\delta\tilde{Z}|mn\rangle}{2} & \frac{\langle mn|\delta\tilde{Z}|m'n'\rangle - \langle m'n'|\delta\tilde{Z}|mn\rangle}{2i} \\ -\frac{\langle mn|\delta\tilde{Z}|m'n'\rangle - \langle m'n'|\delta\tilde{Z}|mn\rangle}{2i} & \frac{\langle mn|\delta\tilde{Z}|m'n'\rangle + \langle m'n'|\delta\tilde{Z}|mn\rangle}{2} \end{pmatrix}$$

and

$$\left\langle mn\left|\delta\tilde{Z}\right|m'n'\right\rangle \equiv \int dxdy\, \phi^{*}_{mn;\omega_0}(x,y)\delta\tilde{Z}(x,y)\phi_{m'n';\omega_0}(x,y)$$

If the mirror is slightly rotated we can write

$$\delta\tilde{Z}(x,y) = \delta\tilde{\theta}_x y - \delta\tilde{\theta}_y x \tag{3.16}$$

and

$$\delta\tilde{L} = \frac{N}{2\pi}\sum_{mn}\sum_{m'n'}\alpha^T_{mn}\left(\delta\theta_x\Gamma^{mn;m'n'}[y] - \delta\theta_y\Gamma^{mn;m'n'}[x]\right)\hat{a}_{m'n'} \tag{3.17}$$

Now we can easily recover the radiation pressure torques,

$$\begin{pmatrix}\tilde{M}_x\\ \tilde{M}_y\end{pmatrix} = \begin{pmatrix}\frac{d}{d\theta_x}\delta\tilde{L}\\ \frac{d}{d\theta_y}\delta\tilde{L}\end{pmatrix} = \frac{N}{2\pi}\sum_{mn}\sum_{m'n'}\begin{pmatrix}\alpha^T_{mn}\Gamma^{mn;m'n'}[y]\,\hat{a}_{m'n'}\\ -\alpha^T_{mn}\Gamma^{mn;m'n'}[x]\,\hat{a}_{m'n'}\end{pmatrix}$$

Note that the matrix element of x are different from zero only when $|m-m'|=1$ and $|n-n'|=0$,

$$\langle m'n'\,|x|\,mn\rangle = \delta_{n,n'}\left(\gamma^{(+)}_m\delta_{m',m+1} + \gamma^{(-)}_m\delta_{m',m-1}\right)$$

where

$$\begin{aligned}\gamma^{(+)}_m &= \int x\phi^*_{m+1n;\omega_0}(x,y)\phi_{mn;\omega_0}(x,y)dxdy\\ \gamma^{(-)}_m &= \int x\phi^*_{m-1n;\omega_0}(x,y)\phi_{mn;\omega_0}(x,y)dxdy\end{aligned} \tag{3.18}$$

and similarly

$$\langle m'n'\,|y|\,mn\rangle = \delta_{m,m'}\left(\gamma^{(+)}_n\delta_{n',n+1} + \gamma^{(-)}_n\delta_{n',n-1}\right)$$

Explicitly this means

$$\tilde{M}_x = \frac{N}{2\pi}\sum_{mn}\left(\gamma^{(+)}_n\underline{\alpha}^T_{mn}\underline{\hat{a}}_{m+1n} + \gamma^{(-)}_n\underline{\alpha}^T_{mn}\underline{\hat{a}}_{m-1n}\right) \tag{3.19}$$

$$\tilde{M}_y = -\frac{N}{2\pi}\sum_{mn}\left(\gamma^{(+)}_m\underline{\alpha}^T_{mn+1}\underline{\hat{a}}_{mn} + \gamma^{(-)}_m\underline{\alpha}^T_{mn}\underline{\hat{a}}_{m-1n}\right) \tag{3.20}$$

We see from previous expressions that torque appears only when more modes are present. In particular it is generated by two modes that differ only by one index. It can be seen looking at an intensity profile of the modes (Figure(2.4))and noting how a superposition of the modes HG_{11} and HG_{10},for example, will determine a non-symmetric intensity profile and then a non-zero torque on the mirror.

3.2.2.3 Rotation modulation

Now we look for a general expression for the first order modulations in case our incoming field is not a plane wave but a superposition of HG modes and the mirror displacement is a function of x and y. The reflected field is related to the incoming one by the relation

$$E_r(x,y,t) = r\exp\left(\frac{2i\omega_o\delta Z(x,y,t)}{c}\right)E(x,y,t)$$

where $\delta Z(x,y,t)$ is the mirror displacement from its zero position, which is small compared with the wavelength, so we can linearize in δZ and find

$$E_r(x,y,t) = r\left(1+\frac{2i\omega_o\delta Z(x,y,t)}{c}\right)E(x,y,t) \tag{3.21}$$

If we write also the field as the sum of a classical part and a fluctuating part we get

$$E(t) = E_{cl}(t) + \delta E(t)$$

which inserted in (3.21) gives

$$E_{r;cl}(x,y,t) + \delta E_r(x,y,t) = r\left(1+\frac{2i\omega_o\delta Z(x,y,t)}{c}\right)(E_{cl}(x,y,t) + \delta E_r(x,y,t))$$

and for the fluctuating part we have

$$\delta E_r(x,y,t) = r\delta E(x,y,t) + \frac{2ir\omega_o\delta Z(x,y,t)}{c}E_{cl}(x,y,t) \tag{3.22}$$

Using again the field expansion (3.10) we get

$$\begin{aligned}\delta\tilde{E}_r(\omega) = {} & \delta\tilde{E}(\omega) \\ & - \frac{2ir\omega_0}{c}\sum_{m,n}\delta\tilde{Z}(x,y,\omega-\omega_0)E_{0;mn}\phi_{mn;\omega_0}(x,y) \\ & - \frac{2ir\omega_0}{c}\sum_{m,n}\delta\tilde{Z}(x,y,\omega+\omega_0)E^*_{0;mn}\phi^*_{mn;\omega_0}(x,y)\end{aligned}$$

Now we construct the quadratures.

$$\delta\tilde{E}_r(\omega_0+\Omega) = r\delta\tilde{E}(\omega_0+\Omega)$$

$$
\begin{aligned}
&- \frac{2ir\omega_0}{c} \sum_{m,n} \delta\tilde{Z}(x,y,\Omega) E_{0;mn}\phi_{mn;\omega_0}(x,y) \\
&- \frac{2ir\omega_0}{c} \sum_{m,n} \delta\tilde{Z}(x,y,2\omega_0+\Omega) E^*_{0;mn}\phi^*_{mn;\omega_0}(x,y) \\
&\simeq r\delta\tilde{E}(\omega_0+\Omega) - \frac{2ir\omega_0}{c} \sum_{m,n} \delta\tilde{Z}(x,y,\Omega) E_{0;mn}\phi_{mn;\omega_0}(x,y)
\end{aligned}
$$

and

$$
\begin{aligned}
\delta\tilde{E}_{r;cl}(\omega_0-\Omega) &= r\delta\tilde{E}(\omega_0-\Omega) \\
&- \frac{2ri\omega_0}{c} \sum_{m,n} \delta\tilde{Z}(x,y,-\Omega) E_{0;mn}\phi_{mn;\omega_0}(x,y) \\
&- \frac{2ri\omega_0}{c} \sum_{m,n} \delta\tilde{Z}(x,y,2\omega_0-\Omega) E^*_{0;mn}\phi^*_{mn;\omega_0}(x,y) \\
&\simeq r\delta\tilde{E}(\omega_0-\Omega) - \frac{2ir\omega_0}{c} \sum_{m,n} \delta\tilde{Z}(x,y,\Omega)^* E_{0;mn}\phi_{mn;\omega_0}(x,y)
\end{aligned}
$$

Projecting on a mode this gives

$$
\begin{aligned}
\left[\delta\tilde{E}_r(\omega_0+\Omega)\right]_{m'n'} &= N\hat{a}_{r;m'n'}(\omega_0+\Omega) \\
&= rN\hat{a}_{m'n'}(\omega_0+\Omega) - \frac{2ir\omega_0}{c} \sum_{m,n} \left\langle m'n' \left| \delta\tilde{Z}(\Omega) \right| mn \right\rangle E_{0;mn} \\
\left[\delta\tilde{E}_r(\omega_0-\Omega)\right]^*_{m'n'} &= N\hat{a}^\dagger_{r;m'n'}(\omega_0-\Omega) \\
&= rN\hat{a}^\dagger_{m'n'}(\omega_0-\Omega) + \frac{2ir\omega_0}{c} \sum_{m,n} \left\langle mn \left| \delta\tilde{Z}(\Omega) \right| m'n' \right\rangle E^*_{0;mn}
\end{aligned}
$$

which can be written in a more compact way as

$$
\begin{aligned}
\begin{pmatrix} \hat{a}_{r;m'n'}(\omega_0+\Omega) \\ \hat{a}^\dagger_{r;m'n'}(\omega_0-\Omega) \end{pmatrix} &= r \begin{pmatrix} \hat{a}_{m'n'}(\omega_0+\Omega) \\ \hat{a}^\dagger_{m'n'}(\omega_0-\Omega) \end{pmatrix} \\
&- \frac{2ir\omega_0}{cN} \begin{pmatrix} \left\langle m'n' \left| \delta\tilde{Z} \right| mn \right\rangle & 0 \\ 0 & -\left\langle mn \left| \delta\tilde{Z} \right| m'n' \right\rangle \end{pmatrix} \begin{pmatrix} E_{0;mn} \\ E^*_{0;mn} \end{pmatrix}
\end{aligned}
$$

or

$$\hat{a}_{r,mn} = r\hat{a}_{mn}$$

$$-\frac{2r\omega_0}{cN}\mathbf{\Sigma}\begin{pmatrix} i\left\langle m'n'\left|\delta\tilde{Z}\right|mn\right\rangle & 0 \\ 0 & -i\left\langle mn\left|\delta\tilde{Z}\right|m'n'\right\rangle \end{pmatrix}\mathbf{\Sigma}^{-1}\alpha_{mn}$$

and finally

$$\hat{a}_{r,mn} = r\hat{a}_{mn} - \frac{2r\omega_0}{cN}\left(\Gamma\left[\delta\tilde{Z}\right]^{mn;m'n'}\right)^T\begin{pmatrix}0 & 1\\ -1 & 0\end{pmatrix}\alpha_{mn} \tag{3.23}$$

This general result can be specialized for different $\delta\tilde{Z}(x,y,\Omega)$. In particular for a rotation using (3.16) we get

$$\begin{aligned}\hat{a}_{r;mn} = r\hat{a}_{mn} &- \delta\tilde{\theta}_x\frac{2r\omega_0}{cN}\left(\Gamma[y]^{mn;m'n'}\right)^T\begin{pmatrix}0 & 1\\ -1 & 0\end{pmatrix}\alpha_{mn}\\ &+ \delta\tilde{\theta}_y\frac{2r\omega_0}{cN}\left(\Gamma[x]^{mn;m'n'}\right)^T\begin{pmatrix}0 & 1\\ -1 & 0\end{pmatrix}\alpha_{mn}\end{aligned}$$

and recalling (3.18) we obtain the expression for the modulation induced by a rotation along the x axis

$$\begin{aligned}\underline{\hat{a}}_{r;mn} &= r\underline{\hat{a}}_{i;mn}\\ &+ \frac{2\omega_0}{cN}\delta\tilde{\theta}_x(\Omega)\begin{pmatrix}\frac{\gamma_n^{(+)}-\gamma_{n+1}^{(-)}}{2i} & \frac{\gamma_n^{(+)}+\gamma_{n+1}^{(-)}}{2}\\ -\frac{\gamma_n^{(+)}+\gamma_{n+1}^{(-)}}{2} & \frac{\gamma_n^{(+)}-\gamma_{n+1}^{(-)}}{2i}\end{pmatrix}\underline{\alpha}_{i;mn+1}\\ &+ \frac{2\omega_0}{cN}\delta\tilde{\theta}_x(\Omega)\begin{pmatrix}\frac{\gamma_n^{(-)}-\gamma_{n-1}^{(+)}}{2i} & \frac{\gamma_n^{(-)}+\gamma_{n-1}^{(+)}}{2}\\ -\frac{\gamma_n^{(-)}-\gamma_{n-1}^{(+)}}{2} & \frac{\gamma_n^{(-)}-\gamma_{n-1}^{(+)}}{2i}\end{pmatrix}\underline{\alpha}_{i;mn-1}\end{aligned} \tag{3.24}$$

and along the y one

$$\begin{aligned}\underline{\hat{a}}_{r;mn} &= r\underline{\hat{a}}_{i;mn}\\ &- \frac{2\omega_0 r}{c}N^{-1}\delta\tilde{\theta}_y(\Omega)\begin{pmatrix}\frac{\gamma_m^{(+)}-\gamma_{m+1}^{(-)}}{2i} & \frac{\gamma_m^{(+)}+\gamma_{m+1}^{(-)}}{2}\\ -\frac{\gamma_m^{(+)}+\gamma_{m+1}^{(-)}}{2} & \frac{\gamma_m^{(+)}-\gamma_{m+1}^{(-)}}{2i}\end{pmatrix}\underline{\alpha}_{i;m+1n}\\ &- \frac{2\omega_0 r}{c}N^{-1}\delta\tilde{\theta}_y(\Omega)\begin{pmatrix}\frac{\gamma_m^{(-)}-\gamma_{m-1}^{(+)}}{2i} & \frac{\gamma_m^{(-)}+\gamma_{m-1}^{(+)}}{2}\\ -\frac{\gamma_m^{(-)}-\gamma_{m-1}^{(+)}}{2} & \frac{\gamma_m^{(-)}-\gamma_{m-1}^{(+)}}{2i}\end{pmatrix}\underline{\alpha}_{i;m-1n}\end{aligned} \tag{3.25}$$

For a longitudinal displacement

$$\delta\tilde{Z}(x,y,\Omega) = \delta\tilde{Z}(\Omega)$$

and we recover Eq. (3.8).

$$\underline{\hat{a}}_{r;mn} = r\underline{\hat{a}}_{i;mn} + \frac{2\omega_0 r}{c} N^{-1}\delta\tilde{Z}(\Omega) \begin{pmatrix} 0 & 1 \\ -1 & 0 \end{pmatrix} \underline{\alpha}_{i;mn} \tag{3.26}$$

3.2.3 Schematic representation of the opto-mechanical interactions observed

Previous results strongly suggest that a specialization of Equation (3.15) of the form

$$\delta\tilde{L} = \frac{N}{2\pi} \sum_{mn} \sum_{m'n'} \sum_{i} \alpha^{T}_{mn} \Gamma^{mn;m'n'} \left[\mathcal{O}_i\right] \hat{a}_{m'n'} \delta\tilde{q}_i \tag{3.27}$$

where $\delta\tilde{q}_i = \left\{\delta\tilde{Z}, \delta\tilde{\theta}_x, \delta\tilde{\theta}_y\right\}$ and $\mathcal{O}_i = \{1, y, -x\}$ can be used to completely describe the interaction between the mirror and the light, with the approximations used here.

As a matter of fact we could follow this approach to formalize the dynamics and its simulation. Here we will use it only to get a better qualitative understanding of the rich phenomenology that can be studied with the implemented simulation code. The interaction (3.27) can be schematised by means of three simple diagrams shown in the Table 3.1.

Each diagram accounts for a possible interaction and can be read in two direction. For example the first diagram, when read from left to right, says that the coupling of the classical amplitude (continuous line) of a mode with its quantum fluctuations (wavy line) causes a longitudinal displacement δZ of the mirror which is described by Eq. 3.14. If we read it from right to left, it says that in presence of a longitudinal displacement δZ, a classical carrier interacts with it generating an additional reflected quantum fluctuation in the same mode. This effect is described by Eq. 3.26.

The same happens for the other two interaction, but this time the carrier and the fluctuation which couple together belong to modes which differ by ± 1 in just one index and the mechanical mode of the mirror is associated with its rotation.

Suppose now that we want to evaluate the field reflected by a mirror. At the linear order this will be given by two contributions, namely

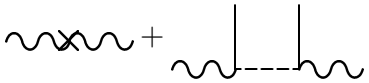

(3.28)

Interaction 1	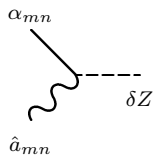
Interaction 2	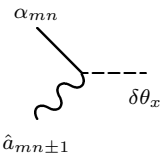
Interaction 3	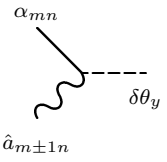

Table 3.1: Schematic diagrams representing the interaction between the light and the longitudinal and rotational degrees of freedom of a mirror. Continuous line represents a classical amplitude of a given mode, while a wavy line is associated with a quantum fluctuation fluctuation. Finally, the dashed line represents a mechanical degree of freedom.

where the first represent a simple reflection of an incoming fluctuation, the second the modulation of the carrier field done by the mirror moved by an incoming fluctuation. Note that the excitation of the field propagates between the two interactions, and this propagation is associated to its dynamics.[2]

The analysis will be more involved for a resonant cavity: in this case the connection between input and output field will be given by an infinite set of contributions as follows:

The first two terms are the same of (3.28), and represent the interaction with the frontal mirror of the cavity. The last one represent two transmissions (one for entering the cavity and one for exiting from it, labeled with the arrow) and the interaction with the cavity, which can be defined by

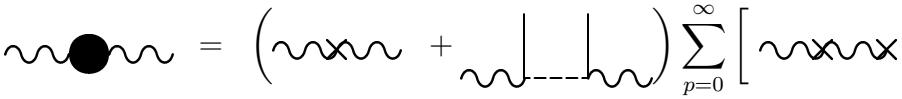

[2]As a matter of fact, this propagator is the mirror's Green function.

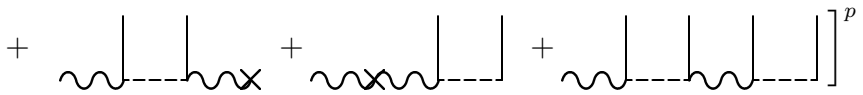

where the product means that the graphs should concatenated.

3.3 Implementation of the simulation

We attempted to implement a modular code: the system to be simulated is considered as a set of fundamental objects connected each other in an appropriate way. Each object has a set of properties that must be specified, and a given number of input and output ports.

In order to understand better the idea we show in Listing 3.1 the definition of a simple resonant optical cavity.

```
1  cavity = qnSystem[
2      {
3      qnMirror[
4          "MIRROR1",
5          reflectivity -> Sqrt[1-(33/1000)],
6          inverseCurvatureRadius->-1/(2*CavityLength),
7          mechanicalTransferFunction -> pendulumMirror1
8      ],
9      qnMirror[
10         "MIRROR2",
11         reflectivity -> 1,
12         inverseCurvatureRadius -> 1/(2*CavityLength),
13         mechanicalTransferFunction -> pendulumMirror2,
14         forces -> {
15             0,
16             0,
17             -1/2 CavityLength qnOmega^2 mirrorMass1,
18             0,
19             0,
20             0
21         }
22     ],
23     qnPropagator[
24         "RightPropagator",
25         detuningFundamental -> d,
26         length -> CavityLength
27         ],
28     qnPropagator[
```

```
29          "LeftPropagator",
30          detuningFundamental -> d,
31          length -> CavityLength
32      ],
33      qnSource[
34          "Laser",
35          carriers -> {
36              HG[0, 0] -> {Sqrt[Power00], 0},
37              HG[1, 0] -> {Sqrt[2 Power10], 0}
38          }
39      ],
40      qnDetector[
41          "Reflected"
42      ],
43      qnSource[
44          "Vacuum"
45      ],
46      qnDetector[
47          "Transmitted"
48      ]
49      },
50      {
51          "Laser"."OUT1" -> "MIRROR1"."IN1",
52          "MIRROR1"."OUT1" -> "Reflected"."IN1",
53          "MIRROR1"."OUT2" -> "RightPropagator"."IN1",
54          "RightPropagator"."OUT1" -> "MIRROR2"."IN1",
55          "MIRROR2"."OUT1" -> "LeftPropagator"."IN1",
56          "LeftPropagator"."OUT1" -> "MIRROR1"."IN2",
57          "MIRROR2"."OUT2" -> "Transmitted"."IN1",
58          "Vacuum"."OUT1" -> "MIRROR2"."IN2"
59      },
60      modes -> {
61      HG[0, 0],HG[1,1]
62      },
63      temperature -> 300,
64      carrierwavelength -> lambda
65  ];
```

Listing 3.1: The definition of a simple resonant cavity, with a semitransparent front mirror and a completely reflective back one.

We see that to completely specify the system we must give three different kind of information, namely

1. the list of the objects which compose it. These are specified from line 3 to

line 49, and in the example are two mirrors, two propagators for the light inside the cavity, two sources of light and a detector.

2. The connections among the different objects composing the system. These are given from line 50 to line 59. For example, the directive at line 51 specify that the output of the “Laser” source is connected with the input “IN1” of the front mirror “MIRROR1”.

3. A list of general parameters, in this case the list of HG modes that are used in the simulation, the temperature and the carrier wavelength.

A “map” for the geometry of our system can be generated by our program: in Figure 3.3 the map for the Fabry-Pérot cavity described in Listing 3.1 is shown.

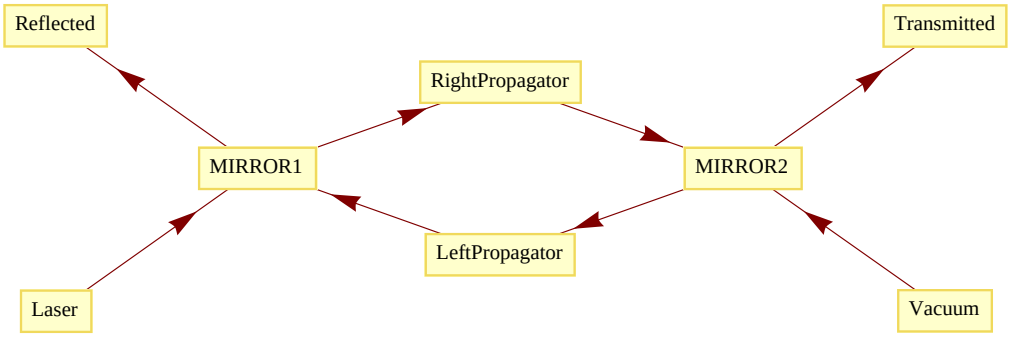

Figure 3.3: Map of the geometry of a Fabry-Pérot cavity printed by the simulation

3.3.1 Objects

Several objects are defined in the code. We give some details on the three fundamental ones, which are the mirror (qnMirror), the light propagator (qnPropagator) and the light source (qnSource).

qnSource

This is a simple object which represents a source of light. It has just a single output port (see Listing 3.2, line 4) which can be connected to the input port of another object. It can provide a superposition of several modes, with given values of the carrier fields. In the current version each mode is a coherent state, but with trivial modifications which are foreseen for the future it will be able to provide a squeezed state with the required parameters.

```
1  qnSource[name_, OptionsPattern[]] := qnSource[
2      name,
3      {
4          qfield[name,"OUT1"]
5      },
6      {
7      },
8      {
9          qsource[name,"OUT1"]
10     },
11     {
12         {
13             "CARRIERS",
14             OptionValue[carriers]
15         }
16     }
17 ];
```

Listing 3.2: The basic structure of a qnSource object.

qnPropagator

This object represent the free propagation of light from two different points. It has a single input port (Listing 3.3, line 4), which should be connected with the start point for the propagation, and a single output port (Listing 3.3, line 5), which should be connected with the end point.

It has an important parameter, which is the detuning of the fundamental HG_{00} mode, which should be specified.

```
1  qnPropagator[name_, OptionsPattern[]] := qnPropagator[
2      name,
3      {
4          qfield[name,"IN1"],
5          qfield[name,"OUT1"]
6      },
7      {
8      },
9      {
10     },
11     {
12     {
13         "DETUNINGFUNDAMENTAL",
14         OptionValue[detuningFundamental]
```

```
15      },
16      {
17          "LENGTH",
18          OptionValue[length]}
19      }
20  ];
```

Listing 3.3: The basic structure of a qnPropagator object.

qnMirror

This is a more complex object, which represent a semitransparent mirror. In has two input ports (Listing 3.4, lines 4,6) and two output ports (Listing 3.4, lines 5,7). The input ports represent the end points for the incident fields (from the two side of the mirror). The output ports represent the starting point for the reflected fields.

This object has some internal mechanical degrees of freedom, represented in (Listing 3.4 from line 10 to line 15). They are the six degrees of freedom of a rigid body (though in the current version only the ones corresponding to δZ, $\delta\theta_x$ and $\delta\theta_y$ are used).

```
 1  qnMirror[name_, OptionsPattern[]] := qnMirror[
 2      name,
 3      {
 4          qfield[name,"IN1"],
 5          qfield[name,"OUT1"],
 6          qfield[name,"IN2"],
 7          qfield[name,"OUT2"]
 8      },
 9      {
10          mfield[name,"x"],
11          mfield[name,"y"],
12          mfield[name,"z"],
13          mfield[name,"rx"],
14          mfield[name,"ry"],
15          mfield[name,"rz"]
16      },
17      {
18      },
19      {
20          {
21              "INVERSECURVATURERADIUS",
22              OptionValue[inverseCurvatureRadius]
```

```
23          },
24          {
25              "FORCESCALING",
26              OptionValue[forceScaling]
27          },
28          {
29              "REFLECTIVITY",
30              OptionValue[reflectivity]
31          },
32          {
33              "MECHANICALTRANSFERFUNCTION",
34              OptionValue[mechanicalTransferFunction]
35          },
36          {
37              "FORCES",
38              OptionValue[forces]
39          },
40          {
41              "LOSSES",
42              OptionValue[losses]
43          }
44      }
45  ];
```

Listing 3.4: The basic structure of a qnMirror object.

Several interesting parameters can be defined, both optical (the inverse curvature radius, the reflectivity, the losses) and mechanical. In particular, an arbitrary mechanical transfer function for the mirror can be specified. The idea is that the motion equations for the relevant degrees of freedom of the mirror can be written in the frequency domain as

$$\boldsymbol{\chi} \begin{pmatrix} \delta\tilde{Z} \\ \delta\tilde{\theta}_x \\ \delta\tilde{\theta}_y \end{pmatrix} = \begin{pmatrix} \tilde{F}_z \\ \tilde{M}_x \\ \tilde{M}_y \end{pmatrix}$$

where $\boldsymbol{\chi}$ is a (frequency dependent) matrix. Two examples are given in Listing 3.5. The first one describes a free rigid body, the second a mirror subject to restoring forces (for example, a suspended one) that can be described by three independent harmonic oscillators.

```
1  pendulumMirror1[omega_] := DiagonalMatrix[
2      {
3      1,0,0,0,0,0,
```

```
4       0,1,0,0,0,0,
5       0,0,-mirrorMass1 omega^2,0,0,0,
6       0,0,0,-mirrorIx omega^2,0,0,
7       0,0,0,0,-mirrorIy omega^2,0,
8       0,0,0,0,0,1
9       }
10  ];
11  pendulumMirror2[omega_] := DiagonalMatrix[
12      {
13      1,0,0,0,0,0,
14      0,1,0,0,0,0,
15      0,0,mirrorMass1*(omegaP^2-omega^2),0,0,0,
16      0,0,0,mirrorIx*(omegaTx^2-omega^2),0,0,
17      0,0,0,0,mirrorIy*(omegaTy^2-omega^2),0,
18      0,0,0,0,0,1
19      }
20  ];
```

Listing 3.5: Two different specifications for the (inverse) mechanical transfer function of a mirror.

It is quite easy to introduce more complicated models, in particular

- dissipations, which are relevant for the dynamics but above all for the valuation of the thermal noise;
- coupling between degrees of freedom and additional (hidden) degrees of freedom, for example the ones which are needed to describe a suspension used for seismic noise attenuation.

3.3.2 Modelization

Objects can have a different number of ways in and ways out, which represent the "ports" of the system and the places where we want to know the fields values. If an optical element has k output ports it also provides k relations which allow to evaluate outputs when inputs and internal degrees of freedom are known. For example a mirror has four nodes (two input and two output) and provides two relations. A propagator has two nodes, connected by one relation. Sources have just one output node and one relation. Ultimately we will have N equations, which results by multiplying the number of nodes for the number of quadratures and the number of modes, when relevant.

There are several task that must be done in order to obtain the final result, which is the information about the statistical properties of the fluctuations of the variables of interest, namely

- the basis for HG modes to be used must be evaluated, given the parameters of the optical elements;
- the classical fields at each port must be evaluated: in order to do that the previous step must be completed first;
- the amplitude of fluctuations for the optical and mechanical fields of interest must be evaluated at each port. This requires the previous two steps to be completed first.

Conceptually all these steps requires the solution of a system of equations which is constructed following the same procedure we just explained.

Basis evaluation

Since we are not dealing with plane waves but with HG modes which need to be matched to the cavities, we associate to the optical fields in every point the parameter $q(z)$ we defined in (2.5a). It keeps all information about the mode shape and could be "propagated" throw different optical elements using the relations we gave in (2.1.2). Each object provides a peculiar rule that connect the q parameter value at its ports, which is obtained using the ABCD formalism described in Section 2.1.2.

```
1  qnQParameterRule[o_qnPropagator] := Block[{a,b,c,d},
2      a = 1;
3      b = gparameter[o,"LENGTH"];
4      c = 0;
5      d = 1;
6      {
7          gqfield[o,2] == (a*gqfield[o,1]+b)/(c*gqfield[o,1]+d)
8      }
9  ];
10
11 qnQParameterRule[o_qnMirror]:= Block[{a,b,c,d},
12     a = 1;
13     b = 0;
14     c=-2*gparameter[o,"INVERSECURVATURERADIUS"];
15     d = 1;
16     {
17         gqfield[o,2]==(a*gqfield[o,1]+b)/(c*gqfield[o,1]+d),
18         gqfield[o,4]==(a*gqfield[o,3]+b)/(-c*gqfield[o,3]+d),
19         gqfield[o,2]==gqfield[o,3],
20         gqfield[o,4] == gqfield[o,1]
```

```
21      }
22  ];
```

Listing 3.6: The equations which connect the q parameters defined at different ports of an object, for the qnPropagator and for the qnMirror.

We give a couple of examples in Listing 3.6, where the functions defined for the qnPropagator and the qnMirror object are shown. These correspond simply to the rules M_L and M_R defined in Section 2.1.2.

Classical fields evaluation

Each object provides also the rules which connect classical fields defined at its ports.

```
qnRule0[o_qnPropagator,qpar_,mode_]  := Block[
    {res,inf,outf,phase,q1,q2},
    q1 = gqfield[o,2] /. qpar;
    q2 = gqfield[o,1] /. qpar;
    phase = gparameter[o,"DETUNINGFUNDAMENTAL"]
        +gouy[q1,q2]*index[mode];
    inf = {gqfield0[o,2,"0"],gqfield0[o,2,"1"]};
    outf = propagator0[phase].{
        gqfield0[o,1,"0"],
        gqfield0[o,1,"1"]
    };
    res=Thread[Equal[inf,outf]];
    Return[res]
];

qnRule0[o_qnMirror,qpar_,mode_] := Block[{res,r,t},
    r = gparameter[o,"REFLECTIVITY"];
    t = Sqrt[1-r^2-gparameter[o,"LOSSES"]^2];
    res = {
        gqfield0[o,2,"0"] == -r gqfield0[o,1,"0"]
            + t gqfield0[o,3,"0"],
        gqfield0[o,4,"0"] == r gqfield0[o,3,"0"]
            + t gqfield0[o,1,"0"],
        gqfield0[o,2,"1"] == -r gqfield0[o,1,"1"]
            + t gqfield0[o,3,"1"],
        gqfield0[o,4,"1"] == r gqfield0[o,3,"1"]
            + t gqfield0[o,1,"1"]
    };
    Return[res]
```

```
30 ];
```

Listing 3.7: The equations which connect the classical (carrier) fields defined at different ports of an object, for the qnPropagator and for the qnMirror.

We give once again two examples in Listing 3.7, where the functions defined for the qnPropagator and the qnMirror are shown. In the first case this is just the implementation of Equation 3.5, in the second of Equation 3.6.

Fluctuation evaluations

Conceptually this step is very similar to the previous one. The main difference is that the rule which each object provides depends from the classical fields, and this is the reason why these must be evaluated first.

Another difference is that, besides the optical fluctuations, an additional set of variables can be defined by an object. These can be mechanical degrees of freedom, thermal force sources, additional fields which describe losses effects.

```
1  gammaP[n_] := -1/2 Sqrt[n+1];
2  gammaM[n_] := -1/2 Sqrt[n];
3
4  tiltP[n_] := {
5      {
6      (gammaP[n]-gammaM[n+1])/(2 I ),
7      (gammaP[n]+gammaM[n+1])/(2)
8      },
9      {
10     -(gammaP[n]+gammaM[n+1])/(2),
11     (gammaP[n]-gammaM[n+1])/(2 I)
12     }
13 };
14
15 tiltM[n_] := {
16     {
17     (gammaM[n]-gammaP[n-1])/(2 I),
18     (gammaM[n]+gammaP[n-1])/(2)
19     },
20     {
21     -(gammaM[n]+gammaP[n-1])/(2),
22     (gammaM[n]-gammaM[n-1])/(2 I)
23     }
24 };
25
```

```
26 qnRule1[o_qnMirror,qpar_,rule0_,sysopt_] := Block[
27     {
28     r,t,
29     outfa,outfb,
30     mira,mirb,
31     modza,modzb,
32     modrxa,modrxb,
33     modrya,modryb,
34     m,n,
35     gmx,gmy,
36     res,modg,omegac,modes,gopt,lambda,wc,gf,frc,outf,
37     Fz,Mx,My,
38     tfrcs,tf1,tf2,tf3,tf4,tf5,tf6
39     },
40     r = gparameter[o,"REFLECTIVITY"];
41     t = Sqrt[1-r^2-gparameter[o,"LOSSES"]^2];
42     modes = gparameterfromlist[sysopt,"MODES"];
43     lambda = gparameterfromlist[sysopt,"CARRIERWAVELENGTH"];
44     wc = 2 Pi/lambda*qnC;
45     gopt = 2 wc/(qnC Sqrt[qnHbar wc]);
46     outfa = {
47         gqfield1[o,2,"0",HG[m,n]],
48         gqfield1[o,2,"1",HG[m,n]]
49     };
50     outfb = {
51         gqfield1[o,4,"0",HG[m,n]],
52         gqfield1[o,4,"1",HG[m,n]]
53     };
54     mira = {
55     -r gqfield1[o,1,"0",HG[m,n]] + t gqfield1[o,3,"0",HG[m,n]],
56     -r gqfield1[o,1,"1",HG[m,n]] + t gqfield1[o,3,"1",HG[m,n]]
57     };
58     mirb = {
59     r*gqfield1[o,3,"0",HG[m,n]] + t gqfield1[o,1,"0",HG[m,n]],
60     r*gqfield1[o,3,"1",HG[m,n]] + t gqfield1[o,1,"1",HG[m,n]]
61     };
62     modza = r*gopt*gmfield[o,3]*propagator0[-Pi/2].{
63         gqfield0[o,1,"0",HG[m,n]],
64         gqfield0[o,1,"1",HG[m,n]]
65     };
66     modzb = r*gopt*gmfield[o,3]*propagator0[-Pi/2].{
67         gqfield0[o,3,"0",HG[m,n]],
68         gqfield0[o,3,"1",HG[m,n]]
```

```
69      };
70      modrxa = r*gopt*gmfield[o,4]*(
71          tiltP[n].{
72              gqfield0[o,1,"0",HG[m,n+1]],
73              gqfield0[o,1,"1",HG[m,n+1]]
74              }
75          + tiltM[n].{
76              gqfield0[o,1,"0",HG[m,n-1]],
77              gqfield0[o,1,"1",HG[m,n-1]]
78          }
79      );
80      modrxb = r*gopt*gmfield[o,4]*(
81          tiltP[n].{
82              gqfield0[o,3,"0",HG[m,n+1]],
83              gqfield0[o,3,"1",HG[m,n+1]]
84          }
85          +   tiltM[n].{
86              gqfield0[o,3,"0",HG[m,n-1]],
87              gqfield0[o,3,"1",HG[m,n-1]]
88          }
89      );
90      modrya = r*gopt*gmfield[o,5]*(
91          tiltP[m].{
92              gqfield0[o,1,"0",HG[m+1,n]],
93              gqfield0[o,1,"1",HG[m+1,n]]
94          }
95          +   tiltM[m].{
96              gqfield0[o,1,"0",HG[m-1,n]],
97              gqfield0[o,1,"1",HG[m-1,n]]
98          }
99      );
100     modryb = r*gopt*gmfield[o,5]*(
101         tiltP[m].{
102             gqfield0[o,3,"0",HG[m+1,n]],
103             gqfield0[o,3,"1",HG[m+1,n]]
104         }
105         +   tiltM[m].{
106             gqfield0[o,3,"0",HG[m-1,n]],
107             gqfield0[o,3,"1",HG[m-1,n]]
108         }
109     );
110     res = Join[
111         MapThread[
```

```
112             Equal,
113             {outfa,mira+modza+modrxa+modrya}
114         ],
115         MapThread[
116             Equal,
117             {outfb,mirb+modzb+modrxb+modryb}
118         ]
119     ];
120
121     (* All modes *)
122     res = Map[
123         (res /. {m->#[[1]],n->#[[2]]})&,
124         modes
125     ];
126     res = res /. {
127         qfield1[_,_,_,mode_HG] :> 0 /; Not[MemberQ[modes,mode]]
128     };
129     res = res /. {
130         qfield0[_,_,_,mode_HG] :> 0 /; Not[MemberQ[modes,mode]]
131     };
132     res = Flatten[res /. rule0];
133
134     (* radiation pressure *)
135     outf = gparameter[o,"MECHANICALTRANSFERFUNCTION"][qnOmega].{
136         gmfield[o,1],
137         gmfield[o,2],
138         gmfield[o,3],
139         gmfield[o,4],
140         gmfield[o,5],
141         gmfield[o,6]
142     };
143
144     gopt = Sqrt[qnHbar wc/qnC^2];
145
146     gf[f_] :=
147         gqfield0[o,f,"0",HG[m,n]]
148             *gqfield1[o,f,"0",HG[m,n]]
149         +gqfield0[o,f,"1",HG[m,n]]
150             *gqfield1[o,f,"1",HG[m,n]];
151
152     gmx[f_] :=
153         gammaP[n]*(
154             gqfield0[o,f,"0",HG[m,n]]
```

```
155                 *gqfield1[o,f,"0",HG[m,n+1]]
156             +gqfield0[o,f,"1",HG[m,n]]
157                 *gqfield1[o,f,"1",HG[m,n+1]]
158         )
159         +gammaM[n]*(
160             gqfield0[o,f,"0",HG[m,n]]
161                 *gqfield1[o,f,"0",HG[m,n-1]]
162             +gqfield0[o,f,"1",HG[m,n]]
163                 *gqfield1[o,f,"1",HG[m,n-1]]
164         );
165
166     gmy[f_] :=
167         -gammaP[m]*(
168             gqfield0[o,f,"0",HG[m,n]]
169                 *gqfield1[o,f,"0",HG[m+1,n]]
170             +gqfield0[o,f,"1",HG[m,n]]
171                 *gqfield1[o,f,"1",HG[m+1,n]]
172         )
173         -gammaM[m]*(
174             gqfield0[o,f,"0",HG[m,n]]
175                 *gqfield1[o,f,"0",HG[m-1,n]]
176             +gqfield0[o,f,"1",HG[m,n]]
177                 *gqfield1[o,f,"1",HG[m-1,n]]
178         );
179
180     Fz = gopt*(gf[1]+gf[2]-gf[3]-gf[4]);
181     Mx = gopt*(gmx[1]+gmx[2]-gmx[3]-gmx[4]);
182     My = gopt*(gmy[1]+gmy[2]-gmy[3]-gmy[4]);
183
184     frc = { 0, 0, Fz, Mx, My, 0 };
185
186     (* all modes *)
187     frc = Map[
188         (frc /. {
189             m->#[[1]],n->#[[2]]
190             })&,
191         modes
192     ];
193
194     frc = frc /. {
195         qfield1[_,_,_,mode_HG] :> 0 /; Not[MemberQ[modes,mode]]
196     };
197     frc = frc /. {
```

```
198         qfield0[_,_,_,mode_HG] :> 0 /; Not[MemberQ[modes,mode]]
199     };
200     frc = Apply[Plus,frc];
201     frc = frc /. rule0;
202
203     (* apply scaling *)
204     frc = frc.gparameter[o,"FORCESCALING"];
205
206     (* add external forces *)
207     frc = frc + qsource1["EXTERNAL"]*gparameter[o,"FORCES"];
208
209     (* add thermal forces if needed *)
210     If[
211         gparameterfromlist[sysopt,"TEMPERATURE"]>0,
212         tfrcs = Im[
213             gparameter[o,"MECHANICALTRANSFERFUNCTION"][qnOmega]
214         ]
215     ];
216
217     tfrcs = Eigensystem[tfrcs];
218     tfrcs = DiagonalMatrix[Sqrt[tfrcs[[1]]]].tfrcs[[2]];
219     frc = frc
220         +Sqrt[4*qnKB*gparameterfromlist[sysopt,"TEMPERATURE"]]*
221         Transpose[tfrcs].Table[
222             qsource1["THERMAL",Unique[]],
223             {6}
224         ];
225     ];
226
227     frc = MapThread[Equal,{outf,frc}];
228     Return[Join[frc,res]]
229 ];
```

Listing 3.8: The equations which connect the fluctuating fields defined at different ports of an object in the case of qnMirror.

In Listing 3.8 we show an example of the function which provides the relation between fluctuations, in the qnMirror case. Basically the rules (3.26), (3.24) and (3.25) for the modulation are implemented, together with the motion equations (3.14) for the radiation pressure forces and the analogous ones (3.19), (3.20) for the radiation pressure torques. The final result is a linear relation between the fluctuating variables $\underline{f}$ and the sources $\underline{s}$

$$\boldsymbol{C}_{N\times N}\,\underline{f}_N = \boldsymbol{P}_{N\times k}\,\underline{s}_k$$

which must be inverted, obtaining

$$\underline{f}_N = \boldsymbol{C}^{-1}_{N\times N}\,\boldsymbol{P}_{N\times k}\,\underline{s}_k$$

Once we know this relation we can extract information about noise and squeezing. To begin with, we calculate the spectral density matrix associated with the fields, which is given by

$$\begin{aligned}\boldsymbol{\Sigma} \equiv \left\langle \underline{f}_N \underline{f}_N^\dagger \right\rangle &= \left\langle \boldsymbol{C}^{-1}_{N\times N}\,\boldsymbol{P}_{N\times k}\,\underline{s}_k\,\underline{s}_k^\dagger\,\boldsymbol{P}^\dagger_{k\times N}\,\boldsymbol{C}^{-1\dagger}_{N\times N} \right\rangle \\ &= \boldsymbol{C}^{-1}_{N\times N}\,\boldsymbol{P}_{N\times k}\left\langle \underline{s}_k\,\underline{s}_k^\dagger \right\rangle \boldsymbol{P}^\dagger_{k\times N}\,\boldsymbol{C}^{-1\dagger}_{N\times N} \end{aligned} \tag{3.29}$$

where we indicate with $\langle\cdots\rangle$ the expectation value and we used the fact that the arrays $\boldsymbol{C}$ and $\boldsymbol{P}$ are not stochastic. Assuming that the statistical properties of the sources are known, we can evaluate the matrix $\left\langle \underline{s}_k\,\underline{s}_k^\dagger \right\rangle$[3].

From the real part of $\boldsymbol{\Sigma}$, called covariance matrix (see Section 2.6.3) we know the correlation of phase and amplitude fluctuations, both for a single mode and for quadratures of different modes. Notable quantities which can be used to describe the squeezing are the squeezing parameter, the squeezing angle and the way the vary with the sidebands angular frequency Ω.

```
1  qnEvalCovarianceArray[obj_qnSystem, pattern_, OptionsPattern[]]
2    := Block[{w, qf, sol, res, flds, srcs, ca, eqns},
3    qf = qnEvalQuantumFields[obj];
4    If[
5      !MatchQ[OptionValue[frequency], False],
6      w = OptionValue[frequency];
7      qf = qf /. qnOmega -> w
8    ];
9    Message[qnEvalCovarianceArray::step0];
10
11   sol = qnSolve[qf];
12   Message[qnEvalCovarianceArray::step1];
13
14   res = Select[sol[[1]], MatchQ[#[[1]], pattern]&];
15   If[
16     OptionValue[thermalnoise]==False,
17     res = res /. qsource1["THERMAL", _] :> 0
18   ];
19   If[
```

[3] As we said currently it is assumed that all the sources are described by coherent states, but it is easy to generalize this.

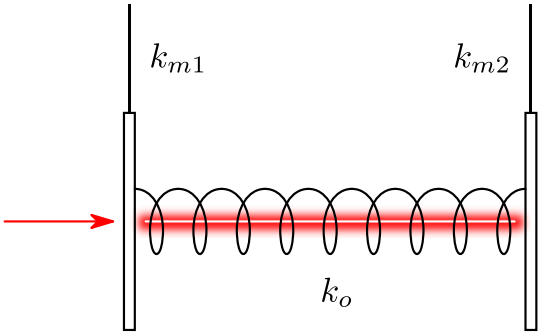

Figure 3.4: A generic model for the cavities considered. The parameters k_{m1} and k_{m2} represent the restoring mechanical forces of the mirrors, and k_o the optical stiffness induced by the optical spring effect discussed.

```
20      OptionValue[quantumnoise]==False,
21      res = res  /. qsource1[_,_,_,_] :> 0
22    ];
23    If[OptionValue[externalforces]==False,
24      res = res /. qsource1["EXTERNAL"] :>0
25    ];
26    flds = Map[#[[1]]&,res];
27    eqns = Map[#[[2]]&,res];
28    srcs = Union[Cases[eqns,qsource1[__],-1]];
29    ca = CoefficientArrays[eqns,srcs];
30
31    (* assuming coherent sources *)
32    res = qnCovarianceArray[
33        Normal[ca[[2]].Transpose[Conjugate[ca[[2]]]]],
34        flds
35    ];
36    Return[res];
37  ];
```

Listing 3.9: The evaluation of the covariance array.

The procedure used to evaluate the covariance array is listed in 3.9. We stress that the covariance array is a function of the frequency Ω. Contributions from external forces and thermal noise can be added to the result under request.

3.4 Some results for the fundamental mode

Although our code is explicitly built to deal with more than one carrier in different HG modes, it is worth starting taking into account only the fundamental mode. That allows to check the code in a simplified configuration, without tilting effect on the mirrors, comparing the results with the ones obtained for plane waves. A study of the squeezing of the fundamental mode will also help us to point out its interrelation with the system parameters (mirrors masses and reflectivity, laser power, cavity detuning etc..) and to discuss some interesting issues such as losses and optical spring effect. We will use the code in two particular configurations:

- "Large" cavity (LC): a kilometer scale Fabry-Pérot cavity of a large interferometer, such as VIRGO or LIGO, built to detect gravitational waves. Though the ponderomotive squeezing is rather a “by-product” for such cavities, some techniques to exploit it in order to reduce quantum noise has been proposed [4];

- SC: a smaller meter scale Fabry-Pérot cavity as the one proposed in [12] or in "*Progetto PRIN di Ponderomotive Squeezing*" (PPPS), see `http://www.ppps.it/`, especially designed to produce ponderomotive squeezed light.

In both cases the cavity can be schematized as the one depicted in Figure 3.4. The choice for the default parameters values, shown in Table 3.2, reflects the different purpose of the two optical systems. In the following we will present the effect of varying some of them.

	LC	SC
cavity length	4000 m	1 m
Laser Power	1 W	4 W
Laser wavelength	10^{-6}m	10^{-6}m
Input mirror transmission	$3.3 \cdot 10^{-2}$	$8 \cdot 10^{-4}$
end mirror transmission	0	0
front mirror mass	30 kg	0.25 kg
end mirror mass	30 kg	0.001 kg

Table 3.2: The main parameters of the two cavities studied. When not otherwise specified, these are the values used in the simulations.

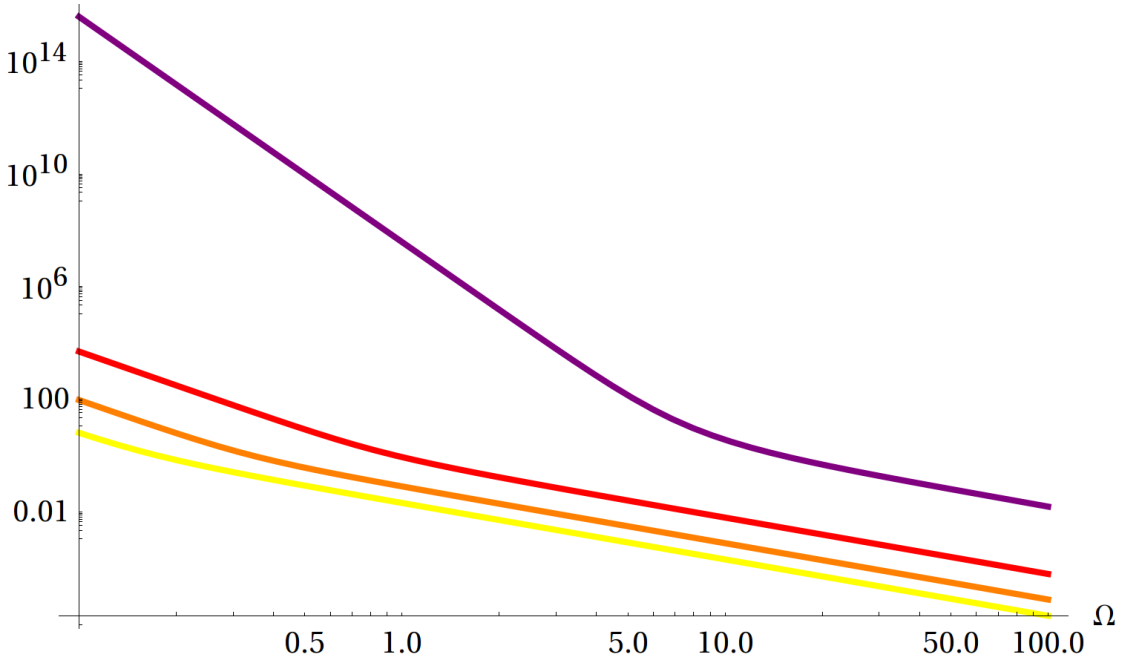

Figure 3.5: Plot of the Squeezing ratio ρ for a resonant LC in function of the sideband angular frequency Ω for different values of the end mirror reflectivity r_2: $r_2 = 1$ (purple), $r_2 = 0.95$ (red), $r_2 = 0.9$ (orange), $r_2 = 0.7$ (yellow). The bi-logarithmic scale shows that ρ decreases approximatively with different power law in regions where the effect of r_2 is relevant or not.

3.4.1 Lower values of the end mirror reflectivity: losses and squeezing deterioration

In order to give a simple characterization of the level of squeezing we will use a squeezing ratio, defined as the ratio between the larger and the smaller eigenvalue of the covariance array $\mathbf{\Sigma}$ for the two quadratures of the mode. In Fig. 3.5 the squeezing ratio of the outgoing field in a LC is plotted in function of the sideband angular frequency Ω for different values of the end mirror reflectivity r_2. It is evident that the squeezing level decreases whit the reflectivity. It can be attributed to two different effects.

The first is the reduction of the radiation force on the mirrors, due to the reduction of the power inside the cavity. The second is the introduction of non-squeezed vacuum fluctuations which enter the cavity from the back mirror. As discussed previously, they are needed in order to preserve the correct commutation relations for quantum operators associated with quantum fluctuations. This

mechanism can be derived from the simple model for mirror losses discussed previously (see Section 3.2.2). Suppose that a coherent field $\hat{a}$ is impinging on a movable mirror. If the mirror is completely reflective the outgoing field $\hat{b}$ will be

$$\hat{b} = \begin{pmatrix} 1 & 0 \\ -k & 1 \end{pmatrix} \hat{a}$$

where we see that amplitude and phase fluctuation are correlated because of radiation pressure. The squeezing ratio for the field $\hat{a}$ will be

$$\rho \equiv \frac{\lambda_{\text{max}}}{\lambda_{\text{min}}} = \left[1 + \frac{k}{2}\left(\sqrt{k^2+4} + k\right)\right]^2 \simeq k^4$$

where the last equality is true when $k \gg 1$. If the mirror has a reflectivity r, the total outgoing field $\hat{c}$ will be the sum of the reflected part of $\hat{b}$ and the transmitted vacuum fluctuation $\vec{w}$ (see Figure 3.2).

$$\hat{c} \;=\; r \begin{pmatrix} 1 & 0 \\ -k' & 1 \end{pmatrix} \hat{a} + \sqrt{1-r^2}\hat{w} = r\hat{b} + \sqrt{1-r^2}\hat{w} \tag{3.30}$$

Since the parameter k depends on the radiation pressure, which in turn depends on r, it changes from the completely reflective case. If we suppose k real the correlation matrix of $\hat{c}$ is

$$\begin{aligned} \boldsymbol{C} = \left\langle \hat{c}\,\hat{c}^\dagger \right\rangle &= r^2 \left\langle \hat{b}\,\hat{b}^\dagger \right\rangle + \left(1-r^2\right) \left\langle \hat{w}\,\hat{w}^\dagger \right\rangle + r\sqrt{1+r^2} \left\langle \hat{b}\,\hat{b}^\dagger + \hat{w}\,\hat{b} \right\rangle \\ &= r^2 \begin{pmatrix} 1 & -k \\ -k & 1+k^2 \end{pmatrix} + \left(1-r^2\right) \begin{pmatrix} 1 & 0 \\ 0 & 1 \end{pmatrix} \\ &= \begin{pmatrix} 1 & -r^2 k \\ -r^2 k & 1+r^2 k^2 \end{pmatrix} \end{aligned} \tag{3.31}$$

where we used the fact that $\hat{w}$ is a coherent state while $\left\langle \vec{b}\,\vec{w} + \vec{w}\,\vec{b} \right\rangle = 0$ since $\vec{b}$ and $\vec{w}$ are not correlated. In this case the squeezing ratio is given by

$$\frac{\lambda_{\text{max}}}{\lambda_{\text{min}}} = \frac{2 + k\left(\sqrt{k^2+4} + k\right) r^2}{2 - k\left(\sqrt{k^2+4} - k\right) r^2}$$

In Figure 3.6, we plotted the error ellipse associated with this covariance matrix for decreasing values of the reflectivity r. It is evident that the squeezing deteriorates when the reflectivity decreases.

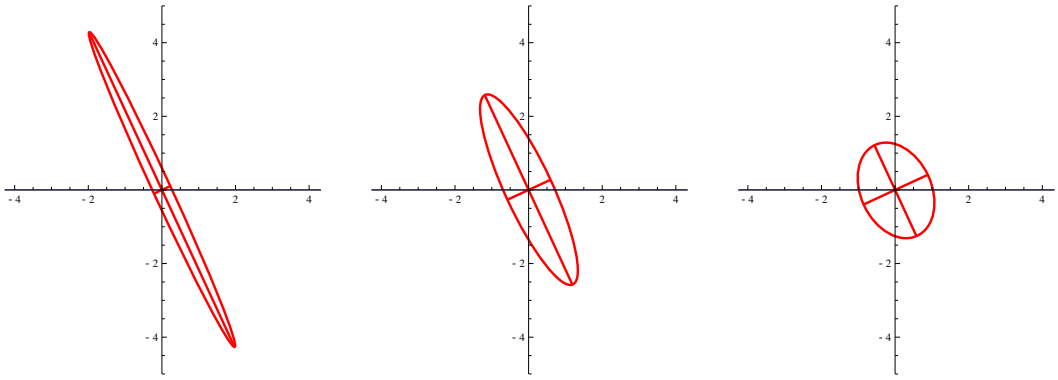

Figura 3.6: Error ellipse associated with this covariance matrix for different value of the reflectivity r: $r = 1$, $r = 0.6$ e $r = 0.25$. A deterioration of the squeezing for lower level of reflectivity can be clearly observed.

3.4.2 Mirror masses and laser power influences on the squeezing

The plot in Figure 3.7 represents the squeezing ratio as a function of the sideband angular frequency Ω for a resonant LC with four different values of the end mirror mass. It is evident how with lighter mirror an higher level of squeezing is achieved. This is clearly due to a more effective response to radiation force (i.e. amplitude fluctuations) which result in a stronger correlation between amplitude and phase noises.

This effect is achievable, for the same reason, enhancing the laser power, as we can see in Fig. 3.8 where the squeezing ratio is plotted for four different values of the laser power, while the mirror masses are kept fixed.

This explain why in SC it has been opted for lighter mirrors and a more powerful laser.

3.4.3 Squeezing in a detuned cavity: optical spring effect

As previously discussed in 2.1.6, in a detuned cavity the movables mirrors behave as two harmonic oscillators coupled by means of an optical spring. The optical spring constant will modify the total spring constant of the system and will shift the frequency at which resonances occur. So far we have left out the pendulum mechanical frequency of the mirrors (and treated them as free masses) because it is usually very small compared to the the frequencies where we are looking for squeezing effects. In fact usually the mechanical frequency of the mirrors affects the squeezing in regions where thermal and seismic noises are so high that a reduction of quantum noise can't be appreciated. For a complete discussion of

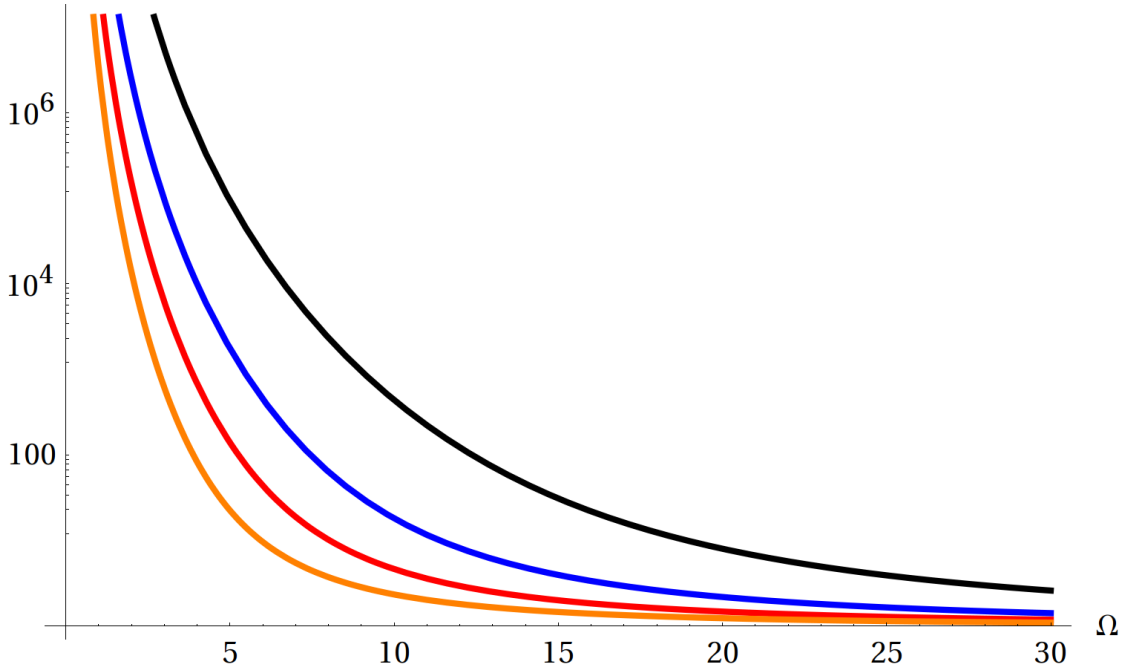

Figure 3.7: Squeezing ratio for a resonant LC as a function of the sideband angular frequency Ω with four different values of the end mirror mass: $3\mathrm{kg}$ (black), $10\mathrm{kg}$ (blue), $30\mathrm{kg}$ (red), $300\mathrm{kg}$ (yellow).

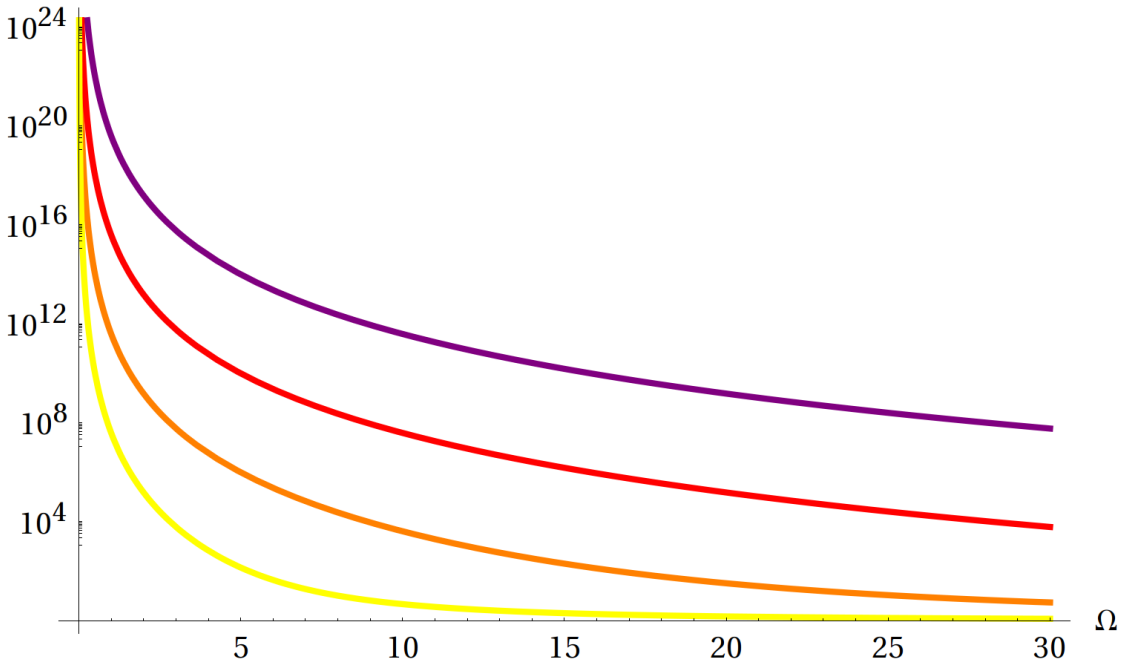

Figure 3.8: Squeezing ratio for a resonant LC in function of the sideband angular frequency Ω with four different values of the end mirror mass: $1\mathrm{W}$ (yellow), $10\mathrm{W}$ (orange), $100\mathrm{W}$ (red), $1000\mathrm{W}$ (purple).

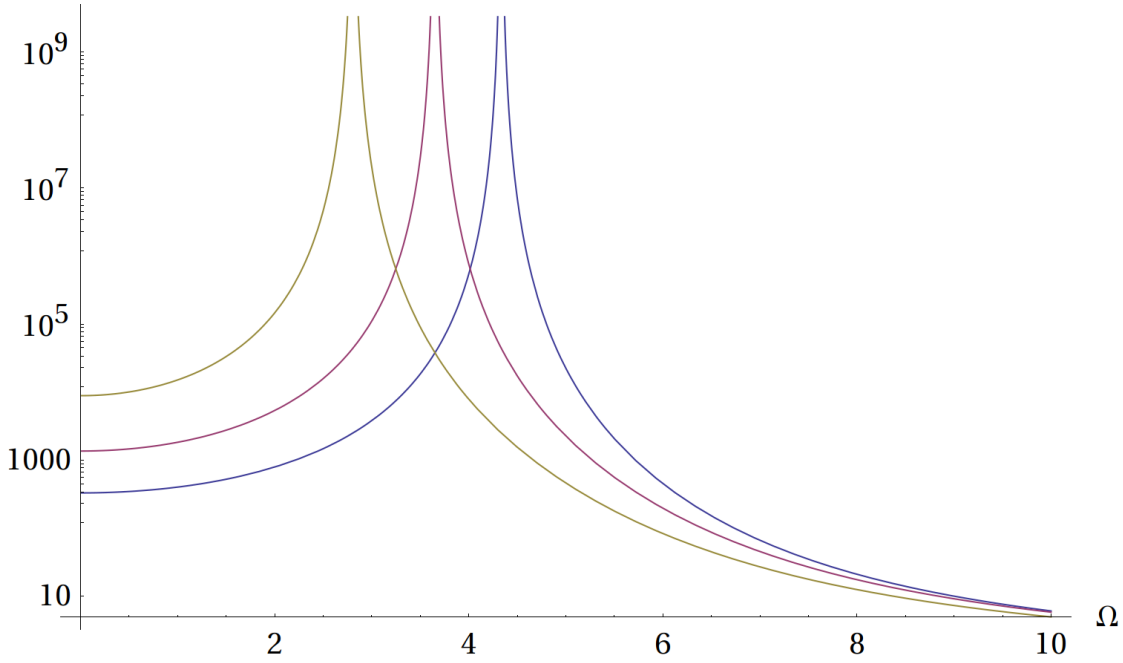

Figure 3.9: Squeezing ratio for a resonant LC as a function of the sideband angular frequency Ω with four different values of the detuning. In the central plot (purple curve) cavity is not detuned ($\Delta = 0$) and we see that it is shifted to the right (blue curve) when $\Delta = -1.2 \times 10^{-5}$ and the optical stiffness is positive, and to the left when $\Delta = +1.2 \times 10^{-5}$ and the optical stiffness is negative. We set $\omega_{m1} = \omega_{m2} = 3.65 \mathrm{rad\,s^{-1}}$

the mirror motions we now assume for the mirrors a pendulum frequency ω_m.

Figure 3.9 shows the squeezing in function of Ω for a LC with three different values of detuning $\Delta = 0$, $\Delta = \pm 1.2 \cdot 10^{-5}$. The central peak represents the resonance when the cavity is not detuned ($\Delta = 0$) and we see that it is shifted to the right when $\Delta < 0$ and the optical stiffness is positive, and to the left when $\Delta > 0$ and the optical stiffness is negative. This simple example suggests that it is possible to exploit the optical spring effect, caused by detuning, to shift the squeezing curve and make it larger in frequency regions which are more interesting to us. We will see that this strategy results more convenient in terms of thermal noise reduction than to use an higher pendulum frequency in a resonant cavity.

In general the squeezing curve is obtained from the noise information of the outgoing fields which are found solving the system we illustrate before. However, it is possible to infer something about its resonances by looking at the motion equations of the mirrors, assuming that, for high-finesse cavity, the squeez-

ing is linked to its relative motion $x_1 - x_2$. The mirrors are regarded as a pair of coupled harmonic oscillators

$$\begin{aligned} -m_1\Omega^2 x_1 &= k_o\,(x_2 - x_1) - k_{m1}x_1 - F \\ -m_2\Omega^2 x_2 &= k_o\,(x_1 - x_2) - k_{m2}x_2 + F \end{aligned}$$

where k_o is the optical spring constant, depending on detuning, power and cavity finesse; k_{m1} and k_{m2} are the mechanical pendulum constants of the mirrors and the radiation pressure force F is assume to be the same (with opposite direction) because of the high finesse[4].

$$\begin{aligned} \left[-\Omega^2 + \frac{k_0}{m_1} + \frac{k_{m1}}{m_1}\right] x_1 - \frac{k_o}{m_1}x_2 &= -\frac{F}{m_1} \\ \left[-\Omega^2 + \frac{k_0}{m_2} + \frac{k_{m2}}{m_2}\right] x_2 - \frac{k_o}{m_2}x_1 &= \frac{F}{m_2} \end{aligned}$$

the systems can be written as

$$\begin{pmatrix} \omega_{o1}^2 + \omega_{m1}^2 - \Omega^2 & -\omega_{o1}^2 \\ -\omega_{o2}^2 & \omega_{o2}^2 + \omega_{m2}^2 - \Omega^2 \end{pmatrix} \begin{pmatrix} x_1 \\ x_2 \end{pmatrix} = \begin{pmatrix} -\frac{F}{m_1} \\ \frac{F}{m_2} \end{pmatrix}$$

by calling M the coefficient matrix, it becomes

$$\begin{pmatrix} x_1 \\ x_2 \end{pmatrix} = \frac{1}{\det M} \begin{pmatrix} \omega_{o2}^2 + \omega_{m2}^2 - \Omega^2 & \omega_{o1}^2 \\ \omega_{o2}^2 & \omega_{o1}^2 + \omega_{m1}^2 - \Omega^2 \end{pmatrix} \begin{pmatrix} -\frac{F}{m_1} \\ \frac{F}{m_2} \end{pmatrix} \tag{3.32}$$

in the case of Fig 3.9 $\omega_{o1}^2 = \omega_{o2}^2 = \omega_o^2$, $\omega_{m1}^2 = \omega_{m2}^2 = \omega_m^2$, the system (3.32) becomes

$$\begin{pmatrix} x_1 \\ x_2 \end{pmatrix} = \frac{1}{\det M} \begin{pmatrix} \omega_o^2 + \omega_m^2 - \Omega^2 & \omega_o^2 \\ \omega_o^2 & \omega_o^2 + \omega_m^2 - \Omega^2 \end{pmatrix} \begin{pmatrix} -\frac{F}{m} \\ \frac{F}{m} \end{pmatrix}$$

and $\det M = (\Omega^2 - \omega_m^2)\,(\Omega^2 - 2\omega_o^2 - \omega_m^2)$.

$$\begin{pmatrix} x_1 \\ x_2 \end{pmatrix} = \frac{1}{\det M} \begin{pmatrix} \frac{F}{m}(\Omega^2 - \omega_m^2) \\ \frac{-F}{m}(\Omega^2 - \omega_m^2) \end{pmatrix}$$

We see that the opposite forces gives a factor $(\Omega^2 - \omega_m^2)$ which cancels the pole in

[4] In the high finesse regime we could neglect the radiation pressure applied by the laser on the external side of the front mirror, because the power inside the cavity dominates.

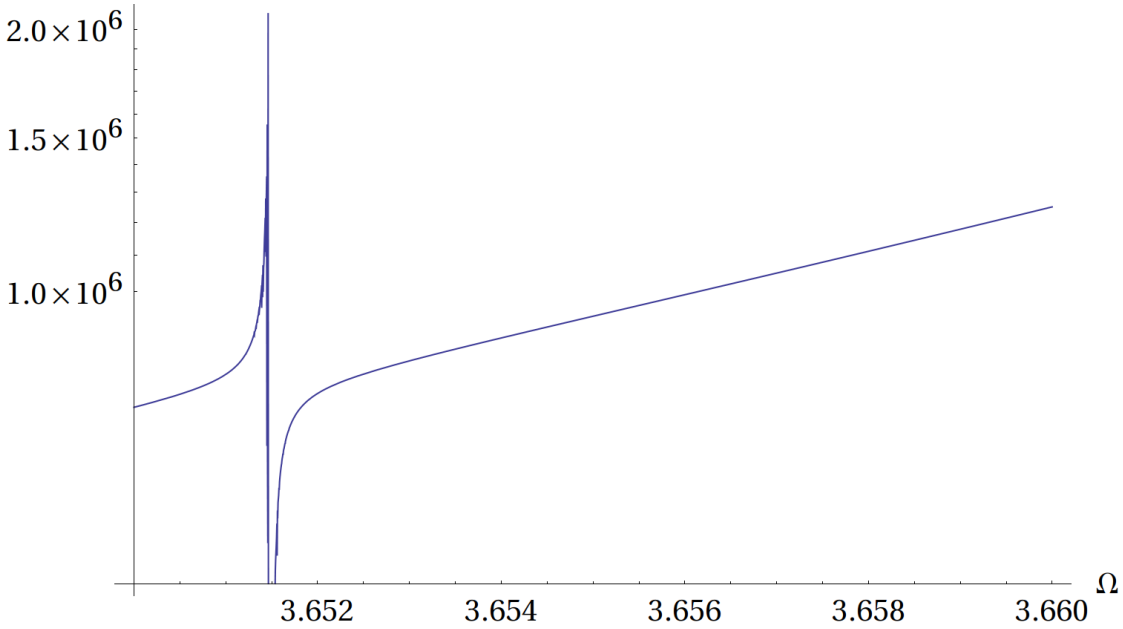

Figure 3.10: Squeezing ratio for a resonant LC in function of the sideband angular frequency Ω an effect of non-exact cancellation of the pole can be observed in correspondence of the mirror mechanical resonance ω_m.

$\Omega = \omega_m$. Consistently with that, we observe only one resonance for the squeezing occurring when

$$\Omega^2 = \omega_m^2 + 2\omega_o^2$$

This pole in $\Omega = \omega_m$ corresponds to the normal mode where the two mirrors oscillate in phase and cannot be excited by two opposite forces. If we reduce the cavity finesse (i.e choosing a lower reflectivity for the front mirror) the forces acting on the mirror cannot be considered the same and the cancellation of the pole is not exact (namely, radiation pressure couples both to the symmetric and antisymmetric mechanical normal modes of the cavity). We see in Figure 3.10 a sign of this effect in correspondence of the mirror mechanical resonance ω_m .

We can estimate ω_o^2 , with reference to the Figure 3.9, comparing the resonance shifting in case of positive and negative detuning. Since

$$\omega_+^2 = \omega_m^2 + 2\omega_o^2$$
$$\omega_-^2 = \omega_m^2 - 2\omega_o^2$$

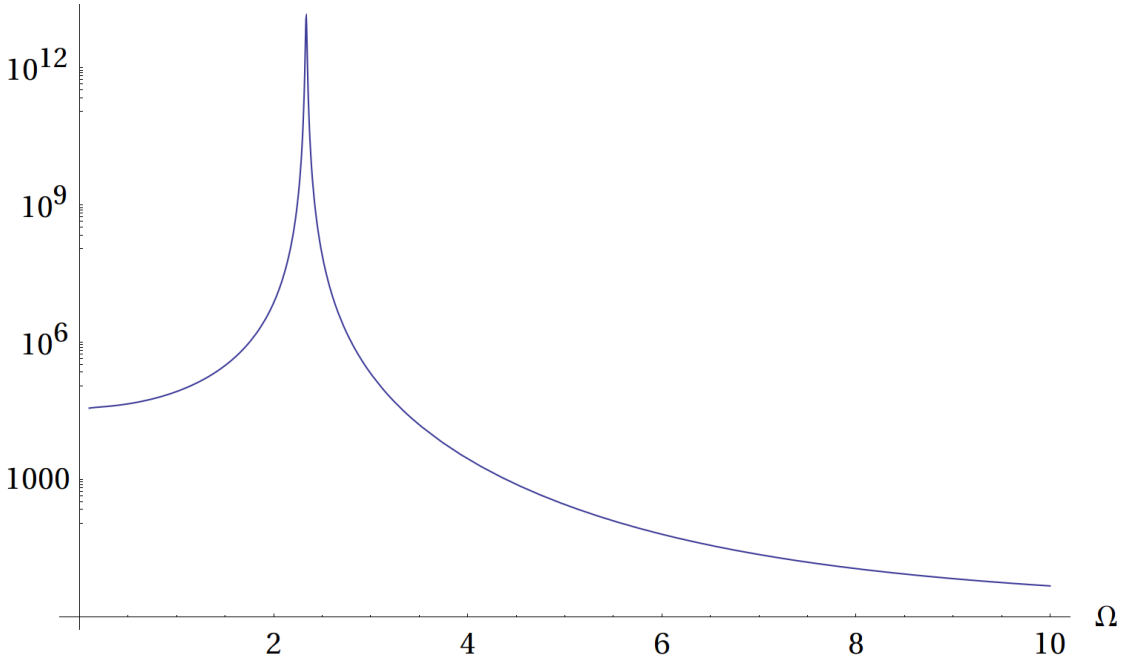

Figure 3.11: Squeezing ratio for a detuned cavity ($\Delta = -1.2 \times 10^{-5}$), without a mechanical stiffness ($\omega_m = 0$). Only optical spring effects contributes to the resonance.

we find that

$$\omega_o^2 = \frac{\omega_+^2 + \omega_-^2}{2}$$

We tested this value by observing the resonance frequency for a negative detuned cavity, when we set $\omega_m^2 = 0$. This is showed in Fig. 3.11

In the general case of (3.32) resonances occur when $\det M = 0$. This happens for

$$\Omega^2 = \frac{1}{2}(\omega_1^2+\omega_2^2+\omega_{o1}^2+\omega_{o2}^2 \pm \sqrt{\left(-\omega_1^2 - \omega_2^2 - \omega_{o1}^2 - \omega_{o2}^2\right)^2 - 4\left(\omega_1^2\omega_2^2 + \omega_2^2\omega_{o1}^2 + \omega_1^2\omega_{o2}^2\right)} \tag{3.33}$$

Figure 3.12 shows the squeezing curve for a cavity whose mirrors have different masses and pendulum frequencies. As expected, there are two resonance.

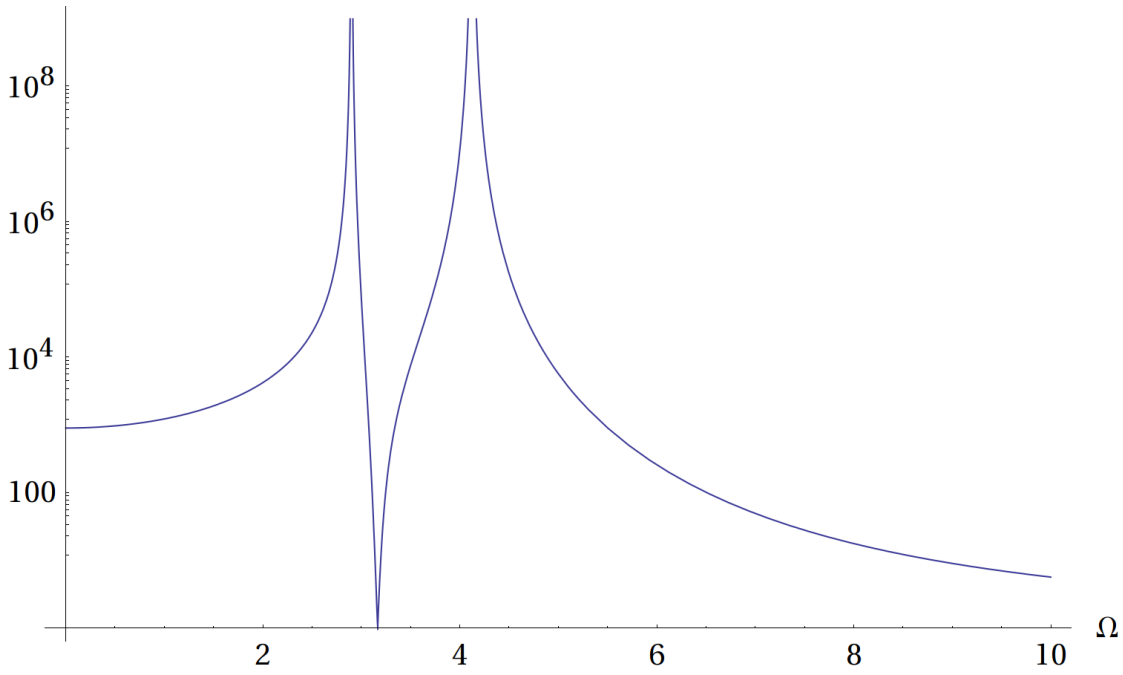

Figure 3.12: Squeezing ratio in function of the sideband angular frequency Ω for a resonant LC cavity whose mirrors has different masses and pendulum frequencies. Two resonance can be observed which corresponds to the two solutions of Eq. 3.33.

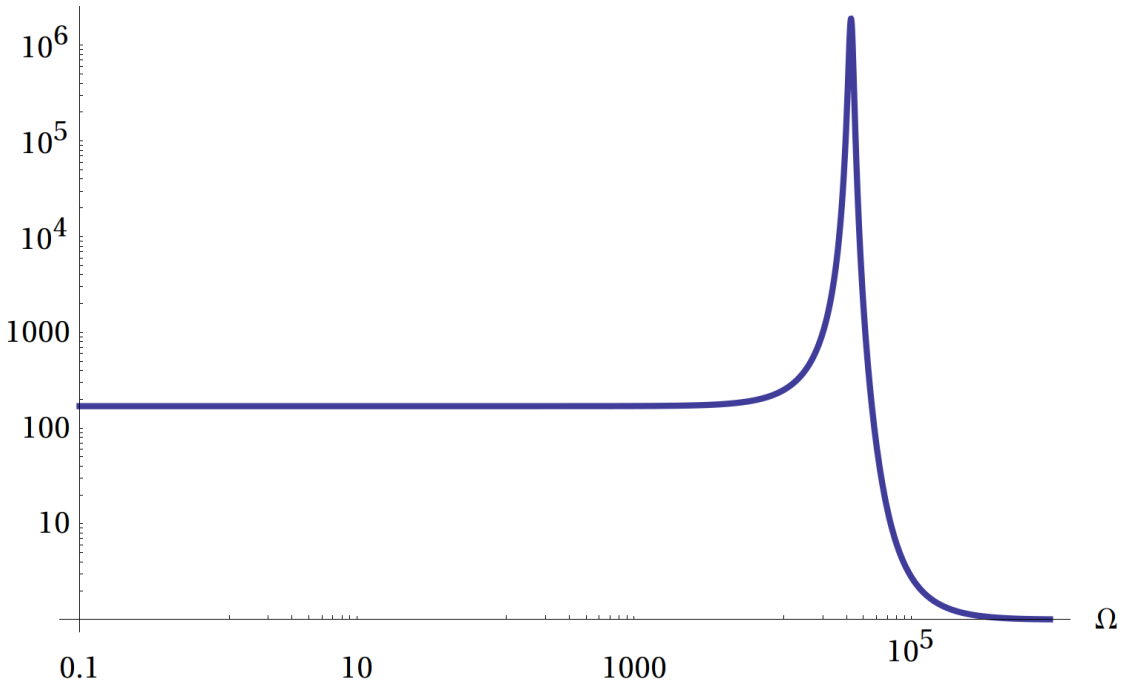

Figure 3.13: Squeezing ratio in function of the sideband angular frequency Ω for a SC with a detuning $\Delta = -1.20083 \times 10^{-4}$.

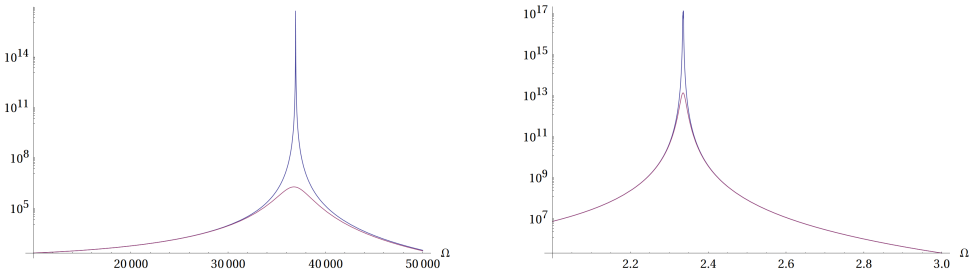

Figure 3.14: Squeezing ratio as a function of the sideband angular frequency Ω for a SC (left figure) and a LC (right figure). The blue curves are obtained as usual while the purple ones are obtained without taking into account the side bands delay, which was switched to zero explicitly in the simulation.

3.4.4 Squeezing in SC

In Fig. 3.13 the squeezing ratio is plotted as a function of Ω for a detuned SC. As previously said, a convenient choice of the cavity parameters allows to achieve an higher level of squeezing and to better exploit the optical spring effect. In this configuration, the resonance associated to the optical spring has a frequency of several kHz: this allows to have a wide region with an high and frequency independent squeezing.

It can be observed that the peak in correspondence of the resonance is smoother compared to the one obtain for a LC. This effect is due to the phase delay associated with side bands propagation (3.4). Since it depend on Ω, it becomes more evident when resonance occurs for higher values of the frequency. In Fig. 3.14 we made a comparison between the resonance curves obtained with and without taking into account the sidebands delay, for the two different type of cavity. The smoothing effect is stronger as the resonance frequency increases.

The trend of the squeezing can be divided in three different regimes: when $\Omega \ll \omega_{res}$ the squeezing parameter is constant and we have a frequency independent squeezed state; when $\Omega \gg \omega_{res}$ the squeezing parameter tends to one and the state is not squeezed anymore. The third regime is when $\Omega \simeq \omega_{res}$, as we have see, the squeezing goes through a resonance which is smoother the higher is ω_{res}.

In Figure 3.15 we plotted the squeezing angle (the rotation angle of the error ellipse) as a function of Ω. Comparing it with the squeezing parameter, it can be noticed that in the region where $\Omega \ll \omega_{res}$ also the squeeze angle is frequency-independent while it is strongly frequency dependent in correspondence of the resonances.

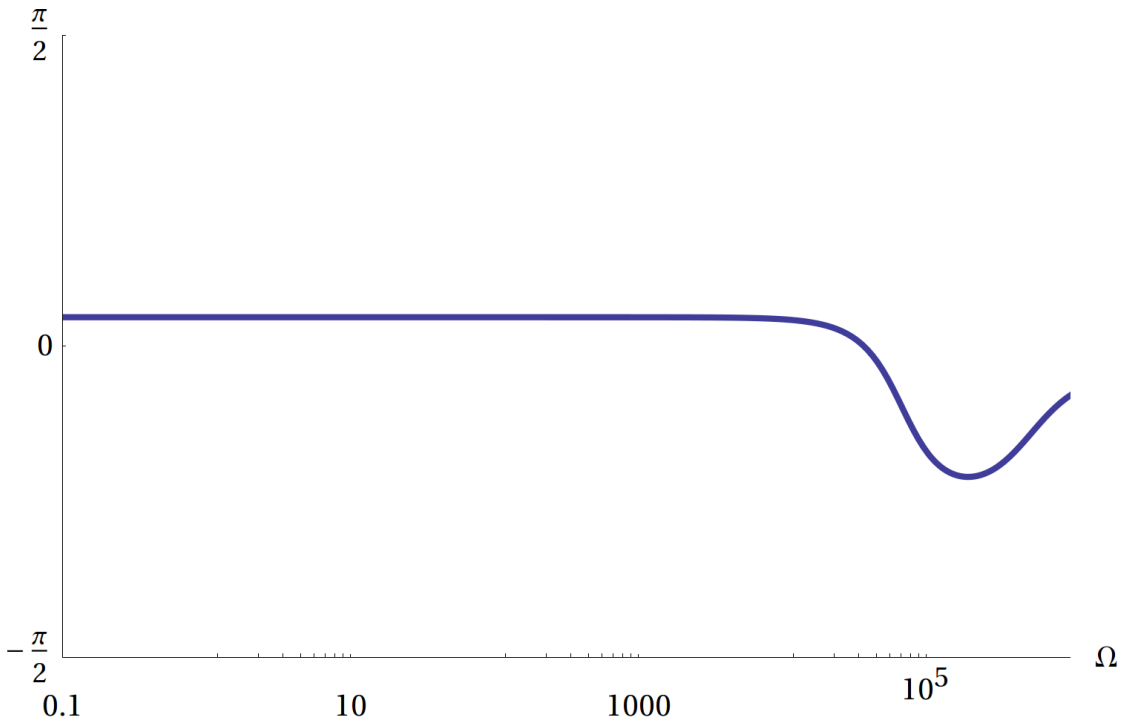

Figure 3.15: Squeezing angle as a function of Ω for a SC with a detuning $\Delta = -1.20083 \times 10^{-4}$. It presents a wide region where it is frequency-independent while it is strongly frequency dependent in correspondence of the resonance.

3.5 Thermal noise simulation

Thermal noise, due to the fact that each vibration mode of the mirrors and of their suspension is randomly excited with an energy proportional to the temperature of the system, is one of the dominant noise sources in interferometric gravitational waves detector. This noise, which is not avoidable in principle, can be concentrated in narrow frequency regions in order to improve the sensitivity at other frequencies: heavily damped modes tend to have broad linewidths, and the relative thermal energy generates a noise which can affect large parts of the spectrum while the noise of lightly damped modes is concentrated around their resonance frequencies.

We will not discuss thermal noise mechanisms in detail but just how it couples with quantum noise and how some configurations of optical cavities used to generate ponderomotive squeezing result more convenient in terms of thermal noise reduction.

The fluctuation-dissipation theorem [22] can be used to deduce the power spectral density of a force F_{th} responsible for thermal fluctuations: if $x(t)$ is the variable of a linear system and $\dot{x}(t) = v(t)$ is the velocity, the equation of motion in the frequency domain can always be written as

$$F_{th}(\omega) = Z(\omega)\,\tilde{v}(\omega) \tag{3.34}$$

where $Z(\omega)$ is a complex quantity defined impedance. According to the theorem, power spectrum of the thermal fluctuation force $S_F(\omega)$ is given by

$$S_F(\omega) = 4k_bT\,\mathrm{Re}\left[Z(\omega)\right] \tag{3.35}$$

From this we compute the power spectral density of the position of the mass: in the frequency domain $\tilde{v}(\omega) = i\omega x(\omega)$ and Eq. (3.34) can be written as

$$x(\omega) = Z^{-1}\frac{\tilde{F}_{th}(\omega)}{i\omega}$$

from which

$$S_x = |Z|^{-2}\frac{S_F}{\omega^2} = \frac{4k_bT}{\omega^2}\frac{\mathrm{Re}\left[Z(\omega)\right]}{|Z|^{-2}} = \frac{4k_bT}{\omega^2}\mathrm{Re}\left[Z(\omega)^{-1}\right]$$

If we model the thermal noise by assuming that the dissipative force is proportional to velocity (viscous damping), the motion equation of the mirror is the one of a damped harmonic oscillator undergoing a force F_{th}

$$m\ddot{x}(t) + f\dot{x}(t) + kx(t) = F_{th}(t)$$

which after switching to the frequency domain, it becomes

$$\left(-m\omega^2 + if\omega + k\right)\tilde{x}\left(\omega\right) = \tilde{F_{th}}\left(\omega\right)$$

It can also be written as

$$-\frac{i}{\omega}\left(-m\omega^2 + if\omega + k\right)\dot{x}\left(\omega\right) = \tilde{F_{th}}\left(\omega\right)$$

which compared to Eq. (3.34) gives the impedance

$$Z = f + i\left(m\omega - \frac{k}{\omega}\right)$$

From (3.35), we find

$$S_F\left(\omega\right) = 4k_bTf$$

and for the position

$$S_x = \frac{4k_bT\,\mathrm{Re}\left[Z\left(\omega\right)^{-1}\right]}{\omega^2} = \frac{4k_bTf}{\omega^2 f^2 + \left(m\omega^2 - k\right)^2} \tag{3.36}$$

The oscillator undergoes a resonance in $\omega_0 = \sqrt{\frac{k}{m}}$ whose sharpness is characterized by $Q = \frac{\omega_0}{\Delta\omega}$, with $\Delta\omega$ the full width at half high, and in this model we have $Q = \frac{\sqrt{km}}{f}$.

In suspended mirrors, as the ones we deal with, dissipative forces causing thermal noise cannot be always modeled as proportional to velocity [23]. In fact the prevalent dissipative effects in such mirrors is due to internal damping and the force can be regarded as an extension of Hooke law

$$F = k\left[1 + i\phi\left(\Omega\right)\right]x \tag{3.37}$$

We have chosen this model to simulate thermal noise in our system. We need to specify, when defining the mirrors, a given model for the mechanical equation of motions. There are no problems in including imaginary parts of the stiffness constant as in (3.37) because the model is defined in the frequency domain.

The equations which relate the mechanical and optical fields to the the thermal forces are added to the linear system which describes the cavity, and we end with a system which can be written as

$$\underline{\tilde{F}}_{th} = i\Omega\boldsymbol{Z}\underline{\tilde{q}}$$

where $\boldsymbol{Z}$ is the impedance matrix, the generalization of the impedance for a

linear system with many degrees of freedom $\underline{\tilde{q}}$. As a consequence of the fluctuation dissipation theorem the thermal forces will be stochastic variables with a covariance matrix given by

$$\boldsymbol{\Sigma}_{F_{th}} = 4k_b T\Omega \mathrm{Im}\boldsymbol{Z}$$

and we can represent the thermal forces as a vector

$$\underline{\tilde{F}}_{th} = \sqrt{4k_B T\Omega}\,(\mathrm{Im}\boldsymbol{Z})^{1/2}\,\underline{\tilde{\eta}}$$

where $\underline{\tilde{\eta}}$ is a vector of random normal and uncorrelated variables, and $\boldsymbol{M}^{1/2}$ is the matrix square root defined for a symmetric matrix by $\boldsymbol{M}^{1/2}\boldsymbol{M}^{1/2} = \boldsymbol{M}$.

We stress that Im$\boldsymbol{Z}$ needs not to be diagonal, so thermal forces coupled to different degrees of freedom can be correlated.

By inserting the thermal forces as additional sources we can evaluate the covariance arrays of the system accordingly with the general method explained previously (see in particular Eq. (3.29)).

Since thermal and optical fluctuations are not correlated, it is possible to deal with the covariance matrices associated with quantum and thermal noise separately and to sum them whenever we are interested in the total noise. It is important to note that we need to switch off optical spring effects when we evaluate $\boldsymbol{Z}$, because the laser field is not considered in thermal equilibrium with the system.

Thermal noise acts moving the mirrors and this motion in turn will enhance the phase fluctuations of an impinging optical field, keeping unchanged the amplitude noise. If we take into account just the thermal noise effect, the uncertainty of the reflecting field will not be equally distributed among the two quadrature but it can't be regarded as a proper squeezing state since noise isn't smaller that the one of a coherent state in some direction and the fluctuations are not correlated. Figure 3.16 shows the error ellipses and the polar plots for a coherent state reflected from a mirror which moves just because of thermal noise for different value of the imaginary part of k

In this case (and anytime we don't have a minimum uncertainty state), it would be misleading to look at the squeezing parameter to obtain information about the squeezing. A reasonable choice, when we want to test the effectiveness of ponderomotive squeezing in the presence of thermal noise, is to look at the minimum eigenvalue of the covariance matrix (which is the shortest axis of the correspondent ellipse error) and see if it is smaller then the ones of a coherent state: in that case we know we managed to reduce quantum noise in some direction. Anyway the combined effect of thermal noise and ponderomotive squeezing is not trivially derivable from the sum of the minimum eigenvalues

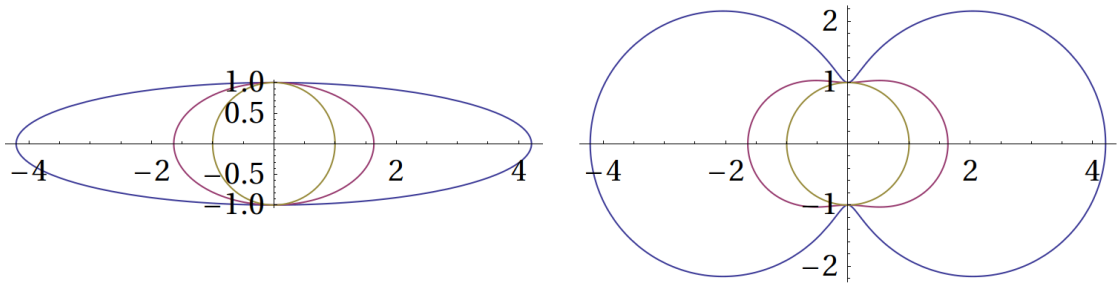

Figure 3.16: The error ellipses and the polar plots for a coherent state reflected from a mirror which moves just because of thermal noise for different value of the imaginary part of k: $\mathrm{Im}\,(k) = 0$ (brown), $\mathrm{Im}\,(k) = 4 \times 10^{-4}$ (purple), $\mathrm{Im}\,(k) = 4 \times 10^{-3}$ (blue)

of the covariance matrices since it strongly depends on the ellipses orientation, that is the squeezing angle. In Figure 3.17 we plotted the minimum axis of the quantum noise ellipse and the minimum axis of the noise ellipse obtained by summing quantum and thermal noise. The plot is done for a resonant cavity where only the end mirror can move and it has an optical spring with a small imaginary part $k_{m2} = 400(1 + 10^{-9}i)$.

We see that the thermal noise spoils the squeezing but its effect does not simply consist in a translation of the quantum noise. In Figure 3.18 we plotted the squeezing angle for the quantum and the thermal noise whose different dependence on Ω explains the total noise behavior shown in Figure 3.17

An additional complication deriving from the introduction of an imaginary part in k_{m2} is the fact that the squeezing state is not a minimum uncertainty state anymore and for example the length of maximum axes cannot be deduced knowing the one of the minimum. The polar plot in Figure 3.19 provides complete information on the noise at a fixed frequency: from it we can deduce quantum noise, thermal noise and their sum in every quadrature and have an intuitive idea of how they combines according to their squeezing angle.

In Figure 3.20 the minimum axes for the total noise is plotted for a resonant cavity at increasing values of the imaginary part of the end mirror mechanical

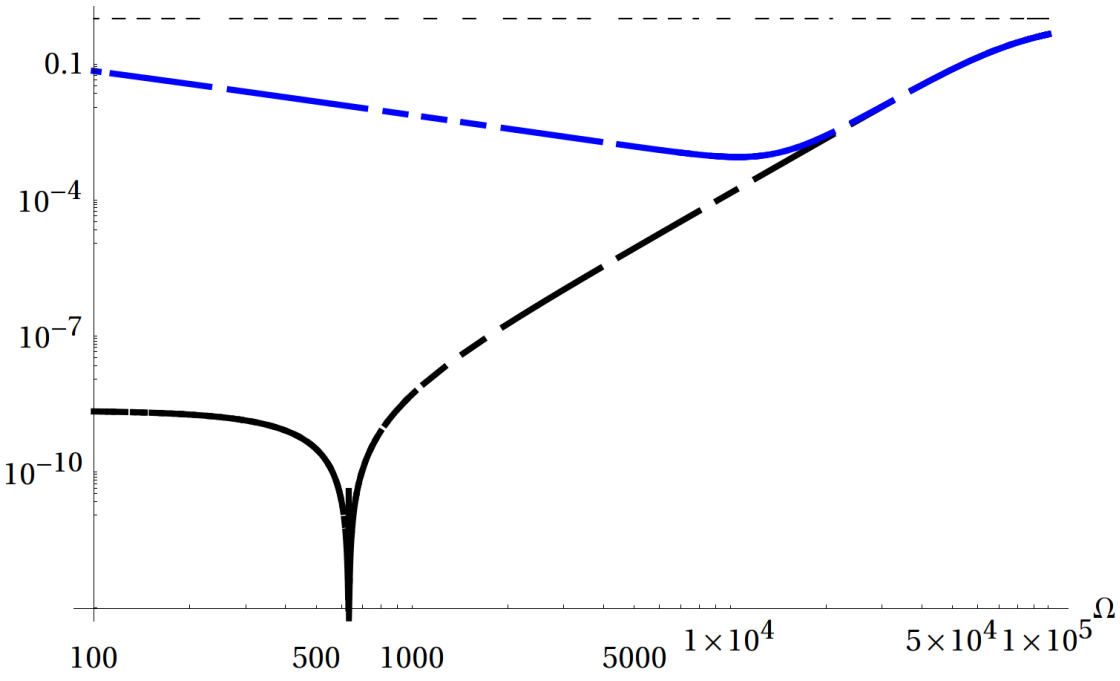

Figure 3.17: Plot of the minimum axis of the quantum noise ellipse and the minimum axis of the noise ellipse obtained by summing quantum and thermal noise. The plot is done for a resonant SC where only the end mirror can move and it has an optical spring with a small imaginary part $k_{m2} = 400(1 + i10^{-9})$. The spoiling effect of the thermal noise is evident. The temperature has been set at 300K

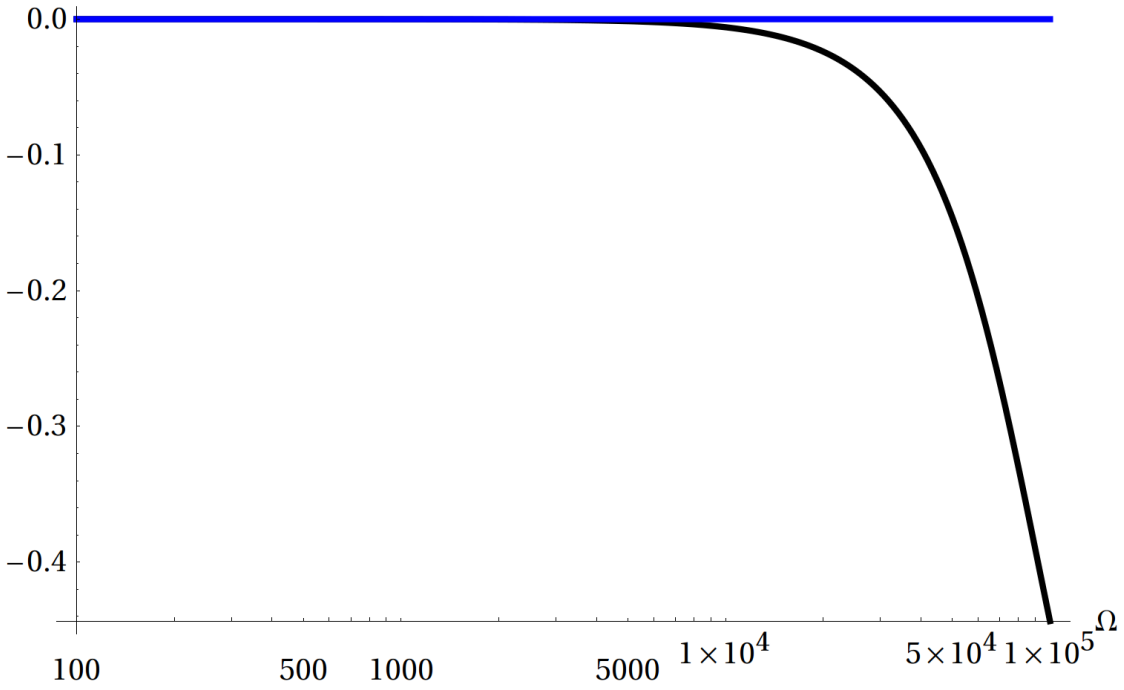

Figure 3.18: The squeezing angle for the quantum and the thermal noise is plotted in function of Ω. Their different dependence on Ω accounts for the total noise behavior shown in Figure 3.17. Obviously the angle or thermal noise "ellipse" is always zero, because there are no thermal fluctuations of the amplitude quadrature.

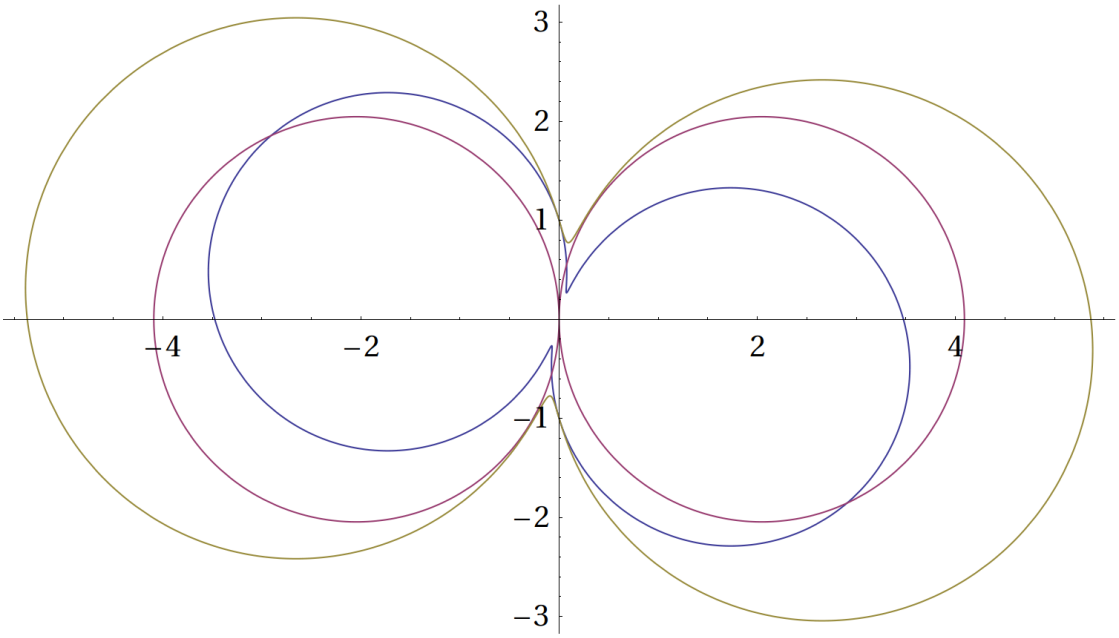

Figure 3.19: Polar plot for quantum noise, thermal noise and their sum in a resonant SC at a fixed sideband angular frequency ($\Omega = 100\mathrm{rad\,s^{-1}}$). It shows how they add up according to their squeezing angle.

stiffness k_{m2} and compared with the minimum noise achievable without thermal fluctuations (dashed, black line). It is evident that thermal noise fluctuations rapidly spoil the squeezing.

The situation is different when we consider a detuned cavity, where the resonance occurs at the optical spring frequency.

In Figure 3.21 we can compare the minimum noise achievable in the case of a resonant cavity with the one of a detuned cavity. The dashed line represents only the quantum noise contribution and shows a similar behavior in both cases but the resonance in the first is obtained with an high mechanical stiffness while in the second case is due to the optical stiffness induced by detuning. The total noise (represented by the thick line) is clearly lower for the detuned cavity and makes it evident that a configuration of that type is preferable in order to preserve the squeezing from thermal noise deterioration. The reason for this is that optical forces acting on the mirrors can be considered as the laser were at zero temperature, namely they does not contribute to thermal noise. As a consequence an optical stiffness associated with these forces will introduce less thermal noise that a mechanical one. This can be understood with the simple model of a single movable mirror whose motion equation in the frequency domain is

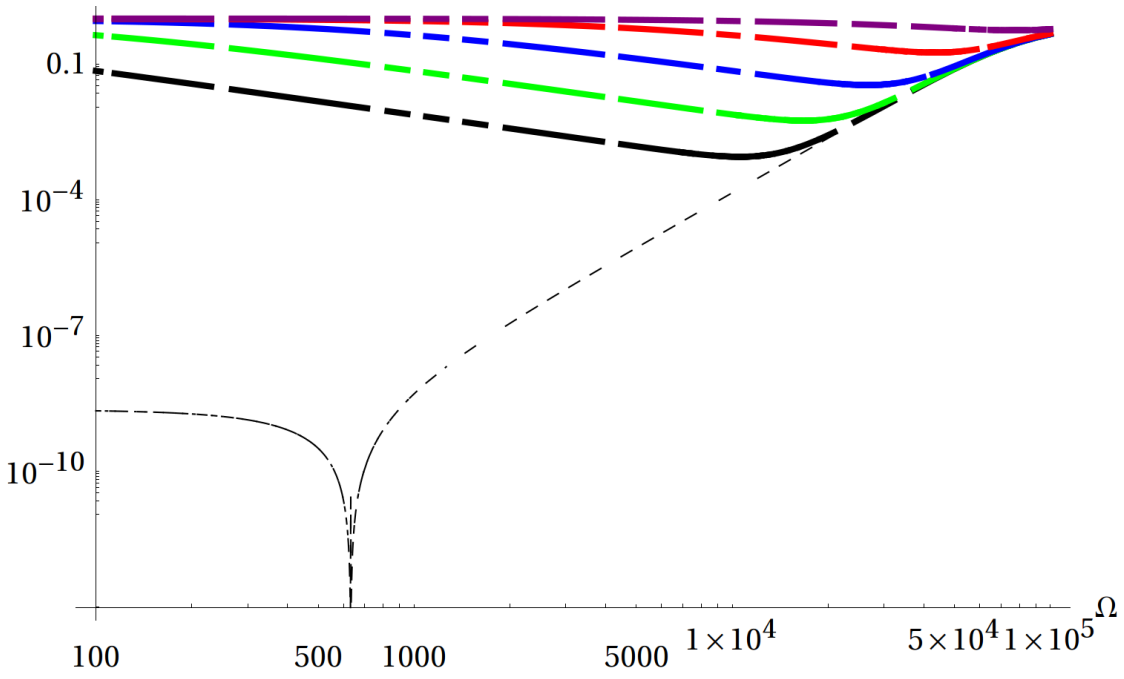

Figure 3.20: Plot of the minimum axes of the total noise error ellipse for a resonant SC as a function of Ω at increasing values of the imaginary part of the end mirror mechanical stiffness k_{m2}. They are compared with the minimum axis for the error ellipse without thermal fluctuations (dashed, black line). Increasing thermal noise values makes the squeezing tend rapidly to one. We used $k_{m2} = 400(1+10^{-n}i)\mathrm{N\,m}$ with $n = 5$ (purple), $n = 6$ (red), $n = 7$ (blue), $n = 8$ (green) and $n = 9$ (black).

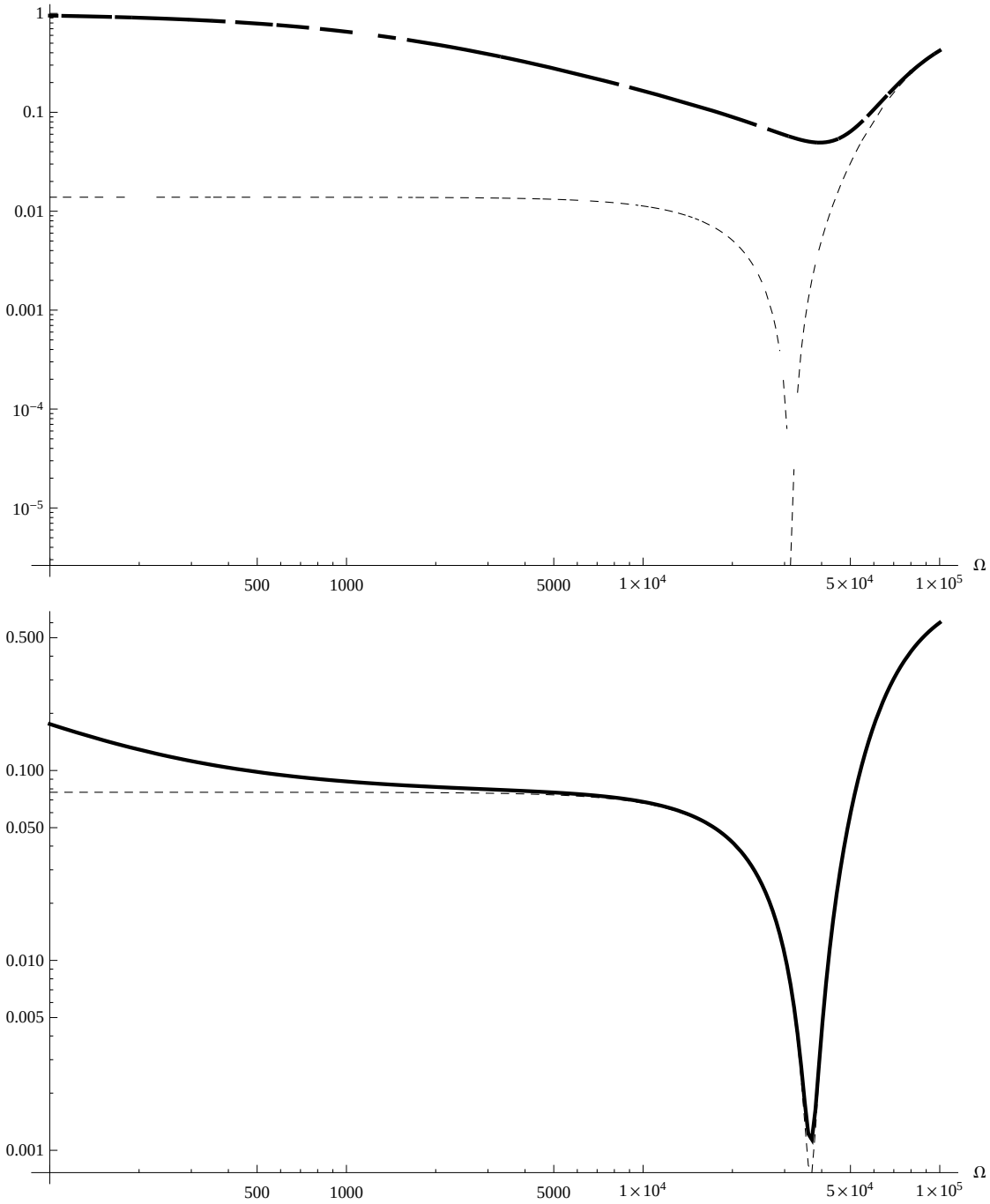

Figure 3.21: Plot of the minimum axes of the quantum and total noise error ellipse in function of Ω in the case of a resonant SC (upper figure) and detuned SC (lower figure). The resonance in the first is obtained with an high mechanical stiffness while in the second case is due to the optical stiffness induce by detuning. The quantum noise (dashed line) shows a similar behavior in both case while total noise (thick line) is clearly lower for the detuned cavity.

$$-m\omega^2\tilde{x} + k\left(1 + i\phi\right)\tilde{x} = \tilde{F}_{th} + \tilde{F}_{opt} \tag{3.38}$$

and if we assume $\tilde{F}_{opt} = -\left(k_{opt} + i\omega\Gamma_{opt}\right)\tilde{x}$, it becomes

$$\left[-m\omega^2 + k\left(1 + i\phi\right) + k_{opt} + i\omega\Gamma_{opt}\right]\tilde{x} = \tilde{F}_{th}$$

whose power spectrum is

$$S_x = \frac{S_{th}}{\left(k + k_{opt} - m\omega^2\right)^2 + \left(k\phi + \omega\Gamma_{opt}\right)^2} \tag{3.39}$$

Now, if we assume that F_{th} does not contribute to thermal fluctuations, S_{th} can be deduced applying to Eq. (3.38) the fluctuation-dissipation theorem, after having set $\tilde{F}_{opt} = 0$. We find the relative impedance

$$Z = \frac{k\phi}{\omega} - i\left(m\omega + \frac{k\phi}{\omega}\right)$$

and from it

$$S_{th} = 4k_bT\mathrm{Re}\left[Z\right] = 4k_bT\frac{k\phi}{\omega}$$

The position power spectrum (3.39) becomes

$$S_x = \frac{4k_bTk\phi}{\omega\left[\left(k + k_{opt} - m\omega^2\right)^2 + \left(k\phi + \omega\Gamma_{opt}\right)^2\right]}$$

which is less noisy than if we simply had chosen a bigger mechanical stiffness, (eg. $k_{mech} = k + k_{opt}$) in a resonant cavity[8].

3.6 Simulation for more than one mode

3.6.1 One carrier

So far we presented the results obtained from our simulation considering just the fundamental mode in the cavity. The next step we take is to include the first order modes HG_{10} and HG_{01}. Our code provides for the possibility of introducing more than one carrier but we start by not putting classical power into higher modes and simply by taking into account their vacuum fluctuations. As we have seen in Section 3.2.2.2 the presence of modes that differs by one index are capable of producing a non-zero torque that results in a rotation of the mirror. If we now consider the input-output relation for a mirror rotated by a small amount

we see that the reflected quadrature in a mode are affected by the presence of a carrier in a mode which differs from it by one index. This additional fluctuation is also proportional to the mirror rotation which in turns depends on the torque generated by a modes superposition. If we specialize the case to the modes HG_{00} and HG_{10}, where only the first has a classical intensity, the reflected fluctuations of the first order mode are (Eq. (3.25))

$$\hat{a}_{r;10} = \underline{\hat{a}}_{i;10} + \frac{2\omega_0}{c} N^{-1} \delta\tilde{\theta}_y(\Omega) \left[\begin{pmatrix} \frac{\gamma_1^{(-)} - \gamma_0^{(+)}}{2i} & \frac{\gamma_1^{(-)} + \gamma_0^{(+)}}{2} \\ -\frac{\gamma_1^{(-)} + -\gamma_0^{(+)}}{2} & \frac{\gamma_1^{(-)} - \gamma_0^{(+)}}{2i} \end{pmatrix} \underline{\alpha}_{i;00} \right] \tag{3.40}$$

and from Eq. (3.20)

$$\delta\tilde{\theta}_y(\Omega) = \frac{M_y}{I\left(\Omega^2 - \omega_y^2\right)} = \frac{N}{I\left(\Omega^2 - \omega_y^2\right)} \left(\gamma_0^{(-)} \alpha_{00} \cdot \hat{a}_{10}\right)$$

From this we see that this superposition causes a correlation between HG_{01} quantum fluctuations which depends on the classical amplitude of the fundamental mode α_{00}. This mechanism can be represented by composing the interactions shown in Table 3.1 to obtain the the diagram

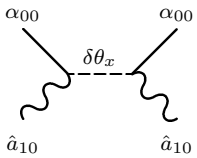

In Figure 3.22 the squeezing parameter of the mode HG_{01} is plotted as a function of the sidebands frequency Ω. The plot shows a clear squeezing effect which vanishes when the mirrors cannot tilt. The resonance is not in zero even if for the harmonic oscillator associated with the mirror tilt we set $\omega_{pendolum} = 0$ (free mass).

This is caused by an optical spring effect which arises since the cavity length has been set to make the mode HG_{00} resonate while the higher modes like HG_{10} are detuned because of the Gouy Phase. In Figure we show that is possible to shift the squeezing resonance adding a $\omega_{pendulum}$ different from zero. All these effects are just the same if we consider the mode HG_{10} instead of HG_{01}.

3.6.2 Two carriers

We have observed the effect of squeezing on the vacuum fluctuations of a mode caused by the coupling of such fluctuations with a carrier in another mode

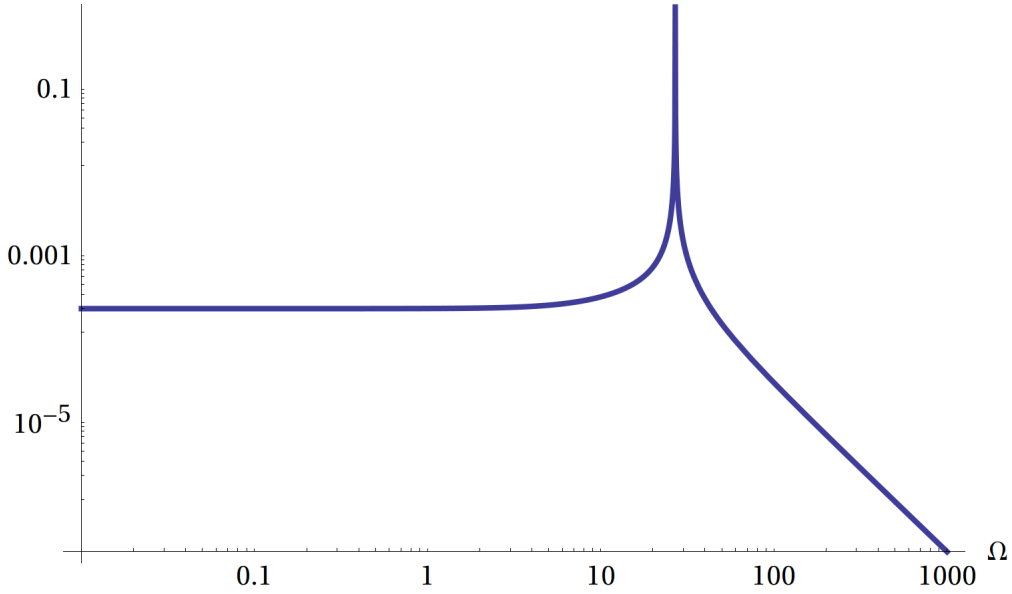

Figure 3.22: Squeezing parameter of the mode HG_{01} as a function of the sidebands frequency Ω

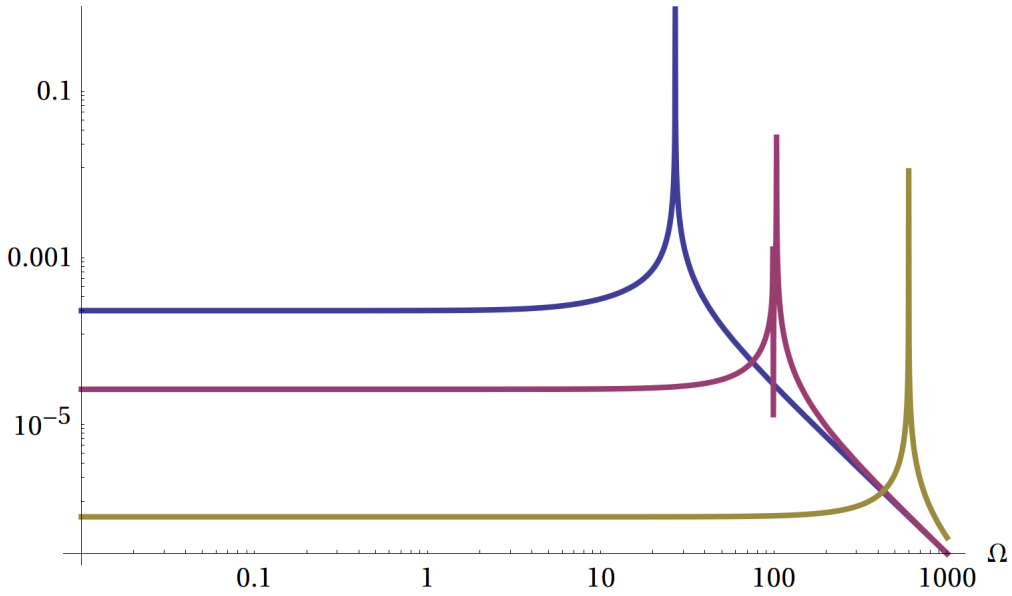

Figure 3.23: Shift of the resonance of the squeezing parameter for the mode HG_{01} for different values of $\omega_{pendulum}$, namely $\omega_{pendulum} = 30\mathrm{rad\,s^{-1}}$ (blue), $\omega_{pendulum} = 100\mathrm{rad\,s^{-1}}$ (purple) and $\omega_{pendulum} = 600\mathrm{rad\,s^{-1}}$ (green).

(which differ from it by one index). However this configuration is not capable of introducing correlations between fluctuations of different modes.

In order to understand this we consider the case where classical light is injected both in the HG_{00} and in the HG_{10}. Here the the behavior of the two mode is symmetric: both undergo a squeezing effect due to the radiation pressure force and also a "tilt" squeezing effect due to the torque, proportional to the amplitude of the carrier of the other mode and to the rotation $\delta\tilde{\theta}_y(\Omega)$. For example in the case of HG_{10} we have:

$$\begin{aligned}\hat{a}_{r;01} = \underline{\hat{a}}_{i;10} + \underbrace{\left[\frac{2\omega_0}{c} N^{-1} \delta\tilde{Z}(\Omega) \begin{pmatrix} 0 & 1 \\ -1 & 0 \end{pmatrix} \underline{\alpha}_{i;10}\right]}_{traslation} \\ + \underbrace{\frac{2\omega_0}{c} N^{-1} \delta\tilde{\theta}_y(\Omega) \left[\begin{pmatrix} \frac{\gamma_1^{(-)} - \gamma_0^{(+)}}{2i} & \frac{\gamma_1^{(-)} + \gamma_0^{(+)}}{2} \\ -\frac{\gamma_1^{(-)} + -\gamma_0^{(+)}}{2} & \frac{\gamma_1^{(-)} - \gamma_0^{(+)}}{2i} \end{pmatrix} \underline{\alpha}_{i;00}\right]}_{tilt}\end{aligned} \tag{3.41}$$

However $\delta\tilde{\theta}_y(\Omega)$ is proportional to the torque M_y which in this configuration is generated by a mixed combination of carriers and fluctuations of the two mode

$$\begin{aligned}\delta\tilde{\theta}_y(\Omega) &= \frac{M_y}{I\left(\Omega^2 - \omega_y^2\right)} \\ &= \frac{N}{I\left(\Omega^2 - \omega_y^2\right)} \left[\left(\gamma_0^{(-)} \alpha_{00} \cdot \hat{a}_{10}\right) + \left(\gamma_1^{(-)} \alpha_{10} \cdot \hat{a}_{00}\right)\right]\end{aligned} \tag{3.42}$$

While $\delta\tilde{Z}(\Omega)$ is proportional to the radiation pressure force F_z which is proportional to the sum on the modes of the product of carriers and fluctuations of the same mode. In this case we have

$$\begin{aligned}\delta\tilde{Z}(\Omega) = \frac{F_z(\Omega)}{M\left(\Omega^2 - \omega_z^2\right)} &= \frac{N}{M\left(\Omega^2 - \omega_z^2\right)} \sum_{mn} \alpha_{mn} \cdot \hat{a}_{mn} \\ &= \frac{N}{M\left(\Omega^2 - \omega_z^2\right)} \left[\left(\alpha_{00} \cdot \hat{a}_{00}\right) + \left(\alpha_{10} \cdot \hat{a}_{10}\right)\right]\end{aligned}$$

When we put Eq. 3.42 in the Eq. 3.41 we observe that it has been created a correlation between fluctuation of two different modes:

$$\hat{a}_{r;01} = \underline{\hat{a}}_{i;10} + \frac{2\omega_0}{cM\left(\Omega^2-\omega_z^2\right)}\left[(\alpha_{00}\cdot\hat{a}_{00})+(\alpha_{01}\cdot\hat{a}_{10})\right]\left[\begin{pmatrix}0 & 1\\ -1 & 0\end{pmatrix}\underline{\alpha}_{i;10}\right]$$
$$+\frac{2\omega_0}{cI\left(\Omega^2-\omega_y^2\right)}\left[\left(\gamma_0^{(-)}\alpha_{00}\cdot\hat{a}_{10}\right)+\left(\gamma_1^{(-)}\alpha_{10}\cdot\hat{a}_{00}\right)\right]$$
$$\times\begin{pmatrix}\frac{\gamma_1^{(-)}-\gamma_0^{(+)}}{2i} & \frac{\gamma_1^{(-)}+\gamma_0^{(+)}}{2}\\ -\frac{\gamma_1^{(-)}+-\gamma_0^{(+)}}{2} & \frac{\gamma_1^{(-)}-\gamma_0^{(+)}}{2i}\end{pmatrix}\underline{\alpha}_{i;00} \tag{3.43}$$

An equation analogous to Eq. (3.43) can be found for $\hat{a}_{r;00}$ and the correlation between fluctuations HG_{00} and HG_{10} are now evident.

In Table 3.3 are shown all the mechanisms which contribute to create the correlations for the fluctuations in the basis subspace HG_{00}, HG_{10} and HG_{01}. One of the lower leg is the incoming fluctuation and the other is the fluctuation which is correlated to it. Each diagram in the table accounts for a term in the Eq. (3.43). S_z and D_z are connected with a longitudinal displacement of the mirror while the others are connected with its rotations.

Accordingly with these diagrams we can see that since a squeezed state of light with a correlation between fluctuations of different modes can only be generated by graphs D_z and $D_{\theta_{x,y}}$, in order to observe it we need to introduce more than one carrier. From our simulation we can extract the covariance matrix extended to the two modes considered. As we said, it is a 4×4 matrix which correspond to an ellipsoid in the $4-$dimensional quadrature space and can be seen as a generalization of the error ellipse we presented before. We can work out the coherence values between quadratures belonging to different modes and observe that they are not zero. A plot for these coherences as a function of the sidebands frequency Ω is shown in Figure 3.24. It can be confronted with the squeezing parameter (which we used previously to quantify the correlations between quadrature belonging to the same mode) shown in Figure 3.25 for the modes HG_{00} and HG_{10}. It is evident that the correlation between modes is stronger when the squeezing parameter of each modes is higher.

3.6.3 Coupling between mechanical modes of the mirror

So far we considered the mechanical modes of the mirror connected with a longitudinal displacement δZ and with its tilt $\delta\theta_x$ and $\delta\theta_y$ as independent harmonic oscillators. However in a realistic model they are coupled and a tilt can be caused just by a longitudinal displacement. In terms of the diagrams represented in Table 3.3 this means that the "mechanical propagator" can change a δZ fluctuation into a $\delta\theta_x$ one, allowing a correlation between quadratures belonging to differ-

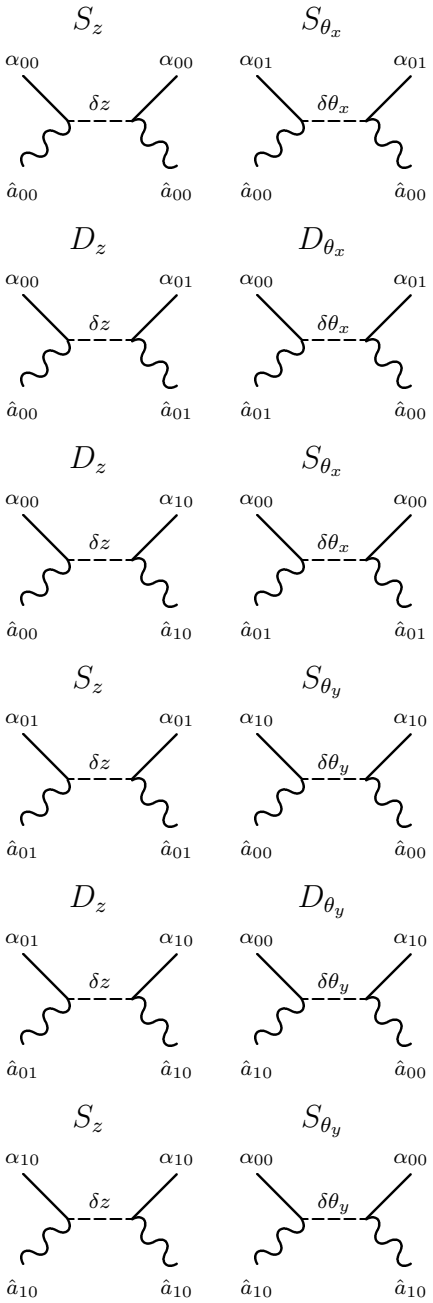

Table 3.3: The basic ponderomotive squeezing mechanisms generated by the longitudinal displacement and by the rotations of the mirror, in the linear approximation in the subspace HG_{00}, HG_{10} and HG_{01}. The D-type interactions requires two carriers, the S-type only one.

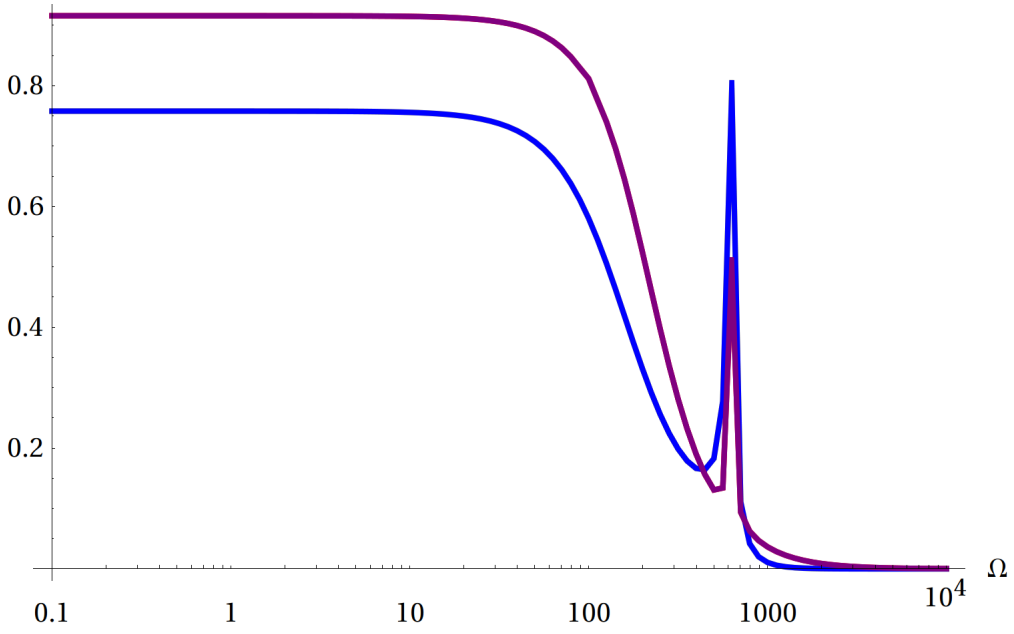

Figure 3.24: Coherences between quadratures of different modes as a function of the sidebands frequency Ω. Correlations between $HG^A_{00} - HG^A_{10}$ and $HG^P_{00} - HG^A_{10}$ (which are the same) are shown in blue while those between $HG^A_{00} - HG^P_{10}$ and $HG^P_{00} - HG^P_{10}$ (which are also the same) are shown in purple.

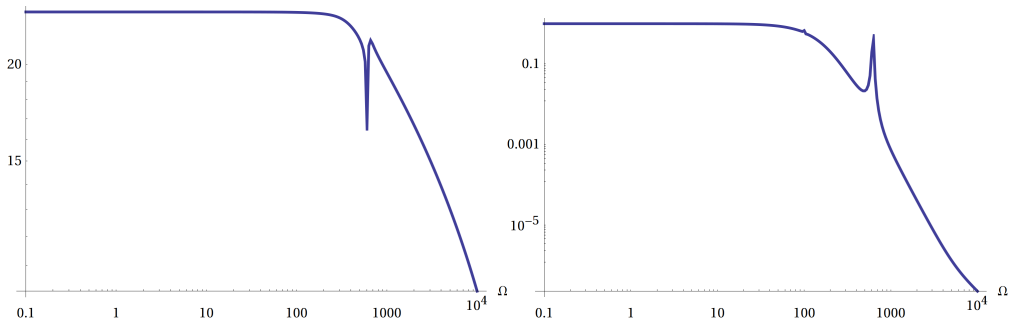

Figure 3.25: Squeezing parameter for the modes HG_{00} and HG_{10} plotted as a function of Ω.

ent modes even in the presence of only one carrier. This further possibility is represented by the diagrams in Table 3.4

It is easy to obtain the mechanical coupling described in a laboratory setup. For example, in a suspended mirror δZ and $\delta\theta_x$ are coupled. An even simpler possibility is to consider a laser beam which is not centered on the center of mass of the mirror.

It is easy to understand that quantum correlations between different modes are to be expected also in a setup with a single carrier with amplitude different from zero. This can be seen as a problem (a source of losses from the mode we are interested to) or a possibility to explore.

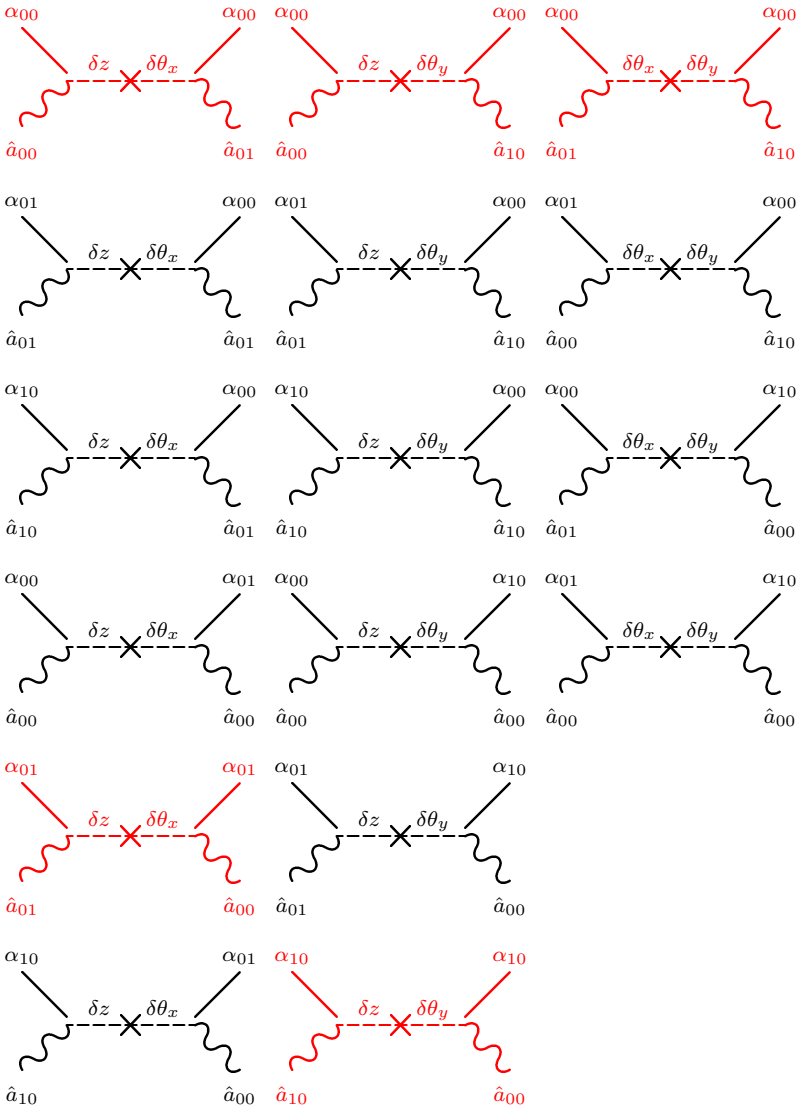

Table 3.4: Additional ponderomotive squeezing mechanisms generated by the longitudinal displacement and by the rotations of the mirror, in the linear approximation in the subspace HG_{00}, HG_{10} and HG_{01}, when cross couplings between mechanical degrees of freedom are present. The graphs in red can correlate different optical modes when a single carrier is available.

4 Conclusions and perspectives

In this work we studied the coupling of light and mechanical modes of movables mirrors in a cavity and developed a simple and accurate code, linear in the quantum fluctuations, which we used to predict the ponderomotive squeezed effects achievable by means of this couping.

The code is an useful tool to test different configurations of the system parameters and to find those which optimize the effect we want to see. For example we verified that the stiffness induced by the opto-mechanical coupling in a cavity (optical spring effect) can be successfully exploited to reduce thermal noise.

The decompositions in HG modes of the fields, introduced to improve the accuracy of our simulation, permitted to take into account more complex opto-mechanical interactions. For the HG modes up to the first order, we developed a scheme which tells how these modes "talk to each other" by means of the mirror mechanical modes. This interaction results in a correlation between fluctuations in the quadrature of the modes, namely a squeezing effect.

In particular configurations (more than one carrier, coupling between mechanical modes) we found that this effect takes place between fluctuations belonging to different modes, showing a more complex structure for the squeezing.

The interest of this results is twofold. From one side, in a realistic optical apparatus there are always couplings between modes at some level, induced by misalignments and/or imperfections in couplings. Current experience with the implementation of noise reduction strategies based on squeezed states shows that this is a crucial problem [24], and codes which allow for the study of mode coupling effects are a really useful and important tool.

From a different point of view, we think that there are possibilities to take advantage of these effects in order to design strategies that can be used both for noise reduction and for designing experiments to detect them directly.

4.1 Code improvement

The main focus of the code implementation was not about computational efficiency and scalability. The best advantage of the approach we choose was that the code is relatively simple to extend and to understand. It is possible to obtain

both numerical and symbolic results, and this is very convenient in the prototyping phase, and as a help in theoretical computations. Another advantage is that the accurate results we can obtain can be used as a validation for numerical codes written at a lower level with numerical efficiency in mind.

We plan to extend and to improve the code in the future, mainly by adding more complex optical objects. The first priority is a beam splitter object. This currently can be simulated by connecting together mirrors, but a separate object would be much more convenient. It will be useful also to add code to simulate losses in a more transparent way (currently these have to be introduced by hand), and more specialized detector objects which implements specific detection strategies, such as homodine detection.

Another important set of capabilities that needs to be added are the one connected with feedback loops. This is an important point for the modelization point of view, and it will introduce the possibility of investigating several interesting and subtle effects.

4.2 Applications

The first application of our code will be in the framework of the "*Progetto PRIN di Ponderomotive Squeezing*", for the simulation of the apparatus that must be implemented. The basic scheme is shown in Figure 4.1.

As mentioned before the main point of interest is the study of the effects of misalignments and spurious mode coupling. Another couple of issues worth to be mentioned are the study of the interplay between thermal and quantum noise, and the possibility of introducing modifications in the basic scheme, for example by substituting the two small mirrors at the center of the double cavity with a single one.

We also planned to use the code to study a possible squeezing input bench for Advanced Virgo, and to cross check with other simulations which are going to be released in the immediate future.

4.3 Nonlinear effects

Another line of research which we plan to investigate is the study of possible relevant effects that could arise in specific situations which go beyond the linear approximations used in our approach. We discuss briefly the main ones.

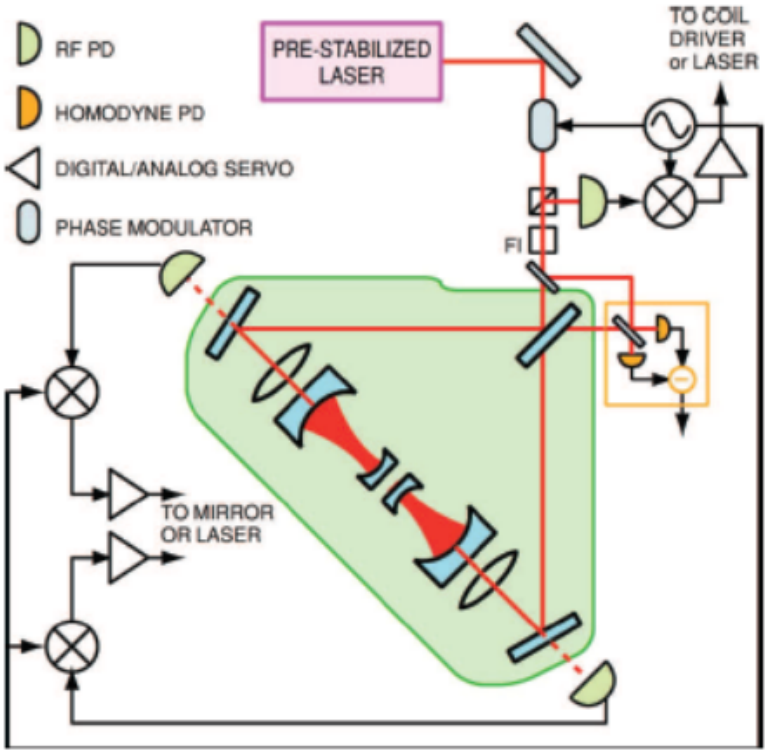

Figure 4.1: The optical apparatus that will be used in the "*Progetto PRIN di Ponderomotive Squeezing*". From the optical point of view it is almost identical to the one proposed in [12].

4.3.1 Higher order modulation effects in the mirror reflection

The reflection by a mirror and the associated phase shift of the reflected fields are described by the reflection operator (2.9) which is a nonlinear function of mirror displacement. We linearized it (see Eq. (2.21)) and as a consequence, for example, the mirror rotation couples only a very reduced number of modes.

This approximation is usually quite well justified, the main requirement being that the size of the typical mirror displacement is much lower than the carrier wavelength λ[1].

When this is not the case, besides the need to add more modes for a consistent representation of the system, many additional interactions between the mirror and the electromagnetic fields appear. They can be represented by the graphs

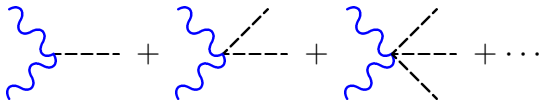

(4.1)

where as before the dashed line represents mirror displacements and the blue wavy line represents the total electromagnetic field (classical part and fluctuations). The first interaction is the only one which we consider, and for this reason the equations we need to solve are linear in the mechanical degrees of freedom.

4.3.2 No linearization in fluctuations

We can retain only the first interaction in (4.1), and still get nonlinear effects. This is because also the simplest ponderomotive interaction is quadratic in the photon fields. The linearization strategy in the standard approach consists in separating the total field (blue wavy line) in a "classical" carrier (black straight line) and in a quantum fluctuation (black wavy line), and to linearize in the fluctuations, graphically

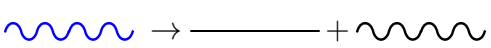

the interaction becomes

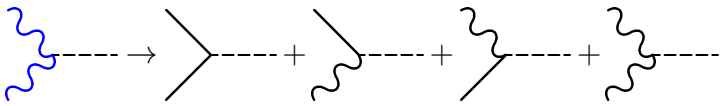

If we neglect the last one (the first can be reabsorbed in a redefinition of the equilibrium point of the system) we get a set of bilinear interactions which give

[1] A discussion about this point, including angular displacements, has been given in Section 2.1.3

the linear set of equations between mechanical degrees of freedom and first order optical quadratures we used.

If we do not discard the last term the dynamics becomes much more complicated. As an example, the reflection on a mirror can correlate together different sidebands, for example with the mechanism described by the graph

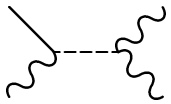

From the computational point of view the code needed to cope with this will be much more demanding in computational power. But it should be stressed that these effects are quite interesting and foreseen in several experimental contexts, so it seems worth the effort needed for further investigations.

Acronyms

SQL Standard Quantum Limit

HG Hermite Gauss

TEM Transverse Electric and Magnetic

FSR Free Spectral Range

qnSource light source

qnPropagator light propagator

qnMirror mirror

PPPS "*Progetto PRIN di Ponderomotive Squeezing*"

SC "Small" cavity

LC "Large" cavity

Bibliography

[1] LIGO Scientific Collaboration, Virgo Collaboration, J. Aasi, J. Abadie, B. P. Abbott, R. Abbott, T. D. Abbott, and others. Prospects for Localization of Gravitational Wave Transients by the Advanced LIGO and Advanced Virgo Observatories. *ArXiv e-prints*, April 2013.

[2] Kip S. Thorne Vladimir B. Braginsky, Farid Ya Khalili. *Quantum measurement*. Cambridge University Press, 1995.

[3] C. M. Caves, K. S. Thorne, R. W. P. Drever, V. D. Sandberg, and M. Zimmermann. On the measurement of a weak classical force coupled to a quantum-mechanical oscillator. i. issues of principle. *Rev. Mod. Phys.*, 52:341–392, Apr 1980.

[4] H. J. Kimble, Y. Levin, A. B. Matsko, K. S. Thorne, and S. P. Vyatchanin. Conversion of conventional gravitational-wave interferometers into quantum nondemolition interferometers by modifying their input and/or output optics. *Phys. Rev. D*, 65:022002, Dec 2001.

[5] H. Grote, K. Danzmann, K. L. Dooley, R. Schnabel, J. Slutsky, and H. Vahlbruch. First Long-Term Application of Squeezed States of Light in a Gravitational-Wave Observatory. *Phys. Rev. Lett*, 110(18):181101, May 2013.

[6] S. Mancini and P. Tombesi. Quantum noise reduction by radiation pressure. *Phys. Rev. A*, 49:4055–4065, May 1994.

[7] C. Fabre, M. Pinard, S. Bourzeix, A. Heidmann, E. Giacobino, and S. Reynaud. Quantum-noise reduction using a cavity with a movable mirror. *Phys. Rev. A*, 49:1337–1343, Feb 1994.

[8] W. Z. Korth, H. Miao, T. Corbitt, G. D. Cole, Y. Chen, and R. X. Adhikari. Suppression of quantum-radiation-pressure noise in an optical spring. *Phys. Rev. A*, 88:033805, Sep 2013.

[9] M. Aspelmeyer, T. J. Kippenberg, and F. Marquardt. Cavity Optomechanics. *ArXiv e-prints*, Mar 2013.

[10] C.M. Caves and B. L. Schumaker. New formalism for two-photon quantum optics. i. quadrature phases and squeezed states. *Phys. Rev. A*, 31:3068–3092, May 1985.

[11] C. M. Caves and B. L. Schumaker. New formalism for two-photon quantum optics. ii. mathematical foundation and compact notation. *Phys. Rev. A*, 31:3093–3111, May 1985.

[12] T. Corbitt, Y. Chen, F. Khalili, D. Ottaway, S. Vyatchanin, S. Whitcomb, and N. Mavalvala. Squeezed-state source using radiation-pressure-induced rigidity. *Phys. Rev. A*, 73:023801, Feb 2006.

[13] H. Kogelnik and T. Li. Laser beams and resonators. *Appl. Opt.*, 5, Oct 1966.

[14] B. S. Sheard, M. B. Gray, C. M. Mow-Lowry, D. E. McClelland, and S. E. Whitcomb. Observation and characterization of an optical spring. *Phys. Rev. A*, 69:051801, May 2004.

[15] U. Leonhardt. *Essential Quantum Optics: From Quantum Measurements to Black Holes*. Cambridge University Press, 2010.

[16] D. F. Walls and G. J. Milburn. *Quantum optics*. Springer, 2007.

[17] W. P. Schleich. *Quantum optics in phase space*. John Wiley & Sons, 2011.

[18] Y. Chen. Macroscopic quantum mechanics: theory and experimental concepts of optomechanics. *Journal of Physics B: Atomic, Molecular and Optical Physics*, 46(10):104001, 2013.

[19] C. K. Law. Interaction between a moving mirror and radiation pressure: A hamiltonian formulation. *Phys. Rev. A*, 51:2537–2541, Mar 1995.

[20] J.Harms. Quantum Noise in the laser-interferometer gravitational wave detector GEO 600. Master's thesis, Hannover Univeristy, 2002.

[21] T. Corbitt, Y. Chen, and N. Mavalvala. Mathematical framework for simulation of quantum fields in complex interferometers using the two-photon formalism. *Phys. Rev. A*, 72:013818, Jul 2005.

[22] H. B. Callen and R. F. Green. On a theorem of irreversible thermodynamics. *Phys. Rev.*, 86:702–710, Jun 1952.

[23] P. R. Saulson. Thermal noise in mechanical experiments. *Phys. Rev. D*, 42:2437–2445, Oct 1990.

[24] S. S. Y. Chua, S. Dwyer, L. Barsotti, D. Sigg, R. M. S. Schofield, V. V. Frolov, K. Kawabe, M. Evans, G. D. Meadors, M. Factourovich, R. Gustafson, N. Smith-Lefebvre, C. Vorvick, M. Landry, A. Khalaidovski, M. S. Stefszky, C. M. Mow-Lowry, B. C. Buchler, D. A. Shaddock, P. K. Lam, R. Schnabel, N. Mavalvala, and D. E. McClelland. Impact of backscattered light in a squeezing-enhanced interferometric gravitational-wave detector. *Classical and Quantum Gravity*, 31(3):035017, 2014.